Regularity underlying complexity: a redshift-independent description of the continuous variation of galaxy-scale molecular gas properties in the mass-star formation rate plane

Article (Published Version)

Published in the Astrophysical Journal, 793, 19
Preprint typeset using LaTeX style emulateapj v. 11/10/09

REGULARITY UNDERLYING COMPLEXITY: A REDSHIFT-INDEPENDENT DESCRIPTION OF THE CONTINUOUS VARIATION OF GALAXY-SCALE MOLECULAR GAS PROPERTIES IN THE MASS-STAR FORMATION RATE PLANE

M. T. Sargent[1, 2, ⋆], E. Daddi[1], M. Béthermin[1], H. Aussel[1], G. Magdis[3], H. S. Hwang[4], S. Juneau[1], D. Elbaz[1], E. da Cunha[5]

Published in the Astrophysical Journal, 793, 19

ABSTRACT

Star-forming galaxies (SFGs) display a continuous specific star formation rate (sSFR) distribution which can be approximated by two log-normal functions: one encompassing the galaxy main sequence, the other a rarer, starbursting population. Starburst sSFRs can be regarded as outcome of a physical process (plausibly merging) taking the mathematical form of a log-normal boosting kernel that enhances star formation activity. We explore the utility of splitting the star-forming population into main-sequence and starburst galaxies – an approach we term "2-Star Formation Mode" (2-SFM) framework – for understanding their molecular gas properties. Star formation efficiency (SFE) and gas fraction variations among SFGs take a simple redshift-independent form, once these quantities are normalized to the corresponding values for average main-sequence galaxies. SFE enhancements during starburst episodes scale supra-linearly with the SFR increase, as expected for mergers. Consequently, galaxies separate more clearly into loci for starbursts and normal galaxies in the Schmidt-Kennicutt plane than in (s)SFR versus $M_\star$ space. Starbursts with large deviations (>10-fold) from the main sequence, e.g. local ULIRGs, are not average starbursts, but are much rarer events whose progenitors had larger gas fractions than typical main-sequence galaxies. Statistically, gas fractions in starbursts are reduced two- to threefold compared to their direct main-sequence progenitors, as expected for short-lived SFR boosts where internal gas reservoirs are depleted more quickly than gas is re-accreted from the cosmic web. We predict variations of the conversion factor $\alpha_{\rm CO}$ in the SFR-$M_\star$ plane and we show that the higher sSFR of distant galaxies is directly related to their larger gas fractions.

Subject headings: cosmology: observations – galaxies: evolution – galaxies: spiral – galaxies: ISM – surveys

1. INTRODUCTION

Studies of star-forming galaxies (SFGs) over the last decade have revealed a positive and tight correlation between their current star formation rate (SFR) and stellar mass $M_\star$, which is intimately linked to the integral of the preceding star formation (SF) activity. Initially observed at low redshift (e.g., Brinchmann et al. 2004, Salim et al. 2007, Wyder et al. 2007), this "star-forming main sequence (MS)" was soon shown to be present out to $z\sim2$ (Noeske et al. 2007, Elbaz et al. 2007, Daddi et al. 2007b). Subsequent work on the relation between SFR and $M_\star$ in SFGs charted its evolution to $z\sim2.5$ using different SFR tracers and selection criteria (e.g., Damen et al. 2009, Dunne et al. 2009, Pannella et al. 2009, Santini et al. 2009, Kajisawa et al. 2010, Oliver et al. 2010, Elbaz et al. 2011, Lee et al. 2011, Rodighiero et al. 2011, Wuyts et al. 2011, Whitaker et al. 2012), has explored factors affecting the exact shape and dispersion of the MS (e.g., Karim et al. 2011, Salmi et al. 2012) and has traced it out to even higher redshifts $z\sim3$–4 (e.g., Daddi et al. 2009, Magdis et al. 2010). The existence of a scaling relation between SFR and $M_\star$ throughout much of cosmic time implies that the (mass-dependent) assembly history of SFGs is characterized by a high degree of homogeneity and simplicity (e.g., Noeske et al. 2007, Bouché et al. 2010, Peng et al. 2010, Leitner 2012, Behroozi et al. 2013) and that the strong decline of the cosmic SFR density since $z\sim2$ (e.g., Reddy & Steidel 2009, Rodighiero et al. 2010, Karim et al. 2011, Magnelli et al. 2011, Cucciati et al. 2012; and references therein) reflects the uniform SFR evolution of the majority of the SFG population rather than a decreased frequency of episodic starburst (SB) events. Nevertheless, the study of SBs remains central to understanding the nature of interacting galaxies and the physics of merging events that may produce the most luminous sources at all redshifts (Sargent et al. 2012; henceforth abbreviated as 'S12').

SF activity at a rate which locally occurs only in strong SBs is common in massive MS galaxies in the distant universe. Hence alternatives to pure luminosity-selection are required for obtaining a census of bursty SF activity at high redshift, e.g., based on their position in the SFR versus $M_\star$ plane (e.g., Rodighiero et al. 2011, Whitaker et al. 2012) or based on their morphology (e.g., Kartaltepe et al. 2012, Kaviraj et al. 2013). The latter approach relies on the assumption that SBs are generally triggered by interactions between galaxies, as observed in the local universe (e.g., Sanders et al. 1988, Barton

⋆ E-mail: Mark.Sargent@sussex.ac.uk
[1] CEA Saclay, DSM/Irfu/Sérvice d'Astrophysique, Orme des Merisiers, F-91191 Gif-sur-Yvette Cedex, France
[2] Astronomy Centre, Department of Physics and Astronomy, University of Sussex, Brighton, BN1 9QH, UK
[3] Department of Physics, University of Oxford, Keble Road, Oxford OX1 3RH, UK
[4] Smithsonian Astrophysical Observatory, 60 Garden Street, Cambridge, MA 02138, USA
[5] Max-Planck-Institut für Astronomie, Königstuhl 17, D-69117 Heidelberg, Germany

et al. 2000), while MS galaxies would represent a "normal", secular channel of stellar mass growth in galaxies that is fueled by the steady accretion of cold, primordial gas (e.g., Bouché et al. 2010).

A series of studies on the star-forming population has improved our understanding of normal (MS) galaxies and SBs and is in qualitative agreement with this picture. Starbursting sources are more compact on average (e.g., Elbaz et al. 2011, Rujopakarn et al. 2011) than MS galaxies, which have a stellar structure that is well described by exponential disks (e.g., Wuyts et al. 2011, Salmi et al. 2012). They display deficits in the intensity of infrared (IR) spectral features (e.g., polycyclic aromatic hydrocarbon (PAH) bands or in the far-IR [CII]-line; Elbaz et al. 2011, Graciá-Carpio et al. 2011), and have warmer IR spectral energy distributions (SEDs; e.g. Heisler & Vader 1994, Sanders & Mirabel 1996, Chapman et al. 2003, Elbaz et al. 2011, Magdis et al. 2011, Béthermin et al. 2012; and references therein). These are telltale features of intense and spatially concentrated SF as are expected to occur in interacting or merging galaxies where gravitational torques funnel gas to their centers (e.g., Mihos & Hernquist 1996, Hopkins et al. 2006).

The efficiency with which gas is converted into stars in such settings may be up to an order of magnitude higher than in the extended gas reservoirs that fuel SF activity in normal galaxies out to $z\sim2$ (e.g., Daddi et al. 2010b, Genzel et al. 2010, Tacconi et al. 2013). This strong contrast in star formation efficiency ($\mathrm{SFE}\equiv\mathrm{SFR}/M_{\mathrm{gas}}$) is often taken as one of the most clear-cut manifestations of the existence of two distinct SF laws – a secular mode in main-sequence galaxies and an SB mode characterized by short depletion timescales ($\lesssim$100 Myr, e.g. Solomon & Vanden Bout 2005; and references therein). Whether or not such a bimodality represents the physical reality has been questioned (e.g., Narayanan et al. 2012) on the grounds of discrete "concordance" values being assumed for the CO-to-H_2 conversion factor α_{CO} and, second, due to the expectation that SF laws at a basic level should be expressed in terms of volumetric quantities rather than observationally more easily accessible surface densities of SFR and gas (e.g., Krumholz et al. 2012). The lack of known sources with SFEs between those measured for normal disk galaxies and strong SBs could also be a selection effect: initial CO follow-up observations of high-redshift galaxies targeted only highly luminous sources experiencing "bursty" SF (submillimeter galaxies and QSOs; e.g., Omont et al. 1996, Frayer et al. 1998, Walter et al. 2003, Greve et al. 2005, Maiolino et al. 2007, Tacconi et al. 2008) and following improvements in the sensitivity of millimeter receivers (Chenu et al. 2007, Perley et al. 2011), dedicated studies of typical MS galaxies were undertaken (e.g., Daddi et al. 2008, 2010a, Tacconi et al. 2010, Geach et al. 2011, Tacconi et al. 2013, Bauermeister et al. 2013a). If, as discussed in Renaud et al. (2012), the gas density distribution function – which reflects the turbulence-driven structure of the interstellar medium (ISM) – is a crucial factor in determining the shape of SF laws, then intermediate SFEs should indeed occur in, e.g., minor mergers or in certain stages of galaxy interactions when the gas density distribution is not modified from the steady state as strongly as during final coalescence. However, a dichotomy in the distribution of SFEs could still occur if the timescales for such variations were short (e.g., Teyssier et al. 2010, Bournaud et al. 2011a).

In this paper we consider a large sample of local and high-redshift SFGs which we use to extend the "2 Star-Formation Mode" (2-SFM) framework introduced in S12 to the molecular gas component of SFGs. The 2-SFM framework relies on basic observables (e.g., the evolution of specific star formation rate (sSFR) in MS galaxies or their stellar mass distribution) and correlations between observables (e.g. the star-forming MS or the Schmidt-Kennicutt (S-K) relation). Our goal is to describe how the SFE and the molecular gas content of galaxies are related to their location with respect to the MS, i.e., to their sSFR, which is the main diagnostic of "starburstiness" within the 2-SFM framework. We will show that the population of massive SFGs that reside on the MS has similar molecular gas properties across a broad range of redshifts ($z\lesssim3$) and we will use our detailed description of the SB population and its SFR-"boosting" developed in Section 4.2 to demonstrate how in the 2-SFM framework a bimodal behavior in terms of SFE arises naturally even in the absence of discrete SF laws for normal galaxies and SBs. The description of SFE in the SFG population developed in this paper forms the basis for the prediction of molecular gas mass functions and CO luminosity functions in a companion paper (M.T. Sargent et al., in prep.; henceforth Paper II).

The outline of this manuscript is as follows. Section 2 introduces the observational data set we use and how it was homogenized. We then employ this reference sample in Section 3 to calibrate galaxy-scale SF laws – both in terms of observables (L_{IR} & L'_{CO}) or intrinsic quantities (SFR & $M_{\mathrm{H_2}}$) – for galaxies at low and high redshift. These calibrations depend on the adopted CO-to-H_2 conversion factor α_{CO}, and the corresponding systematics will also be assessed in Section 3. The mathematical description of the SB population in the 2-SFM framework, and its relation to MS galaxies is the focus of Section 4 where we derive the distribution of the burst amplitudes – the "boost function" – that transforms a theoretical population of pure main-sequence star forming galaxies into the observed distribution of sSFR. We discuss what physical mechanisms could produce this boost function and consider in particular the possible link between SBs and galaxy mergers. In Section 5 we will combine the redshift-independent, integrated S-K law derived in Section 3 with the evolution of the sSFR distribution from S12 to construct prescriptions for the relative variation of molecular gas properties of normal and SB galaxies that are particularly simple (and self-similar) once they are referred to the properties of the average MS galaxy. Our results are presented in three main blocks: the SFE and gas fractions of MS galaxies and SBs are the subject of Section 5.1 and 5.2, respectively; Section 5.3 focuses on the CO-to-H_2 conversion factor and its variation within the MS and among starbursting systems. We then discuss and summarize our findings in Sections 6 and 7.

Throughout this article we adopt the WMAP-7 cosmology ($\Omega_m=0.273$, $\Omega_\Lambda+\Omega_m=1$ and $H_0=70.4$ $\mathrm{km\,s^{-1}\,Mpc^{-1}}$; Larson et al. 2011). SFRs and stellar masses are given for a Chabrier (2003) initial mass function[7] (IMF). All literature values have been adapted ac-

[7] Logarithmic masses and SFRs based on a Salpeter (1955), a

cordingly. Metallicities are given on the Kewley & Dopita (2002; henceforth 'KD02') scale[8] and (molecular) gas mass estimates include a 36% correction for helium.

2. DATA

We discuss two different kinds of data sets in this section. To begin with (Section 2.1), we describe individual, CO-detected SFGs which we will utilize to establish the basic scaling relations (e.g. for SFE or gas fractions) that link the molecular gas content of massive ($M_\star > 10^{10} M_\odot$) SFGs to fundamental galaxy properties like (s)SFR or $M_\star$. In Section 2.2 we introduce statistical samples of SFGs at $z \sim 1$ and 2. These will subsequently be used (1) to visualize/simulate complete samples of galaxies that obey the aforementioned scaling relations, and (2) to extend the analysis to fainter galaxies where the validity of such scaling relations can be verified with image stacking.

2.1. *The Reference Sample of Individual Star-forming Galaxies*

Our "reference sample" of normal galaxies at redshifts $z \lesssim 3$ comprises 131 sources from the recent literature (see Sections 2.1.1 & 2.1.2). We complement these with local and high-redshift starbursts with measured CO-to-H_2 conversion factors (see Section 2.1.3). These are essential for a further investigation of the notion that the "bimodality" of SF is particularly pronounced in terms of SFE (e.g., Daddi et al. 2010a, Genzel et al. 2010).

2.1.1. *Normal Galaxies: Low-redshift CO-detections*

The HERACLES survey (Leroy et al. 2008, 2009, 2013) targeted the CO(J=2→1) transition in nearby ($D \lesssim 15$ Mpc) THINGS galaxies (Walter et al. 2008) with the IRAM 30 m single-dish telescope. Here we select 20 galaxies with spiral galaxy morphology and stellar mass $M_\star \geq 10^{10}\, M_\odot$ from the HERACLES sample. Stellar masses (converted to the Chabrier (2003) scale) and morphological information are taken from the compilations of Skibba et al. (2011) or Leroy et al. (2008, 2009), or from the NASA/IPAC Extragalactic Database (NED)[9] if not listed in either of the former. Metallicity estimates for most of the selected HERACLES spirals are provided in Moustakas et al. (2010). The IR (8-1000 μm) luminosities attributed to the HERACLES galaxies are based on the photometry reported in Dale et al. (2007) and have been calculated following Equation 22 in Draine & Li (2007).

We augment the local MS galaxies from the HERACLES data set with a subset of galaxies from the first release of the COLD GASS survey (Saintonge et al. 2011) for which an accurate IR luminosity could be calculated thanks to the presence of a counterpart in either the *IRAS* Faint Source Catalog (v2; Moshir et al. 1992) or the *AKARI*/Far-Infrared Surveyor (FIS; Kawada et al. 2007) all-sky survey Bright Source Catalog (v1.0; Yamamura et al. 2010). An additional cut in stellar mass (taken from Saintonge et al. 2011) at $M_\star = 10^{10}\, M_\odot$ excluded all less massive sources. Among the 222 sources in the first COLD GASS data release 32 fulfill these criteria; they lie in the redshift range $0.025 < z < 0.05$ and are all late-type galaxies with CO(J=1→0) fluxes measured by the IRAM 30 m telescope at signal-to-noise ratio, $S/N > 4$. IR luminosities for these galaxies were computed using the SED library of Chary & Elbaz (2001) and allowing renormalization of the templates when fitting the reliable[10] *IRAS* or *AKARI* photometry at $\lambda_{\rm rest} \geq 30\,\mu$m (for details on the IR SED-fitting see Hwang et al. 2010).

2.1.2. *Normal Galaxies: Intermediate- & High-redshift CO-detections*

CO-transitions in MS galaxies at $z > 0$ have been targeted by Geach et al. (2009, 2011; CO(J=1→0) at $z \sim 0.4$), Daddi et al. (2010a,b; CO(J=2→1) at $z \sim 0.5$ & 1.5), in the PHIBSS survey by (Tacconi et al. 2013; CO(J=3→2) at $z \sim 1.2$ & 2.3), and by Magdis et al. (2012a; CO(J=3→2) at $z \sim 3$) – all using the IRAM Plateau de Bure interferometer – and by the EGNoG survey (Bauermeister et al. 2013a; CO(J=1→0) at $0.06 \lesssim z \lesssim 0.3$) using the Combined Array for Research in Millimeter-wave Astronomy. These observations have produced line flux measurements at $S/N \gtrsim 4$ toward 70 of 79 observed galaxies (for the remaining galaxies $3\,\sigma$ upper flux limits are available). The stellar masses of these sources are in the range $10^{10} < M_\star/M_\odot \lesssim 5 \times 10^{11}$, as determined by SED fitting of the near-UV to near-IR broad-band photometry.

The derivation of SFRs varies among the different aforementioned studies. EGNoG galaxies have SFRs that are based on emission line fluxes and which were extracted from the MPA-JHU value-added catalog for SDSS DR7 (see Bauermeister et al. 2013a; for details). Geach et al. (2009, 2011) estimate the IR-luminosity from the flux of the 7.7 μm emission, as constrained by the *Spitzer* IR spectrograph, while Daddi et al. (2010b) based the luminosity measurements for their $z \sim 0.5$ sources on *Spitzer*/MIPS 24 μm fluxes. SFR-estimates for $z \sim 1.5$ sBzK galaxies presented in Daddi et al. (2010a) are an average of dust-corrected UV luminosities, mid-IR continuum luminosities from 24 μm imaging, and Very Large Array (VLA) 1.4 GHz radio continuum fluxes, all of which were found to give consistent SFR-estimates. Magdis et al. (2012a) adopted a similar averaging approach but were able to add *Herschel*/PACS and SPIRE photometry to constrain the dust-emission of their $z \sim 3$ Lyman-break galaxies (LBGs). We adopted all of these SFR ($L_{\rm IR}$) measurements without further modifications, but in the interest of maximal sample homogeneity chose to re-compute $L_{\rm IR}$ values for PHIBSS sources at $z \sim 1.2$ as Tacconi et al. (2013) report SFRs based on a combination of extinction-corrected optical emission lines, UV flux and mid-IR photometry. To derive new $L_{\rm IR}$ and SFR estimates we searched the Far Infrared Deep Extragalactic Legacy (FIDEL, PI: M. Dickinson, see also data description in Magnelli et al. 2009) coverage of the Ex-

Kroupa (2001) and a Baldry & Glazebrook (2003) IMF are converted to the Chabrier scale by adding -0.24 dex, 0 dex and 0.02 dex, respectively.

[8] When necessary, metallicity information from the literature was converted to the KD02 calibration by means of the prescriptions in Kewley & Ellison (2008).

[9] `http://ned.ipac.caltech.edu`

[10] Flux quality flags are either "high" or "moderate" for *IRAS* sources and "high" for *AKARI* sources.

tended Groth Strip for associated *Spitzer*/MIPS 24 μm detections and converted these to IR luminosities with the MS SFG IR SED of Elbaz et al. (2011). SFRs for $z\sim1.2$ PHIBSS galaxies are the averages of the SFRs reported in Tacconi et al. (2013) and our IR-based estimates. Two of the 27 PHIBSS sources at $z\sim1.2$ have VLA 1.4 GHz detections from the AEGIS20 catalog (Ivison et al. 2007), such that the original, the 24 μm- and a radio-based SFR could be averaged. For PHIBSS galaxies at $z\sim2.3$ neither IR nor radio flux measurements were available; we hence used the original SFRs reported by Tacconi et al. (2013) which are based on extinction-corrected Hα luminosities and which we converted to an IR-luminosity following Kennicutt (1998b).

To summarize, we have compiled a sample of 131 massive ($M_\star\geq10^{10}\,M_\odot$), MS galaxies[11] with CO-detections of which 46% are low-redshift systems ($z<0.1$) systems and the remaining 54% redshifted to $0.1<z<3.2$. Our sample is thus well-balanced between nearby and distant galaxies, as shown in Figure 1 where we review the most important physical properties of our reference galaxies, e.g., $M_\star$, SFR and (s)SFR-excess with respect to the star-forming MS.

2.1.3. *Starbursting Galaxies with Measured* $\alpha_{\rm CO}$

Starbursting galaxies with the same information as available for our reference sample of normal galaxies are listed in the recent study of Magdis et al. (2012b; SB-like galaxies at $2.3<z<4$) and in Solomon et al. (1997; local starbursting *IRAS* ULIRGs). An accurate assessment of the behavior of SFE during SB episodes – one of the main aims of this paper – requires an observational determination of the CO-to-H_2 conversion factor $\alpha_{\rm CO}$. In the case of the local ULIRGs, we thus restrict ourselves to nine objects – VII Zw 31, Arp 193, Arp 220, Mrk 273, 00057+4021, 02483+4302, 10565+2448, 17208-0014, 23365+3604 – with two independent measurements of $\alpha_{\rm CO}$: one based on dynamical constraints[12] by Downes & Solomon (1998) and the other based on large velocity gradient (LVG) radiative transfer modeling by Papadopoulos et al. (2012).

The flux of the CO(J=1→0) transition toward our subsample of nine $z<0.07$ *IRAS*-detected ULIRGs was measured with the IRAM 30 m single-dish telescope by Solomon et al. (1997). We computed their IR luminosities (and thence SFRs) using spectroscopic redshifts from NED and all available *IRAS* photometry, following the standard recipes provided by Sanders & Mirabel (1996; their Table 1). Stellar masses – which are particularly important for the characterization of these systems in terms of sSFR, our prime indicator of "starburstiness" – have been published for some of the ULIRGs in our sample (e.g., Elbaz et al. 2007, da Cunha et al. 2010,

[11] Three of these – one each from HERACLES, PHIBSS and the sample of Geach et al. (2011) – have an sSFR excess larger than four, the frequently adopted threshold to separate normal from SB galaxies (e.g., Rodighiero et al. 2011), but a clearly disk-like morphology showing now indications of interactions. We have hence included them in our main-sequence reference sample.

[12] In the following we adopt a mass-to-light ratio $\alpha_{\rm CO}$ that is given by the ratio between gas mass and dynamical mass within a ∼1-3 kpc region encompassing both the inner, high-density nuclear disk/ring and an outer, lower-density disk (with volume filling factor ∼0.1 for the gas) of the ULIRGs modeled in Downes & Solomon (1998; see their Tables 3 & 9).

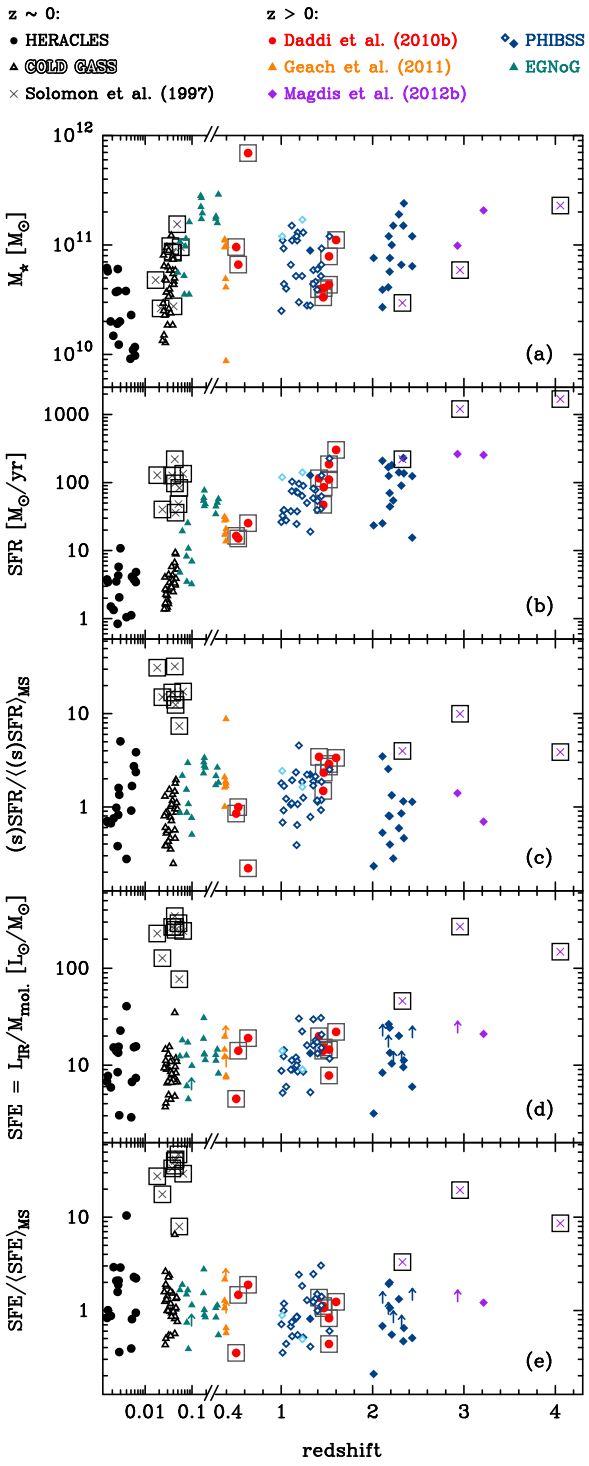

FIG. 1.—: Redshift dependence of physical properties for galaxies in our calibration sample (crosses – starbursting galaxies; all other symbols – massive MS galaxies). (*a*) stellar mass $M_\star$; (*b*) star formation rate SFR; (*c*) offset from the mass- and redshift-dependent mean locus of the star-forming main sequence (MS) (s)SFR/(s)SFR$_{\rm MS}$ (see Appendix A); (*d*) star formation efficiency SFE; (*e*) normalized SFE, i.e. the efficiency normalized to the SFE that a galaxy of equal gas mass would have if it lay directly on the integrated S-K relation (see Figure 2(b)). Boxed symbols are used for galaxies with an observational constraint on the CO-to-H_2 conversion factor $\alpha_{\rm CO}$ (see text for details); symbol coloring depends on the literature source (see legend above figure). The shape of the symbols reflects the CO-transition which was observed to infer molecular gas properties: triangles – CO(J=1→0); dots – CO(J=2→1); diamonds – CO(J=3→2).

Howell et al. 2010, U et al. 2012), but to our knowledge no single study has done this consistently for all sources of interest. We hence re-estimated stellar masses for the Downes & Solomon (1998) ULIRGs based on 2 Micron All Sky Survey K-band fluxes (Skrutskie et al. 2006) and prescriptions for mass-to-light ratios, $M_\star/L_K$, as derived by Arnouts et al. (2007; their Equation 2) and Juneau et al. (2011; their Equation B2). The stellar masses we adopt in the following for the Downes & Solomon (1998) ULIRGs were obtained by averaging the estimates calculated according to these two prescriptions. They agree well with the available literature measurements (median offset 0.1 dex).

In addition to the nine low-redshift SBs just described we also include the three high-z sub-millimeter galaxies GN20 ($z=4.05$), SMMJ2135-0102 ($z=2.325$) and HERMES J105751.1+573027 ($z=2.957$) in our analysis. The recent determination of their conversion factor $\alpha_{\rm CO}$ in Magdis et al. (2012b) by means of the $M_{\rm gas}/M_{\rm dust}$-ratio technique (see also Leroy et al. 2011, Magdis et al. 2011) relied on: (i) a far-IR SED/dust emission that is accurately constrained by *Herschel* and millimetric continuum observations (see Magdis et al. 2012b for a detailed listing), and (ii) CO(J=1→0) line fluxes from the (J)VLA (for GN20; see Carilli et al. 2010, Hodge et al. 2012) and the Green Bank Telescope (for SMMJ2135-0102 and HERMES J105751.1+573027; see Swinbank et al. 2010 and Riechers et al. 2011, resp.). All three sources have sSFR enhancements with respect to the MS of at least a factor three, as constrained by the optical to near-IR and IR SED-fitting of Magdis et al. (2012b). Furthermore, their CO-to-H_2 conversion factors are systematically lower than that of the Milky Way, similar to the values typically measured in interacting local ULIRGs.

2.2. *Statistical Samples of Star-forming Galaxies in GOODS-South*

With the purpose of demonstrating the applicability of our recipes for computing molecular gas properties for observed galaxy samples, based on individual measurements of stellar masses and SFRs, we use two samples of K-selected galaxies in the GOODS-S field, at $z\sim1$ and 2 taken from the work of Daddi et al. (2007a) and Daddi et al. (2007b; see also Salmi et al. 2012 for more details on the $z\sim1$ sample). The same samples were used in the recent papers by Magdis et al. (2012b) and Mullaney et al. (2012a). We refer to the original papers for details of how stellar masses were derived, based on empirical recipes using colors and absolute luminosities. The SFRs of the galaxies at $z\sim1$ and 2 are based on 24 μm and UV observations, respectively, and are known to compare well on average with other tracers including *Herschel*-based SFR measurements (Daddi et al. 2007a, Elbaz et al. 2010, Reddy et al. 2012).

3. GALAXY-SCALE STAR FORMATION LAWS: CORRELATIONS BETWEEN SFR AND GAS MASS AND THE ASSOCIATED OBSERVABLES

Recent reports (e.g., Daddi et al. 2010b, Genzel et al. 2010) of a systematic offset between the power law relation linking the overall surface density of SFR and gas mass (the Schmidt-Kennicutt (S-K) law $\Sigma_{\rm SFR}\propto\Sigma_{\rm gas}^n$; Schmidt 1959, Kennicutt 1998a) of normal galaxies and SBs were highly influential in shaping the notion of "bimodal" SF. These findings are subject to two systematic uncertainties. First, the measured offset between normal and SB galaxies depends on (potentially population-dependent) recipes for CO-to-H_2 conversion factors, which are hard to measure for a statistically significant number of SFGs, especially at $z\gg0$. Second, the sampling of the S-K plane obtained as a result of targeted CO follow-up observations toward selected SFGs is patchy. Constructing a reliable and statistically representative sampling of the distribution of SFGs in the S-K plane is thus not only important to explore different modes of SF. The observed S-K law is also often referred to as a benchmark for the performance/validity of recipes for ISM processes in simulations (e.g., Robertson & Kravtsov 2008, Monaco et al. 2012) and hence used to gauge our understanding of the underlying physics itself. In this section we return to our literature compilation of low- and high-redshift MS galaxies with CO-detections that we presented in Sections 2.1.1 and 2.1.2. We remeasure the slope and dispersion of the galaxy-scale SF law and in doing so for the first time are able to incorporate $\alpha_{\rm CO}$ measurements from the recent study of Magdis et al. (2012b) for a fraction of our reference sample of normal galaxies. Rather than using SFR and gas mass surface densities, we consider the simpler relations between integrated quantities, namely the total SFR and molecular gas mass or the corresponding observables, $L_{\rm IR}$ and $L'_{\rm CO(J=1\rightarrow0)}$. For the rest of this article we will use "$L'_{\rm CO}$" as a shorthand for the line luminosity $L'_{\rm CO(J=1\rightarrow0)}$ of the first rotational transition of ^{12}CO.

3.1. $L'_{\rm CO(J=1\rightarrow0)}$ *versus* $L_{\rm IR}$

We begin with the relation between the observables, $L_{\rm IR}$ and $L'_{\rm CO}$, that are the starting point for estimating SFRs and the molecular gas content of SFGs. As described in Section 2.1 all galaxies considered in the following have stellar masses $M_\star\geq10^{10}\,M_\odot$. Current observations of BzK-selected MS galaxies (e.g., Dannerbauer et al. 2009, Aravena et al. 2010) suggest that typical excitation corrections for the first two higher order transitions J=2→1 and 3→2 are $r_{21}=0.8$-0.9 and $r_{31}\simeq0.5$. Similarly, Leroy et al. (2009) find an average J=2→1/J=1→0 line ratio of 0.8 for nearby HERACLES galaxies and Bauermeister et al. (2013b) report J=3→2/J=1→0 line ratios of 0.46±0.07 for $z\sim0.3$ galaxies in the EGNoG sample. In Figure 2(a) we plot the accordingly corrected CO(J=1→0) luminosities of local (black and white symbols) and redshifted sources (color symbols) against their IR luminosity. We then fitted the CO line luminosity as a function of IR luminosity. While performing a regression of $L_{\rm IR}$ on $L'_{\rm CO}$ would be more natural (as representing the relation between cause and effect, i.e. $M_{\rm mol.}$ and SFR, resp.) our choice is motivated by the aim to provide recipes for the molecular gas content and associated tracer emission beginning with the currently observationally more easily accessible SFR measurements. A Buckley & James (1979; hereafter "BJ'") regression (implemented as described in Isobe et al. 1986), which allows for a statistically correct treatment of the 3 σ upper detection limits for six galaxies from Tacconi et al.

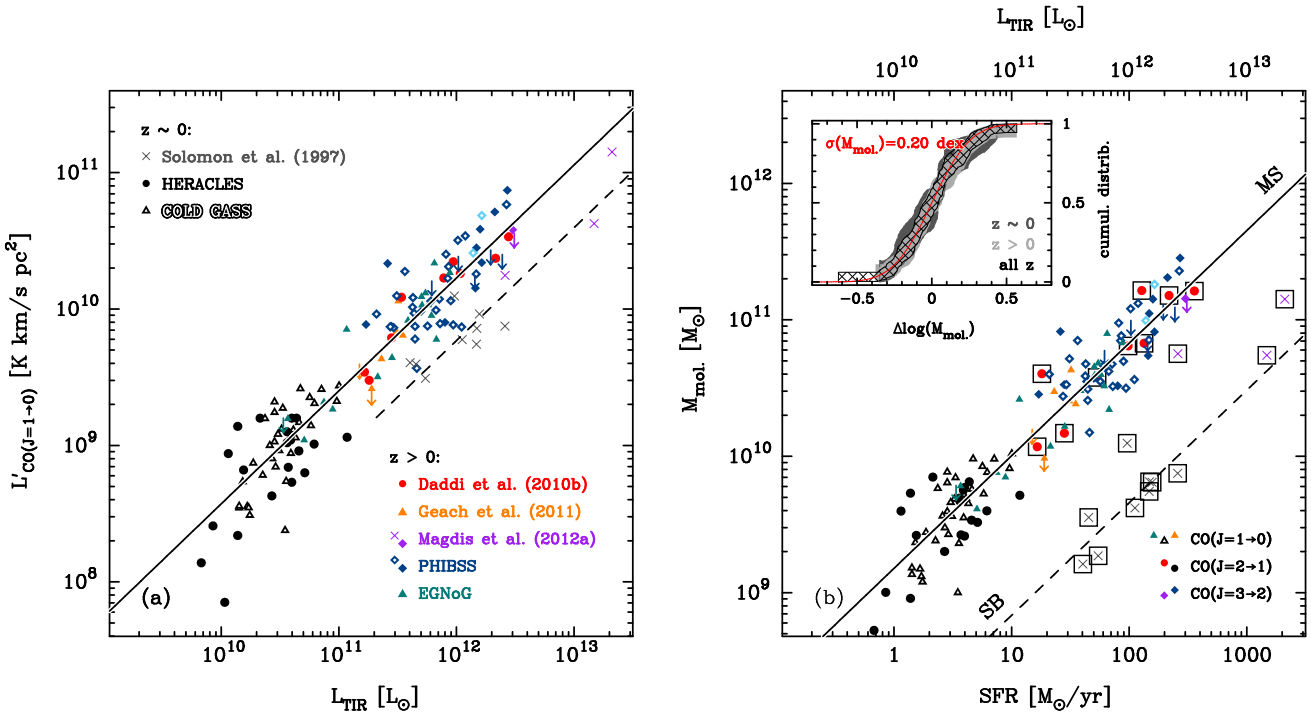

FIG. 2.—: Observed correlation between measures of star formation rate and molecular gas content for massive ($M_\star > 10^{10}\,M_\odot$) main-sequence (MS) galaxies and starbursts (SBs) at low and high redshift. Low-redshift sources (filled/open black symbols – normal galaxies; grey crosses – starbursting (U)LIRGs) are from the HERACLES, GOLD GASS and *IRAS* surveys. Redshifted galaxies from the literature (see legend) are plotted in color (*pine green* – $0.04 \lesssim z \lesssim 0.4$; *orange* – $z \sim 0.4$; *red* – $z \sim 0.55$ & $z \sim 1.5$; *blue* – $z \sim 1.2$ & $z \sim 2.3$; *magenta* – SBs at $2.3 < z < 4$), with arrows indicating $3\,\sigma$ upper limits for CO non-detections. Open blue and cyan symbols indicate modified SFR estimates (see section 2.1.2 for details) based on radio and/or IR data for sources in Tacconi et al. (2013). The shape of the symbol indicates which CO transition was detected toward the individual sources (cf. legend in lower right corner of panel *b*). (*a*) Correlation between infrared luminosity ($L_{\rm IR}$) and CO-luminosity ($L'_{\rm CO(J=1\to0)}$; standard excitation corrections – e.g. Dannerbauer et al. (2009), Leroy et al. (2009) – were applied to $J > 1$ transitions) with the best-fitting relation derived for the MS galaxy sample plotted as a solid black line. The strong SBs considered here (cross symbols) are on average offset to higher $L_{\rm IR}$values by a factor of three (dashed line). (*b*) Inverse, integrated Schmidt-Kennicutt relation between SFR and molecular gas mass ($M_{\rm mol.}$), the latter having been derived based on either (i) observational determinations of $\alpha_{\rm CO}$ (available for sources with boxed symbols) or (ii) using a metallicity-dependent conversion factor (see text of Section 3.2). The dispersion about the best-fit linear trend (solid black line) for MS galaxies is approximately Gaussian with a dispersion $\sigma(M_{\rm mol.}) \sim 0.2$ dex (red curve in inset). Dashed line – offset locus with approx. 15 times higher SFE for strong SB galaxies.

(2010) and Geach et al. (2011), gives

$$\log\left(\frac{L'_{\rm CO(J=1\to0)}}{\rm K\,km/s\,pc^2}\right) = \alpha_1 + \beta_1 \log\left(\frac{L_{\rm IR}}{L_\odot}\right)\ , \quad \text{with} \qquad (1)$$

$$(\alpha_1;\beta_1) = (0.54 \pm 0.02; 0.81 \pm 0.03) \quad \text{for normal galaxies.}$$

The dispersion about this best-fit trend line in the y-direction is 0.21 dex. In performing the linear regression we have down-weighted sources detected in CO(J=3→2) by a factor of two due to the large excitation corrections r_{31}.

Under the assumption that SBs follow a correlation with identical slope, we use our reference sample of SB galaxies (see Section 2.1.3) to solve for the normalization of Equation 1 that best reproduces their average offset. We find

$$(\alpha_1;\beta_1) = (0.08^{+0.15}_{-0.08}; 0.81)\ ,$$

i.e. an offset of 0.46 dex or approx. a factor 2.9 with respect to the locus of MS galaxies. This similar systematic difference was already indicated by Solomon et al. (1997; see their Figure 3) in their pioneering analysis of CO-emission in nearby ULIRGs. Local MS galaxies with the IR luminosities of starbursting ULIRGs are, however, exceedingly rare (e.g., S12) such that this difference could also have been explained by a double power-law nature of the SF law or a single, steeper relation ($L_{\rm IR} \propto {L'_{\rm CO}}^{1.3}$) owing to different probability gas density distributions in mergers and normal galaxies (Narayanan et al. 2008, Juneau et al. 2009). The advent of CO line flux measurements for high-z normal galaxies with ULIRG-luminosities has since added another piece of evidence in support of a systematic offset (e.g., Genzel et al. 2010).

3.2. $M_{\rm mol.}$ *versus SFR*

The integrated S-K law linking the molecular gas mass ($M_{\rm mol.}$) and SFR is expected to have a different slope or curvature than the correlation between logarithmic luminosities $L'_{\rm CO}$ and $L_{\rm IR}$ unless the average CO-to-H_2 conversion factor

$$\alpha_{\rm CO(J=1\to0)} = \frac{M_{\rm mol.}}{L'_{\rm CO(J=1\to0)}}$$

is a constant. Evidence to the contrary has been presented in numerous observational studies, the most recent of which are Leroy et al. (2011), Schruba et al. (2012), Genzel et al. (2012) and Rémy-Ruyer et al. (2014) who show that there is a tendency for $\alpha_{\rm CO}$ to decrease with metallicity both in local galaxies and in massive MS galaxies at $z < 2.5$ in general. Note that Sandstrom et al. (2013) find a similar trend for decreasing $\alpha_{\rm CO}$ with increasing metallicity when considering spatially distinct

regions within nearby galaxies. In the next paragraphs we discuss a scheme for assigning metallicity-dependent $\alpha_{\rm CO}$ values to the normal SFGs in our reference sample (Section 3.2.1) and then proceed to fit the resulting relation between SFR and $M_{\rm mol.}$ in Section 3.2.2. We close this section with an assessment of the robustness of the galaxy-scale SF law obtained in this way (Section 3.2.3).

3.2.1. *Statistically Inferred CO-conversion Factors*

For 9 of the 131 MS galaxies in our reference sample the CO-to-H_2 conversion factor has been measured by Magdis et al. (2012b) and found to be broadly consistent with the trend between $\alpha_{\rm CO}$ and metallicity Z found for galaxy samples in the nearby universe. For the remaining 122 galaxies we assign a metallicity-dependent $\alpha_{\rm CO}$ as explained below, and assume that metallicity can be deduced in a statistical sense from stellar mass $M_\star$ and SFR as proposed by Mannucci et al. (2010) and Lara-López et al. (2010). In the following we use this "fundamental metallicity relation" (FMR; see Figure 3(a)) as parametrized by Mannucci et al. (2010). Since SBs constitute a small fraction of the star-forming population, the FMR primarily reflects the dependence of metallicity on SFR and $M_\star$ for MS galaxies. As the stellar mass and SFR of the CO-detections in our reference sample are known (within observational errors) we can use the FMR to statistically infer metallicities $Z(\mathrm{SFR}, M_\star)$, and thence CO-conversion factors $\alpha_{\rm CO}$ for each of the galaxies in our reference sample[13]. This enables us to calibrate the $M_{\rm mol.}$ versus SFR relation independently from the correlation between $L'_{\rm CO}$ and $L_{\rm IR}$ derived in Section 3.1. Note that more general expectations for $\alpha_{\rm CO}$ variations in the $M_\star$ versus SFR plane that account for (1) changes of the conversion factor within both the normal and starbursting galaxy population, and (2) the relative importance of these to classes of SFGs depending on the location in the plane, are the topic of Section 5.3.2.
A frequently used, first-order description of the metallicity dependence of $\alpha_{\rm CO}$ is the single power-law

$$\log(\alpha_{\rm CO}) = \nu + \xi \log\left({}^{Z}/_{Z_\odot}\right) \ . \qquad (2)$$

Existing literature consistently reports the normalization ν of the $\alpha_{\rm CO}$ versus metallicity relation in Equation 2 to be such that Milky-Way-like conversion factors $\alpha_{\rm CO} = 4.4\ M_\odot/(\mathrm{K\,km/s\,pc^2})$ are reached around solar metallicity. Measurements and expectations for the slope ξ span a larger range which we illustrate in Figure 3(b). Analysis of the varying findings in the literature suggests that the slope measured depends on, e.g., the range of metallicities probed in different samples. This may be linked to a rapid steepening of the $\alpha_{\rm CO}$ versus Z relation that occurs around $Z \sim 1/3$ to $1/2\,Z_\odot$ (e.g., Leroy et al. 2011, Rémy-Ruyer et al. 2014). Models explicitly treating the shielding of CO by dust and (atomic and molecular) hydrogen can reproduce this behavior which arises because CO is more easily photodissociated at low metallicities (see, e.g., Bolatto et al. 2013; and references therein). While a single power law as in Equation 2 may adequately reproduce variations of $\alpha_{\rm CO}$ among galaxies with approximately solar enrichment – and hence among most of the massive SFGs in our reference sample – we will also consider a broader range of metallicities in parts of Section 5.
For this reason, we assign $\alpha_{\rm CO}$ values to those 122 galaxies lacking an observational constraint with the following prescription from Bolatto et al. (2013), which is based on modeling in Wolfire et al. (2010):

$$\frac{\alpha_{\rm CO}(Z')}{\alpha_{\rm CO}(Z'=1)} = \exp\left(\frac{+4.0\,\Delta A_V}{Z'\,\overline{A}_{V,\rm MW}}\right) \exp\left(\frac{-4.0\,\Delta A_V}{\overline{A}_{V,\rm MW}}\right) \ . \qquad (3)$$

Here $Z' = {}^{Z}/_{Z_\odot}$ is metallicity, normalized to solar abundance, and $\overline{A}_{V,\rm MW} = 5$ is the mean visual extinction through a giant molecular cloud (GMC) at $Z_\odot$. ΔA_V, the differential extinction between ISM regions where only the CO molecule or both CO and H_2 are found, is calculated as in Equation 26 in Bolatto et al. (2013), except that we adopt an underlying double power-law relation between gas-to-dust ratio and metallicity in keeping with Rémy-Ruyer et al. (2014). We assume that $\alpha_{\rm CO}(Z'=1) = 4.4\,M_\odot/(\mathrm{K\,km/s\,pc^2})$, i.e. a Millky-Way-like conversion factor at $Z_\odot$. With Equation 3 the equivalent of the logarithmic slope ξ as defined in Equation 2 varies from -0.6 at $Z_\odot$ to a significantly steeper dependence at sub-solar metallicities as illustrated in Figure 3(b) (dotted line).

3.2.2. *Integrated Schmidt-Kennicutt Laws*

Multiplication of the excitation-corrected CO-luminosities of Figure 2(a) with (i) observed CO-to-H_2 conversion factors if available or (ii) the statistical CO-conversion factors discussed in the previous section provides a measure of the molecular gas mass for each of the MS galaxies in our reference sample. These measurements are plotted against their SFR in Figure 2(b). At the stellar masses considered here, the IR-excess $L_{\rm IR}/L_{\rm UV}$ of MS galaxies is in general $\sim$10 or larger (e.g., Whitaker et al. 2012, Pannella et al. 2014, Heinis et al. 2014), leading to a nearly 1:1 correspondence between $L_{\rm IR}$ and SFR, as indicated by the lower and upper scale for the x-axis of Figure 2(b). We convert IR luminosities to SFRs following the prescription of Kennicutt (1998b). BJ regression, applied to the data in Figure 2(b), returns a very similar logarithmic slope as for the correlation between $L'_{\rm CO}$ and $L_{\rm IR}$ due to the relatively narrow range of metallicities spanned by our low- and high-z data:

$$\log\left(\frac{M_{\rm mol.}}{M_\odot}\right) = \alpha_{2,\,\rm SFR} + \beta_2 \log\left(\frac{\rm SFR}{{M_\odot}/{\rm yr}}\right) \ , \quad \text{with} \qquad (4)$$

$$(\alpha_{2,\,\rm SFR}; \beta_2) = \begin{cases} (9.22{\pm}0.02; 0.81{\pm}0.03) \text{ for normal galaxies} \\ (8.05^{+0.29}_{-0.10}; 0.81) \text{ for strong starbursts.} \end{cases}$$

Here the line parameters for the SBs in our reference sample were derived by solving for the normalization under the assumption of an identical, slightly sub-linear slope of the correlation between SFR and $M_{\rm mol.}$ for both MS and SB galaxies. Alternatively, in units of $L_{\rm IR}$,

$$\log\left(\frac{M_{\rm mol.}}{M_\odot}\right) = \alpha_{2,\,\rm IR} + \beta_2 \log\left(\frac{L_{\rm IR}}{L_\odot}\right) \ , \quad \text{with} \qquad (5)$$

$$(\alpha_{2,\,\rm IR}; \beta_2) = \begin{cases} (1.14{\pm}0.02; 0.81{\pm}0.03) \text{ for normal galaxies} \\ (-0.03^{+0.29}_{-0.10}; 0.81) \text{ for strong starbursts.} \end{cases}$$

[13] Mannucci et al. (2010) originally were only able to study the FMR at $z \gg 0$ for massive ($M_\star/M_\odot \geq 10^{10}$) field galaxies. New work has since extended the relation to lower stellar masses (Cresci et al. 2012) and separately verified its validity in the cluster environment at $z \sim 1.4$ (Magrini et al. 2012). The FMR is generally assumed to hold over the range $0 < z < 2.5$, i.e. should apply to almost all galaxies in our reference sample. Beyond $z \sim 2.5$ conflicting evidence for constancy (e.g., Dessauges-Zavadsky et al. 2011, Richard et al. 2011, Lara-López et al. 2013, Belli et al. 2013) and evolution (e.g., Laskar et al. 2011, Sommariva et al. 2012) of the FMR has been presented.

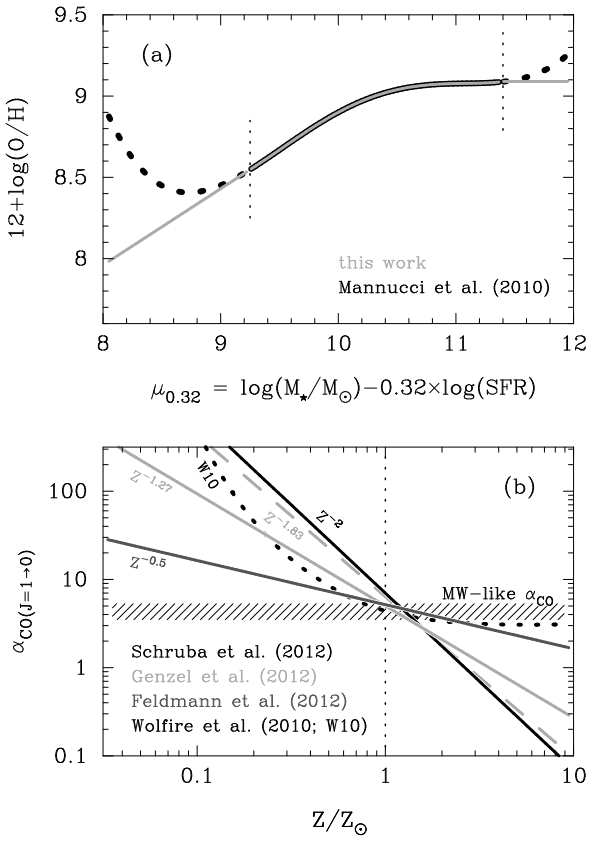

FIG. 3.—: Overview of recipes used to assign CO-to-H_2 conversion factors, α_{CO}, to observed and modeled galaxies based on their SFR and stellar mass. (*a*) Fundamental metallicity relation (FMR) as determined by Mannucci et al. (2010; *thick line section)* and continuation of the FMR assumed in our analytic-empirical modeling to regions of parameter space where the mathematical description of the plane proposed in Mannucci et al. (2010) diverges due to the absence of data. Note that the extension beyond $\mu_{0.32} \in [9.25, 11.4]$ affects only a minority of the galaxies modeled in the present work. (*b*) Recently proposed relations between metallicity (expressed in multiples of the solar metallicity $Z_\odot$ in the system of Kewley & Dopita 2002) and α_{CO} based on simulations (Feldmann et al. 2012a) or observations (Schruba et al. 2012, Genzel et al. 2012; for the latter study the fit derived for both low- and high-z SFGs (*light grey, dashed*) and that for a sample restricted to $z \geq 1$ SFGs (*light grey, solid*) is shown). The dotted line shows the shielding-based prescription of Wolfire et al. (2010) which we adopt here. All recipes predict a Milky-Way-like α_{CO} at approx. solar metallicity but diverge significantly at lower/higher enrichment due to the different measured slopes (see annotations beside trend lines).

The dispersion of the correlation is 0.20 dex and almost equal for the low- and high-z subsamples as shown in the inset panel of Figure 2(b) where we plot the Kaplan & Meier (1958) estimator for the cumulative distribution functions of the offsets $\Delta(M_{\rm mol.})$ of the individual measurements from the best-fitting trend line in Equation 4. The average offset of the reference SBs with respect to the locus for normal galaxies is $1.17^{+0.10}_{-0.29}$ dex or roughly a factor 15 in terms of SFE[14]. It should be emphasized, that this bimodality is arbitrary and merely reflects the properties of our small and incomplete selection of strong SBs. In Sect 5.1.2 we propose an empirical description of the SB population that allows for a continuous enhancement of SFE, depending on the importance of burst-induced SF activity.

[14] In this section we have used the dynamical constraints from Downes & Solomon (1998) to convert $L'_{\rm CO}$ to $M_{\rm mol.}$ for the local starbursting ULIRGs. As discussed in Section 5.3.1, the average offset from the integrated S-K law does not change for this sample when we use the α_{CO} values given by Papadopoulos et al. (2012).

3.2.3. *Robustness of Calibrated $M_{\rm mol.}$ versus SFR Relation*

The integrated S-K law for MS galaxies which we calibrated in the previous section (Equation 4) constitutes a key ingredient for the description of the gaseous component of SFGs in the 2-SFM framework. It is thus essential to ascertain that the shape of our best-fit S-K law is not strongly dependent on assumptions made during the calculation of, e.g., gas masses.

A first potential cause of systematic uncertainty is the shape of the relation between α_{CO} and metallicity discussed in Section 3.2.1. The relation of our choice (see Equation 3), which is based on the models of Wolfire et al. (2010), is equivalent to a continuously varying power law changing from an effective dependence $\alpha_{CO} \propto Z^{-1.4}$ to $Z^{-0.2}$ for metallicities $1/2 < Z/Z_\odot < 2$. This is intermediate between the observed trends that range from Z^0 (e.g., Bolatto et al. 2008) to $Z^{-2.7}$ (e.g., Israel 1997). As representative examples of these different measurements[15] we show in Figure 4(a) the SF laws that we obtain when applying the simulation-based recipe of Feldmann et al. (2012a; $\alpha_{CO} \propto Z^{-0.5}$), and those observationally determined by Genzel et al. (2012; $\alpha_{CO} \propto Z^{-1.27}$) and Schruba et al. (2012; $\alpha_{CO} \propto Z^{-2}$), to the normal galaxies in our reference sample (where we again have assigned metallicities using the FMR). We find that the slope of the different S-K laws are very similar and that their normalization only varies by 0.2 dex, such that they are all consistent within uncertainties among each other and also with our best-fit SF law as given by Equation 4. We also tested the prescription Narayanan et al. (2011) developed based on their simulations of disks and mergers. These authors parametrize α_{CO} as a function of metallicity and CO surface brightness, W_{CO}, which introduces an implicit dependence on galaxy size. Using optical size measurements from the literature[16] and the

[15] Observational studies generally parametrize α_{CO} variations as a function of an absolute value of oxygen abundance rather than relative to the solar metallicity. The inferred oxygen abundances may vary significantly depending on the metallicity calibration and abundance diagnostic used (e.g., Kewley & Ellison 2008). In addition to these systematic uncertainties concerning the normalization of the metallicity scale, transformations between metallicity systems following, e.g., the recipes in Kewley & Ellison (2008) also change the curvature of the α_{CO} versus metallicity relation. As an example, a log-linear relation between α_{CO} and metallicity derived using the R_{23} indicator (e.g., Pilyugin 2001, Kewley & Dopita 2002) may become a convex or concave function of metallicity when converted directly to a system based on the N2 diagnostic (e.g., Denicoló et al. 2002, Pettini & Pagel 2004). In view of these complications we chose to renormalize all literature determinations of the α_{CO} versus metallicity relation considered here to solar metallicity (see Figure 3(b)). In terms of oxygen abundance, solar enrichment generally corresponds to a value of $\log({\rm O/H})+12 \approx 8.7$, but this may change somewhat depending on the metallicity calibration (e.g. $\log(Z_\odot)+12 = 8.9$ in the scale of Kewley & Dopita 2002)

[16] Optical half-light radii for MS galaxies in our reference sample were derived using the following literature sources: Leroy et al. (2008, 2009) for HERACLES galaxies; Förster Schreiber et al. (2009, 2011) and Genzel et al. (2010) for SINS galaxies; Daddi et al. (2010a) for CO-detected sBzK galaxies. No size information was available for the $z \sim 0.4$-0.6 galaxies from Geach et al. (2011) and Daddi et al. (2010b), nor for galaxies in the COLD GASS sample

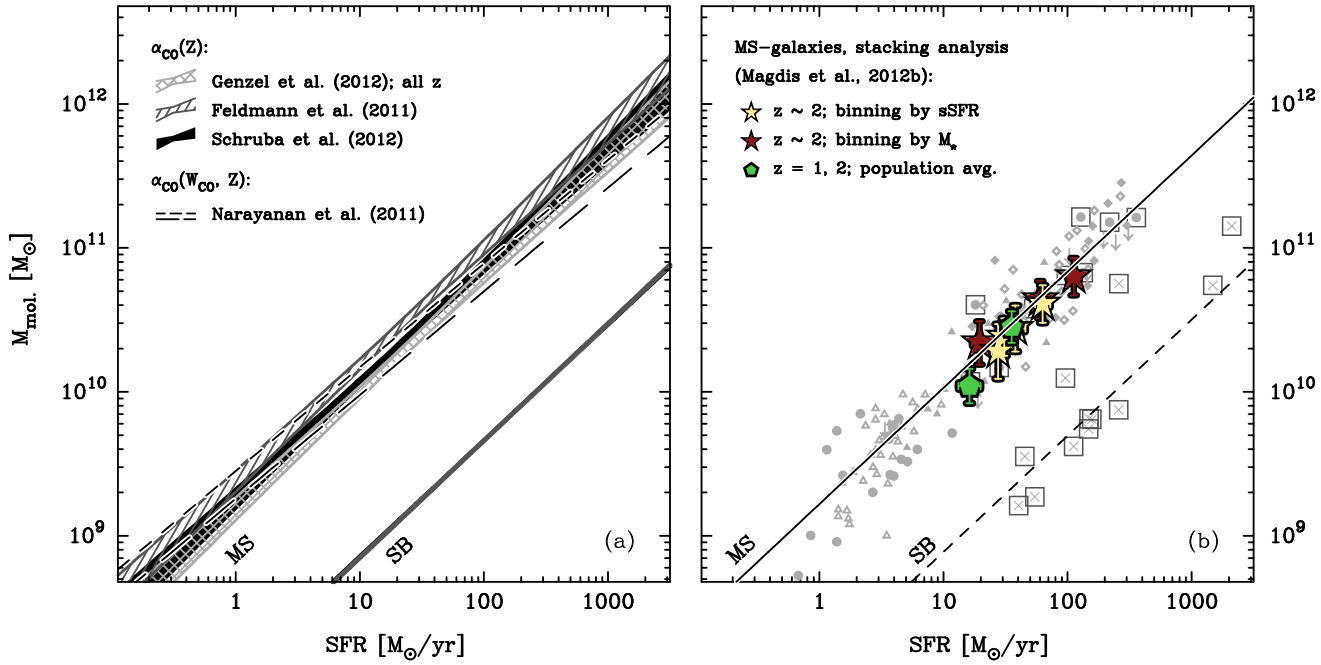

FIG. 4.—: Robustness assessment of the integrated inverse S-K relation calibrated in Figure 2 (see also Equation 4). (*a*) Changes in the best-fit S-K relation, depending on the metallicity dependence, Z^{β}, of the conversion factor, $\alpha_{\rm CO}$, reported by recent observational (Genzel et al. 2012, Schruba et al. 2012) and numerical (Narayanan et al. 2011, Feldmann et al. 2012a) work. (Filled/hatched areas encompass the 95% confidence region of the corresponding best-fit relations.) The additional dependence on the CO surface brightness, $W_{\rm CO}$, proposed by Narayanan et al. (2011) introduces an implicit dependence on galaxy size (long dashes – CO-flux averaged over optical half-light radius; short dashes – CO-flux averaged over two optical half-light radii). (*b*) Extension of high-z S-K relations to the highest SFRs ($\sim$20 $M_\odot$/yr) reached by the $z\sim0$ MS galaxies in our calibration sample. (Grey symbols in background reproduce data plotted in Figure 2.b). After inclusion of the stacked samples of $z\sim2$ MS galaxies from Magdis et al. (2012b; colored symbols), the $z\sim2$ S-K relation is sampled over two orders of magnitude in SFR. The stacked samples bridge the gap between local and $z>0$ calibration sources and are aligned with the best-fit S-K relation determined using these, thereby providing evidence of a universal S-K relation for massive MS galaxies.

CO-fluxes of our reference galaxies we calculated CO-to-H_2 conversion factors and thence molecular gas masses following Narayanan et al. (2011). Our subsequent fit to the data showed that – for reasonable assumptions about the relative spatial distribution of optical and CO emission, see Figure 4(a) – the Narayanan et al. (2011) prescription leads to a SF law that is a bit shallower than our preferred integrated S-K relation ($M_{\rm mol.}\propto{\rm SFR}^{0.72\pm0.04}$ versus ${\rm SFR}^{0.81\pm0.03}$, cf. Equation 4) but still agrees within $1.5\,\sigma$. The good general agreement between all these different recipes is due to the flatness of the mass-metallicity relation at $M_\star>10^{10}\,M_\odot$.

A second source of systematic uncertainty is our assumption that massive galaxies at all redshifts align along a single integrated S-K law relating their SFR and molecular gas mass. By combining high-redshift galaxies from the PHIBSS survey with COLD GASS data Tacconi et al. (2013) recently presented an alternative scenario of parallel and linear S-K laws that are characterized by an SFE that increases with redshift. Tacconi et al. (2013) based their gas surface mass densities on CO(J=3→2) fluxes for $z>1$ SFGs and uniformly applied a Milky-Way-like conversion factor to all sources in their sample, regardless of stellar mass, SFR, and redshift. Both the strong excitation corrections applied to the high-z SFGs that dominate the high-$\Sigma_{\rm gas}$ regime of the S-K relation and the universal $\alpha_{\rm CO}$ are in principle uncertain enough to bring about seemingly systematic shifts between the high- and low-redshift galaxy population in the S-K plane. Given the fact that there is little overlap in $L_{\rm IR}$ between our own subsamples of low- and high-redshift galaxies (see, e.g., Figure 1(b)), we cannot rule out a series of offset and conceivably also curved SF laws. By including average SFE constraints from the stacking analysis of Magdis et al. (2012b), however, it is possible to bridge the luminosity gap between $z>2$ and local SFGs, as shown in Figure 4(b). In combination with the BM/BX-selected galaxies of Tacconi et al. (2010), the $z\sim2$ S-K relation thus spans one and a half orders of magnitude and is seen to extend continuously into the parameter space of intermediate-redshift ($0.4<z<0.6$) and local disks without evidence for a discontinuity. When considering individual detections, the $0.1<z<0.4$ galaxies of Geach et al. (2009, 2011) and the EGNoG sample (Bauermeister et al. 2013a) are aligned with the $z\sim1.2$ and 1.5 sample of Tacconi et al. (2010) and Daddi et al. (2010a). Moreover, the skew and scatter around our universal S-K law are very similar for the subsets of $z\sim0$ and $z>0$ galaxies in our reference sample (see inset of Figure 2(b)). Based on these observations, we conclude that the assumption of a single, slightly sub-linear relation between SFR and $M_{\rm mol.}$ is presently a valid working hypothesis. This is also in line with recent work by Feldmann (2013) who shows that in semi-analytic models a redshift-invariant and approximately linear SF–gas relation is able to reproduce several observed galaxy properties, including gas fractions, metallicities, UV luminosity functions, and the cosmic SF history.

(Saintonge et al. 2011).

4. THE INNER WORKINGS OF THE 2-SFM FRAMEWORK: MAIN-SEQUENCE GALAXIES AND BOOSTED, STARBURSTING SOURCES

While the S-K relation we found in Section 3 for MS galaxies is very well defined, it is much less obvious which concrete form of the SF law should be used to describe the sparse and scattered SB data. Our approach to interpreting the incomplete information on these sources will be to statistically link them to a synthetic and complete SB population where we are able to relate the SB properties to the pre-starburst (MS) state. In the following we describe the "2 Star-Formation Mode" (2-SFM) framework which is the basis for establishing this link.

4.1. *Basic Ingredients and Successes of the 2-SFM Framework*

2-SFM is a simple and self-consistent scheme for the prediction of basic properties of the SFG population that relies on basic observables (e.g. the evolution of sSFR in MS galaxies or their stellar mass distribution) and uses their mathematical description (e.g., the Schechter function parameterization of the stellar mass distribution or slope and normalization of the MS) to produce an analytico-empirical description of the statistical properties of SFGs. It can be both predictive (see, e.g., the indirect measurement of the evolution of molecular gas mass functions in Paper II) or help to (re)interpret existing measurements (e.g., IR luminosity functions or source counts; see S12, Béthermin et al. 2012, Gruppioni et al. 2013).

We introduced the 2-SFM framework in S12 where we demonstrated that the observational constraints on the $z \lesssim 2.5$ IR luminosity functions can be reproduced based on only three observables: (i) the redshift evolution of the stellar mass function for SFGs, (ii) the evolution of the sSFR of MS galaxies, and (iii) a double log-normal decomposition of the sSFR distribution at fixed stellar mass into contributions (assumed redshift- and mass-invariant) from MS and SB activity. The split into (overlapping but offset) (s)SFR distributions associated with MS and SB activity is based on the distributions of sSFR published for massive ($M_\star/M_\odot > 10^{10}$) SFGs at $z \sim 2$ published by Rodighiero et al. (2011). The assumption that this double log-normal decomposition of the (s)SFR distribution is invariant with stellar mass and redshift leads to a good agreement with IR-observables (a mild decrease of the importance of the SB component by <50% between $z < 1$ and 0 leads to additional small improvements; see discussion in S12 and Béthermin et al. 2012).

The distinction between "normal" SFGs (implicitly assumed to be growing their stellar mass in a secular mode on the star-forming MS) and starbursting galaxies is central to the 2-SFM framework and of particular interest since it yields observationally verifiable predictions of the notion that SF is a bimodal process at low and high redshift. In this vein Béthermin et al. (2012) assigned a characteristic (albeit redshift-dependent; see Magdis et al. 2012b) IR SED to MS and SB galaxies and showed that this simple approach is capable of reproducing the IR/radio source counts (incl. new *Herschel* counts) at 24–1100 μm and 1.4 GHz. Given the sensitivity of the source counts, this observation evidences that the 2-SFM framework provides a valid description of the dust emission from SFGs out to at least $z \sim 4$, (i.e. over 84% of the age of the universe). The 2-SFM description of the IR-properties of SFGs has also provided testable predictions which were verified in recent work, e.g. the redshift distribution of SCUBA-2 450 μm sources (Geach et al. 2013) and the redshift distribution of lensed 1.4 mm sources detected with the South Pole Telescope (see Weiss et al. 2013; Figure 9). The good agreement of the predictions with the latter measurement suggests that the basic ingredients of the 2-SFM framework (e.g. the minor role of SBs) remain applicable out to $z \sim 6$.

4.2. *Boosting of Main-sequence Galaxies: Mathematical Description*

Encouraged by the successful reproduction of the IR properties of the SFG population we now further develop the 2-SFM framework with the primary aim of using it for a predictive analysis of the molecular gas properties of SFGs at high redshift. In preparation for this we revisit the key ingredient of the 2-SFM framework – the double log-normal decomposition of the (s)SFR distribution at fixed stellar mass. Analogously to S12 we write this (s)SFR distribution as the sum of two log-normal distribution functions $\mathcal{G}$ describing MS (MS) and starburst (SB) galaxies, respectively:

$$p(\mathrm{sSFR})|_{M_\star} = \mathcal{G}_{\mathrm{MS}}(\mathrm{sSFR}) + \mathcal{G}_{\mathrm{SB}}(\mathrm{sSFR}) \; . \qquad (6)$$

The log-normal shape of the sSFR distribution of MS galaxies, $\mathcal{G}_{\mathrm{MS}}$, is observationally established by numerous studies on independent data sets and covering different redshift ranges (e.g., Rodighiero et al. 2011, Guo et al. 2013; C. Schreiber et al., in prep.). Our assumption that the excess population of high-sSFR objects is drawn from a second log-normal distribution $\mathcal{G}_{\mathrm{SB}}$ is more uncertain, and its parameters are less well constrained (see Section 2.2 in S12). In addition to being fully consistent with observations, the main appeal of our choice of a log-normal $\mathcal{G}_{\mathrm{SB}}$ is that this implies the simplest possible relation (see also discussion at the end of Section 4.2.1 and in Section 6.1.1) between normal galaxies and SBs: SB activity is the consequence of a stochastic process that at any given time acts on only a small subset of the MS population. The natural outcome of this is a random resampling of the parent (MS) distribution, i.e. a second log-normal. Furthermore, note that with this parameterization "starburstiness" is not an all-or-nothing property, but that the *Ansatz* in Equation 6 naturally leads to a continuous spectrum of burst-bearing sources ranging from those with strongly boosted SF activity to others with only a mild enhancement (see Section 4.2.3).

4.2.1. *The Boost Function: basic properties*

Both the burst-bearing and the normal galaxy population are described by an amplitude A_{X} with units of [Mpc^{-3} dex(sSFR)$^{-1}$], a dispersion σ_{X} (units: [dex(sSFR)]) and a mode $\langle \mathrm{sSFR} \rangle_{\mathrm{X}}$ ($\mathrm{X} \in \{\mathrm{MS}, \mathrm{SB}\}$). In

particular, the MS-distribution has the functional form

$$\mathcal{G}_{\rm MS}(\mathrm{sSFR}) = A_{\rm MS}\exp\left(-\frac{[\log(\mathrm{sSFR})-\log(\langle\mathrm{sSFR}\rangle_{\rm MS})]^2}{2\sigma^2_{\rm MS}}\right)\ , \quad \text{or}$$
$$A_{\rm MS}\exp\left(-\frac{x^2}{2\sigma^2_{\rm MS}}\right) \tag{7}$$

if, for the sake of brevity, we introduce an sSFR $x \equiv \log(\mathrm{sSFR}/\langle\mathrm{sSFR}\rangle_{\rm MS})$ that is normalized to the stellar mass- and redshift-dependent average sSFR of MS galaxies, $\langle\mathrm{sSFR}\rangle_{\rm MS}$. Similarly, for starbursting sources, we write

$$\mathcal{G}_{\rm SB}(\mathrm{sSFR}) = A_{\rm SB}\exp\left(-\frac{[\log(\mathrm{sSFR})-\log(\langle\mathrm{sSFR}\rangle_{\rm SB})]^2}{2\sigma^2_{\rm SB}}\right)$$
$$A_{\rm SB}\exp\left(-\frac{[\log(\mathrm{sSFR})-\{\log(\langle\mathrm{sSFR}\rangle_{\rm MS})+B_{SB}\}]^2}{2\sigma^2_{\rm SB}}\right)$$
$$A_{\rm SB}\exp\left(-\frac{[x-B_{\rm SB}]^2}{2\sigma^2_{\rm SB}}\right)\ . \tag{8}$$

Here $B_{\rm SB}$ is the offset between the peak position of the MS and SB component of the sSFR distribution. In our interpretation it represents the average sSFR enhancement – or boost – brought about by the burst-inducing process. In the following we will assume that there is a process (to be discussed in Section 6.1) that boosts the SF activity of an (s)SFR-dependent fraction of MS galaxies with initial sSFR distribution $\mathcal{G}^0_{\rm MS}$. $\mathcal{G}^0_{\rm MS}$ is identical with the log-normal distribution in Equation 7, except for a higher normalization $A_{\rm MS} \rightarrow A^0_{\rm MS} = A_{\rm MS}\times I(\mathcal{G}_{\rm MS}+\mathcal{G}_{\rm SB}:x)/I(\mathcal{G}_{\rm MS}:x)$. (Here $I(f:x)$ stands for the integral of the function f over the range $x\in]-\infty,\infty[$.) The "boost function" describes the spectrum of perturbations that MS galaxies suffer. It is effectively a convolution kernel that transfers galaxies from the MS- to the SB-distribution:

$$\mathcal{G}_{\rm SB}(x) = (\mathcal{G}^0_{\rm MS} * \mathcal{BK})(x) = \int_{-\infty}^{\infty}\mathcal{G}^0_{\rm MS}(y)\,\mathcal{BK}(x-y)\,dy\ . \tag{9}$$

The boost function kernel ($\mathcal{BK}$) is obtained using the convolution theorem which links the Fourier transforms[17]

$$\widehat{\mathcal{G}}_{\rm SB}(k) = \widehat{\mathcal{G}}^0_{\rm MS}(k)\times\widehat{\mathcal{BK}}(k)\ , \tag{10}$$

[17] For the one-dimensional Fourier transform and its inverse we use the following convention

$$\widehat{f}(k) = \int_{-\infty}^{\infty} f(x)e^{-ikx}\,dx$$
$$f(x) = \frac{1}{2\pi}\int_{-\infty}^{\infty}\widehat{f}(k)e^{ikx}\,dk\ .$$

With this definition the Fourier transforms of the log-normal distributions for starbursting sources and the unperturbed MS become

$$\widehat{\mathcal{G}}_{\rm SB}(k) = e^{ikB_{\rm SB}}A_{\rm SB}\sqrt{2\pi}\sigma_{\rm SB}e^{-\left(\frac{\sigma_{\rm SB}k}{\sqrt{2}}\right)^2}\ , \quad \text{and}$$
$$\widehat{\mathcal{G}}^0_{\rm MS}(k) = A^0_{\rm MS}\sqrt{2\pi}\sigma_{\rm MS}e^{-\left(\frac{\sigma_{\rm MS}k}{\sqrt{2}}\right)^2}\ .$$

and by then applying the inverse Fourier transform:

$$\mathcal{BK}(x) = \frac{1}{2\pi}\int_{-\infty}^{\infty}\frac{\widehat{\mathcal{G}}_{\rm SB}(k)}{\widehat{\mathcal{G}}^0_{\rm MS}(k)}e^{ikx}\,dk\ . \tag{11}$$

Equations 10 and 11 will not always have an analytical solution. In the present case however, since both parent and resultant distribution – $\mathcal{G}^0_{\rm MS}$ and $\mathcal{G}_{\rm SB}$, resp. – are log-normal, the boost function kernel also has this functional form:

$$\mathcal{BK}(x) \equiv \mathcal{G}_{\rm BK}(x) = C_{\rm BK}\exp\left(-\frac{[x-\langle x\rangle_{\rm BK}]^2}{2\sigma^2_{\rm BK}}\right)\ . \tag{12}$$

By explicitly solving Equation 9, the three free parameters of the boost function in Equation 12 are found to be

$$C_{\rm BK} = \frac{A_{\rm SB}\sigma_{\rm SB}}{A^0_{\rm MS}\sigma_{\rm MS}}\frac{1}{\sqrt{2\pi}\sigma_{\rm BK}}\ , \quad \text{with}$$
$$\sigma_{\rm BK} = \sqrt{\sigma^2_{\rm SB}-\sigma^2_{\rm MS}}\ , \quad \text{and} \tag{13}$$
$$\langle x\rangle_{\rm BK} = B_{\rm SB}\ .$$

The shape of the boost function with free parameters given by expressions 13 is shown as a solid red line in Figure 5 and compared to distributions of SFR enhancements reported for simulated and observed interacting galaxies.

When writing down Equation 9 we implicitly assume that a statistical link exists between the MS population and high-sSFR outliers. Such a link is expected on the grounds that SBs are transient events, meaning that these galaxies must be drawn from the larger population of active (normal) SFGs. Defining a boost kernel which is independent of an initial distribution of SF activity would hence necessarily involve some arbitrary assumptions. The model we propose here is thus as simple a scenario as one can imagine. It is important to realize that we did not choose the shape of the boost kernel $\mathcal{BK}$ *a priori*. It is the consequence of the fact that the cross-section of the MS has a log-normal shape and that the high-SFR tail can be modelled well by the addition of a second, shifted log-normal distribution as shown in S12. It is natural to expect that the process which statistically/physically links starbursting and normal galaxies is galaxy interactions and merging. In Section 6.1 we discuss in detail whether theory or observations can provide supporting evidence for such a straightforward connection. To summarize, some properties of the 2-SFM boost function are suggestively reminiscent of SFR enhancements in observations and simulations. Other aspects do not conform to the expectations of what a realistic boost distribution should look like if it accounts for, e.g., minor interactions, interactions including passive galaxies and the fact that an observational snapshot of the SB population will catch different objects in different phases of the burst. This difference, however, could be entirely due to the impossibility of statistically distinguishing between normal and only weakly starbursting galaxies in a direct fit to the sSFR distribution; the conventional view that SBs are often tied to galaxy interactions hence remains a viable scenario and we now consider a modification to the boost function that we expect to apply for the idealized case that all SB events are triggered by merging.

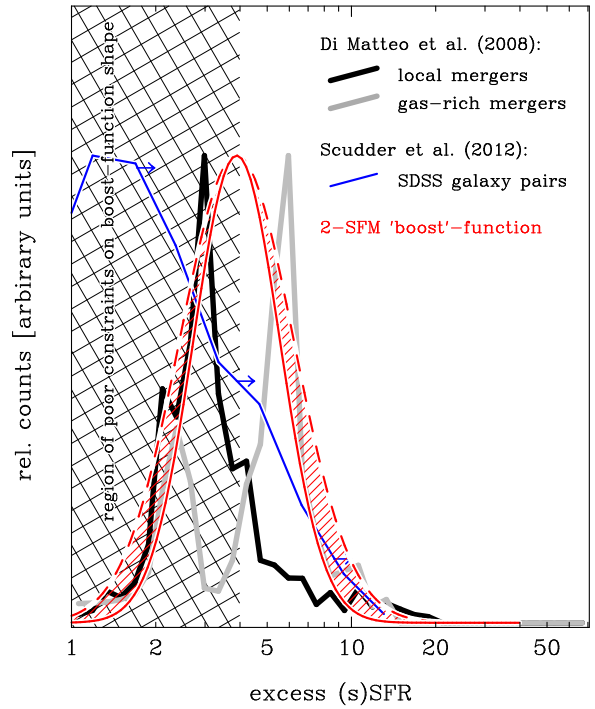

FIG. 5.—: Comparison of the 2-SFM boost function (i.e., the spectrum of (s)SFR-perturbations that move normal galaxies off the MS and into a SB state) with measured and simulated distributions of SFR enhancements induced by galaxy interactions. Red (solid) – "direct" boost function; red (dashes) – boost function including explicit correction for merger statistics (see Section 4.2.2). In the cross-hatched area the shape of the 2-SFM boost function is not known accurately (see discussion in Section 6.1). The distribution of SFR enhancements in massive ($M_\star > 10^{10}\,M_\odot$) members of $z \in [0.02,0.15]$ SDSS galaxy pairs measured by Scudder et al. (2012; blue line) does not include mergers that have already undergone final coalescence and hence represents a lower observational limit to the total local SFR excess distribution caused by interactions. Black and light grey lines – average of peak boosts (relative to isolated galaxies) measured in SPH and grid-based N-body simulations (cf. Di Matteo et al. 2008) of local mergers and gas-rich mergers with gas fraction similar to those of $z \sim 2$ MS galaxies.

4.2.2. *Statistical Correction for Paired, Ante-merger Galaxies*

In our presentation of the 2-SFM boost function we have so far skipped issues that would complicate an immediate interpretation that is based purely on a mathematical description of the problem. A first and strong simplifying assumption is that the boost function is mass- and redshift-independent. However, as discussed in S12 and Béthermin et al. (2012), current observations so far are consistent with this hypothesis. The sSFR distributions of MS galaxies and starbursting sources are snapshots that provide no direct information on the time scale over which SF in MS galaxies is boosted (and over which they, possibly having undergone a merger, later fall back onto the relation or drop below it). The relative redshift-independence of the boost function that is suggested by observations implies that the flux of galaxies into and out of the SB component of the double log-normal distribution also should not evolve strongly with redshift. If the SFR enhancements were always the result of galaxy merging, then this would motivate a modification to the boost function. We regard each pair of merging galaxies as a single system that is composed of two MS galaxies. Because the parent sSFR distribution $\mathcal{G}_{\rm MS}(\rm sSFR)$ is by assumption independent of mass and symmetric, both galaxies involved are drawn from the same distribution and their average SFR will follow a log-normal function that is centered on the same sSFR as the original distribution $\mathcal{G}_{\rm MS}(\rm sSFR)$ but narrowed by a factor $\sqrt{2}$. For the boost function this implies a broader distribution of SFR enhancements while the peak location of the boost spectrum remains identical (see also distribution plotted with a dashed red line in Figure 5):

$$\begin{aligned} \sigma_{\rm BK} &= \sqrt{\sigma_{\rm SB}^2 - \left(\sigma_{\rm MS}/\sqrt{2}\right)^2}\,, \quad \text{and} \\ \langle x\rangle_{\rm BK} &= B_{\rm SB} \qquad\qquad\quad , \quad \text{such that} \\ C_{\rm BK} &= \frac{A_{\rm SB}\sigma_{\rm SB}}{A^0_{\rm MS}\sigma_{\rm MS}}\,\frac{1}{\sqrt{2\pi}\sigma_{\rm BK}}\,. \end{aligned} \tag{14}$$

In the following we will refer to this version of the boost function as "boost function including an explicit correction for mergers" (as opposed to the boost function described by Equations 13 and henceforth called: "direct boost function"). The principle findings of this paper are valid irrespective of the choice of boost function, but for the sake of legibility we will only show results obtained with the direct boost function where plotting both alternatives would reduce rather than improve clarity.

4.2.3. *The Continuously Varying Boost Distribution*

As previously mentioned, the "typical" sSFR increase $B_{\rm SB}$ of starbursting sources is approx. a factor of four, but the average boost varies as a function of (s)SFR, as does the (relative) number of sources undergoing burst-like activity. For example, a source with measured sSFR twice as large as the (redshift- and stellar-mass-dependent) MS average could either display this excess simply due to a larger than average gas fraction and without having suffered any triggering, it could have experienced a modest boost, or – with a lesser probability – it could initially have been a gas-poor, low-(s)SFR outlier to the MS which has been strongly boosted. In the following we quantify these variations that are a consequence of the convolution in Equation 9.
To find the "typical" boost of burst-bearing sources at a given $\rm sSFR_0$ (or $\log(\rm sSFR_0/\langle sSFR\rangle_{MS}) = x_0$) we consider the integrand in Equation 9,

$$\mathcal{G}^0_{\rm MS}(x)\,\mathcal{G}_{\rm BK}(x_0 - x) = \mathcal{G}^0_{\rm MS}(x_0 - b_{\rm sSFR})\,\mathcal{G}_{\rm BK}(b_{\rm sSFR})\,. \tag{15}$$

Here we introduced a variable for the logarithmic boost, $b_{\rm sSFR} = x_0 - x \equiv \log(\rm sSFR_0/sSFR)$, in order to be able to directly locate the peak of the boost distribution, $b^{\rm max}_{\rm sSFR}$, by solving the minimization problem:

$$\frac{\partial}{\partial b_{\rm sSFR}}\left\{\mathcal{G}^0_{\rm MS}(x_0 - b_{\rm sSFR})\,\mathcal{G}_{\rm BK}(b_{\rm sSFR})\right\} \doteq 0\,. \tag{16}$$

Given the properties of the exponential function this is equivalent to requiring

$$\frac{\partial}{\partial b_{\rm sSFR}}\left\{\frac{-\left(x_0 - b_{\rm sSFR}\right)^2}{2\sigma^2_{\rm MS}}\right\} + \frac{\partial}{\partial b_{\rm sSFR}}\left\{\frac{-\left(b_{\rm sSFR} - B_{\rm SB}\right)^2}{2\sigma^2_{\rm BK}}\right\} \doteq 0\,, \tag{17}$$

an equation which has the solution

$$b^{\rm max}_{\rm sSFR} = \frac{B_{\rm SB} + x_0\left(\sigma_{\rm BK}/\sigma_{\rm MS}\right)^2}{1 + \left(\sigma_{\rm BK}/\sigma_{\rm MS}\right)^2}\,. \tag{18}$$

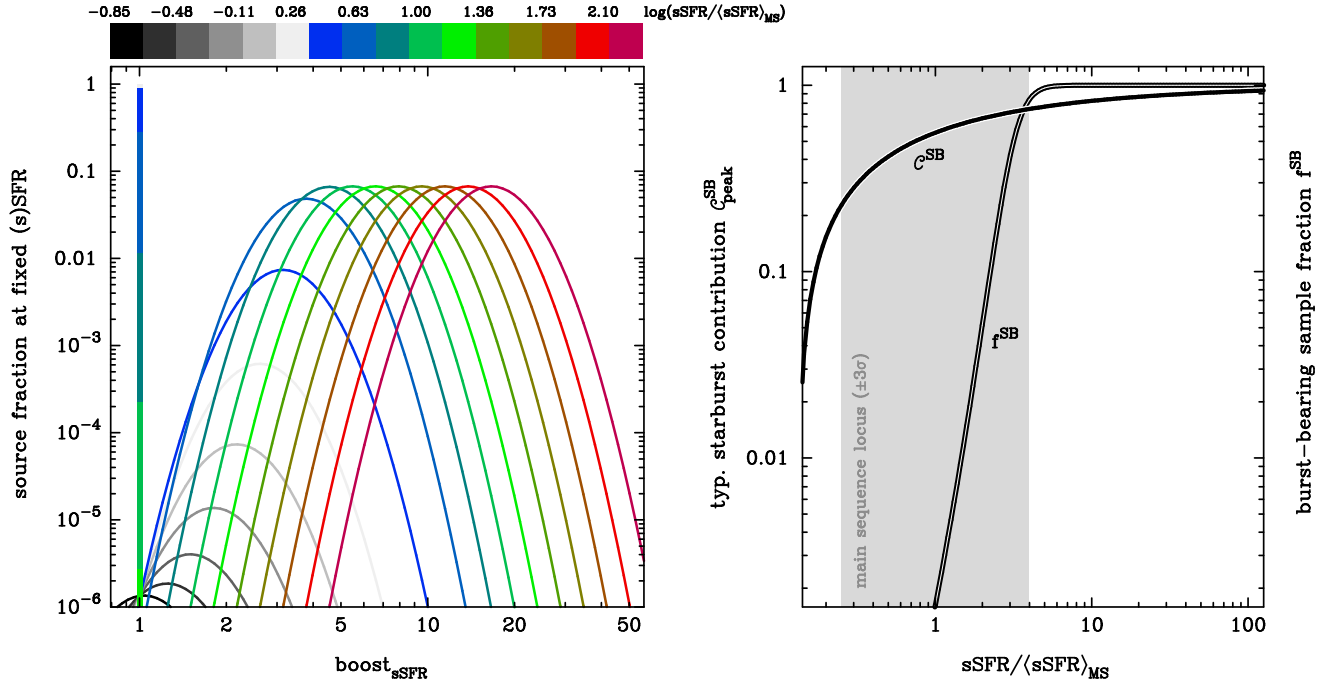

FIG. 6.—: Illustration of the properties of the continuously varying, sSFR-dependent 2-SFM boost distribution (i.e. the distribution of (s)SFR enhancements of starbursting galaxies; see Section 4.2.2). Left – log-normal distribution of boosts (see eqs. 18–20) of SFGs with a specific sSFR. All distributions are normalized to the total number of sources at a given sSFR and colors vary according to the value of sSFR, where sSFR is referenced to the MS average. For example, at $\mathrm{sSFR}/\langle\mathrm{sSFR}\rangle_{\mathrm{MS}} = 10$ the median boost is approx. seven-fold and 95% of the SB population have boosts in the range 2.5-17. Starbursts with $\mathrm{sSFR}/\langle\mathrm{sSFR}\rangle_{\mathrm{MS}} = 1/2$, on the other hand, have on average experienced weak boosting by only approx. 30% and 95% of such systems have boosts that are smaller than a factor three. The relative number of secularly evolving galaxies (plotted at boost = 1 with a bar of appropriate height) and of boosted sources is given by the burst-bearing fraction f^{SB}. Right – variation of the starbursting fraction f^{SB} with normalized sSFR, compared to the evolution of the typical fractional contribution, $\mathcal{C}^{\mathrm{SB}}$, of the burst-induced activity to the total SFR of boosted sources at a given sSFR. (Here 'typical fractional contribution' is defined as the contribution of a source located at the sSFR-dependent peak of the boost distribution.) Directly on the MS locus ($\mathrm{sSFR}/\langle\mathrm{sSFR}\rangle_{\mathrm{MS}} = 1$) starbursting sources are rare ($\mathrm{f}^{\mathrm{SB}} < 2‰$) but in those systems that have experienced boosting the contribution of the burst-activity to the total SFR is significant ($\mathcal{C}^{\mathrm{SB}} \sim 47\%$). At an sSFR excess of $\mathrm{sSFR}/\langle\mathrm{sSFR}\rangle_{\mathrm{MS}} \simeq 3$, above which SBs are more numerous than normal galaxies ($\mathrm{f}^{\mathrm{SB}} \geq 0.5$), the SB contribution to the total SFR of boosted sources is already clearly dominant ($\mathcal{C}^{\mathrm{SB}} \sim 71\%$). These numbers are based on the "direct" boost function that uses the best-fit parameters of the double log-normal sSFR decomposition in S12 (see also Equation 6 in this paper).

To determine the shape of the boost spectrum which peaks at $b^{\mathrm{max}}_{\mathrm{sSFR}}$ we consider the product of the two Gaussians in Equation 15

$$\mathcal{G}^0_{\mathrm{MS}}(x_0 - b_{\mathrm{sSFR}})\,\mathcal{G}_{\mathrm{BK}}(b_{\mathrm{sSFR}}) = \qquad (19)$$
$$A^0_{\mathrm{MS}}\,C_{\mathrm{BK}}\exp\left(-\left\{\frac{[x_0 - b_{\mathrm{sSFR}}]^2}{2\sigma^2_{\mathrm{MS}}} + \frac{[b_{\mathrm{sSFR}} - B_{\mathrm{SB}}]^2}{2\sigma^2_{\mathrm{BK}}}\right\}\right)$$

and examine the exponent

$$\frac{[x_0 - b_{\mathrm{sSFR}}]^2}{2\sigma^2_{\mathrm{MS}}} + \frac{[b_{\mathrm{sSFR}} - B_{\mathrm{SB}}]^2}{2\sigma^2_{\mathrm{BK}}}$$

which can be re-written as

$$\frac{1}{2\frac{(\sigma_{\mathrm{MS}}\sigma_{\mathrm{BK}})^2}{\sigma^2_{\mathrm{MS}}+\sigma^2_{\mathrm{BK}}}}\left\{b^2_{\mathrm{sSFR}} - 2\,\frac{x_0\sigma^2_{\mathrm{BK}} + B_{\mathrm{SB}}\sigma^2_{\mathrm{MS}}}{\sigma^2_{\mathrm{MS}} + \sigma^2_{\mathrm{BK}}}\,b_{\mathrm{sSFR}} + ...\right.$$
$$\left. ... + \frac{x_0^2\sigma^2_{\mathrm{BK}} + B^2_{\mathrm{SB}}\sigma^2_{\mathrm{MS}}}{\sigma^2_{\mathrm{MS}} + \sigma^2_{\mathrm{BK}}}\right\}. \qquad (20)$$

This is again a quadratic form, implying that the boosts at fixed normalized sSFR x_0 are distributed log-normally with a width $\sigma_b = \sqrt{(\sigma_{\mathrm{MS}}\sigma_{\mathrm{BK}})^2/(\sigma^2_{\mathrm{MS}} + \sigma^2_{\mathrm{BK}})}$ that is independent of sSFR.

On the left-hand side of Figure 6 we visualize with different colors the changes in the boost distribution for sSFRs ranging from ∼0.1 to two hundred times the characteristic MS value, $\langle\mathrm{sSFR}\rangle_{\mathrm{MS}}$. Note that the sSFR variations take place within a given bin of stellar mass and that the integral over the boost distributions at all sSFRs would give a total boost-distribution that is equal to the boost function plotted with the red solid line in Figure 5. This is not immediately obvious based on Figure 6 where we have scaled all sSFR-dependent boost distributions such that they give the fraction of sources with boost b_{sSFR} in a specific sSFR bin. This representation highlights the evolution of the fraction f^{SB} of starbursting sources (given by the ratio of the two log-normal curves in Equation 6; see also Figure 6, right) with sSFR while simultaneously compensating for the variation of the total number of sources across the width of the MS. The amplitude of the log-normal boost distributions thus grows until $\mathrm{sSFR}/\langle\mathrm{sSFR}\rangle_{\mathrm{MS}} \simeq 8$ where the number of MS galaxies becomes insignificant with respect to the number of starbursting sources (see also flattening of the evolution of f^{SB} in the right-hand panel of Figure 6).

An alternative quantity which traces the increasing importance of SB activity at successively

higher sSFRs is the typical fractional contribution, $\mathcal{C}^{\rm SB} = ({\rm SFR} - {\rm SFR}_{\rm MS,\,init.})/{\rm SFR} = 1 - 10^{-b_{\rm sSFR}}$, of the burst-induced activity to the total SFR of boosted sources. (Here $\rm SFR_{MS,\,init.}$ is the SFR of the galaxy in the MS state prior to boosting.) $\mathcal{C}^{\rm SB}$ is complementary to the starbursting fraction of the population, $\rm f^{SB}$, in that it describes the impact of the boost on an individual galaxy, while $\rm f^{SB}$ provides the number of galaxies of a given sSFR within the 2-SFM framework that are subject to such boosting. The relative variation of these two quantities is compared in the right-hand panel of Figure 6.

While the 2-SFM boost kernel has the effect of increasing the star-formation activity for the vast majority of the objects affected, its lower tail formally allows for "negative" boosts (boost < 1; i.e. suppression of star formation activity). This only occurs for a tiny fraction of <0.1‰ and 2‰ of the SFG population for the direct and merger-corrected boost function, respectively. Our illustration of the sSFR dependence (see color scale) of boost distributions in the left-hand panel of Figure 6 shows that the mode of these distributions is located at positive boosts at all normalized $\rm sSFR/\langle sSFR\rangle_{MS} \gtrsim 0.1$. Below this sSFR (which lies about 4-5 $\sigma_{\rm MS}$ below the average MS locus) a majority of boost-bearing sources experience a suppression of activity. The exact location of this transition is a somewhat arbitrary mathematical consequence of our choice to describe the boosting-process with a log-normal kernel (but see final paragraph of Section 4.2.1 for why this is a reasonable *Ansatz*). From the observational perspective, however, this arbitrariness and the details of the boost demographics in general on and below the MS locus are inconsequential because (a) the number of boosted galaxies is negligibly small compared to the dominant MS population in this regime ($\rm f^{SB} \ll 10\%$ over much of the MS, cf. right-hand panel of Figure 6) and (b) it is exceedingly hard to distinguish a galaxy with a small boost from a normal MS galaxy. For example, the rare, burst-bearing sources at the lower envelope of the MS typically are predicted to have small SFR enhancements (e.g. by 30% at -2 $\sigma_{\rm MS}$). At an identical positive offset from the MS locus (+2 $\sigma_{\rm MS}$), typical SFR enhancements by about a factor three[18] are expected. This ambiguity between normal MS galaxies and modest SBs reflects that fact that the lower half of our boost kernel is not well constrained by observations, as highlighted by the hatched area in Figure 5. The strengths of the 2-SFM approach thus lie in describing the properties of high-activity outliers rather than characterizing objects that are in practice indistinguishable from normal SFGs.

5. RESULTS

In the following we will show how a simpler understanding of the molecular gas properties of SFGs at all redshifts $z < 3$ emerges when variations of, e.g. SFE or gas fraction, about the typical value of MS galaxies are considered. To be able to establish such normalized trends requires a reliable prescription for the evolution of slope and normalization of the star-forming MS with redshift. In Appendix A we parametrize the evolution of sSFR for MS galaxies as a smoothly varying function of redshift and stellar mass (see Equation A1) which we fit to a compilation of sSFR-data from the literature. We find that on average a sSFR versus $M_\star$ relation $\rm sSFR \propto M_\star^\nu$ with exponent $\nu \simeq$ -0.2 reproduces the systematic shift between the sSFR evolution of galaxies in different mass bins out to $z \sim 3$. The extrapolation of the sSFR evolution to higher redshift (as briefly proposed for the discussion of gas fraction evolution in Section 5.2.2) is speculative, since constraints on the shape of the MS at $z > 3$ are much sparser.

We begin this section with our new description of SFE-variations between normal and starbursting galaxies (Section 5.1) and then discuss gas fractions variations and evolution plus empirical recipes for the CO-to-H_2 conversion factor (Sections 5.2 and 5.3, resp.).

5.1. *Simple Recipes for Star Formation Efficiency in Massive Star-forming Galaxies*

5.1.1. *Star Formation Efficiency in Normal and Starbursting Galaxies: Observations*

The non-linearity of the integrated S-K law found in Section 3.2.2 implies a residual dependence of the gas depletion time, $\tau_{\rm dep.} = M_{\rm mol.}/{\rm SFR}$, and its inverse, the SFE, on SFR. Using our fit for MS galaxies from Equation 4 we obtain

$$\log\left(\frac{\tau_{\rm dep.}}{\rm Gyr}\right) = (\alpha_{2,\,\rm SFR} - 9) + (\beta_2 - 1)\log\left(\frac{\rm SFR}{M_\odot/{\rm yr}}\right) \qquad (21)$$
$$= 0.22(\pm 0.02) - 0.19(\pm 0.03) \times \log\left(\frac{\rm SFR}{M_\odot/{\rm yr}}\right)$$

and

$$\log\left(\frac{\rm SFE}{\rm Gyr^{-1}}\right) = (1 - \beta_2)\log\left(\frac{\rm SFR}{M_\odot/{\rm yr}}\right) - (\alpha_{2,\,\rm SFR} - 9) \qquad (22)$$
$$= 0.19(\pm 0.03) \times \log\left(\frac{\rm SFR}{M_\odot/{\rm yr}}\right) - 0.22(\pm 0.02)\ .$$

The dispersion about this characteristic value is ∼0.2 dex (see Section 3.2). Figure 7 illustrates how the galaxies from our reference sample (see Section 2.1) and the stacked samples of Magdis et al. (2012b) scatter around this average trend which – due to the general redshift evolution of sSFR in SFGs – implies a roughly two-fold decrease of $\tau_{\rm dep.}$ between $z \sim 0$ and $z \sim 2$ for galaxies of $M_\star/M_\odot = 4\times10^{10}$, which contribute most to the cosmic SFRD over this period (Cowie & Barger 2008, Gilbank et al. 2011, Karim et al. 2011). The variation between the depletion times of 1-2 Gyr in local spiral galaxies (e.g., Leroy et al. 2008, Bigiel et al. 2011) and the approx. 0.5-1 Gyr determined for BM/BX- and BzK-selected galaxies at $1.5 < z < 2.5$ (e.g., Daddi et al. 2010b, Tacconi et al. 2013) is much smaller than the difference between normal galaxies and strong SBs (see Figure 1(d) and offset, dashed locus in Figure 7).

We attempt to correct for the implicit redshift dependence of SFE by considering a renormalized efficiency (see Figure 1(e)). For each galaxy in our reference sample the normalization constant, $\langle{\rm SFE}\rangle_{\rm MS}$, is the SFE that a galaxy of equal gas mass would have if it lay directly on the inverse S-K relation given by Equation 4. In Figure

[18] These numbers are for the boost function including the explicit correction for merger statistics. For the direct boost function the typical boost $b^{\rm max}_{\rm sSFR}$ varies more slowly across the MS (see Equation 18 and Figure 9).

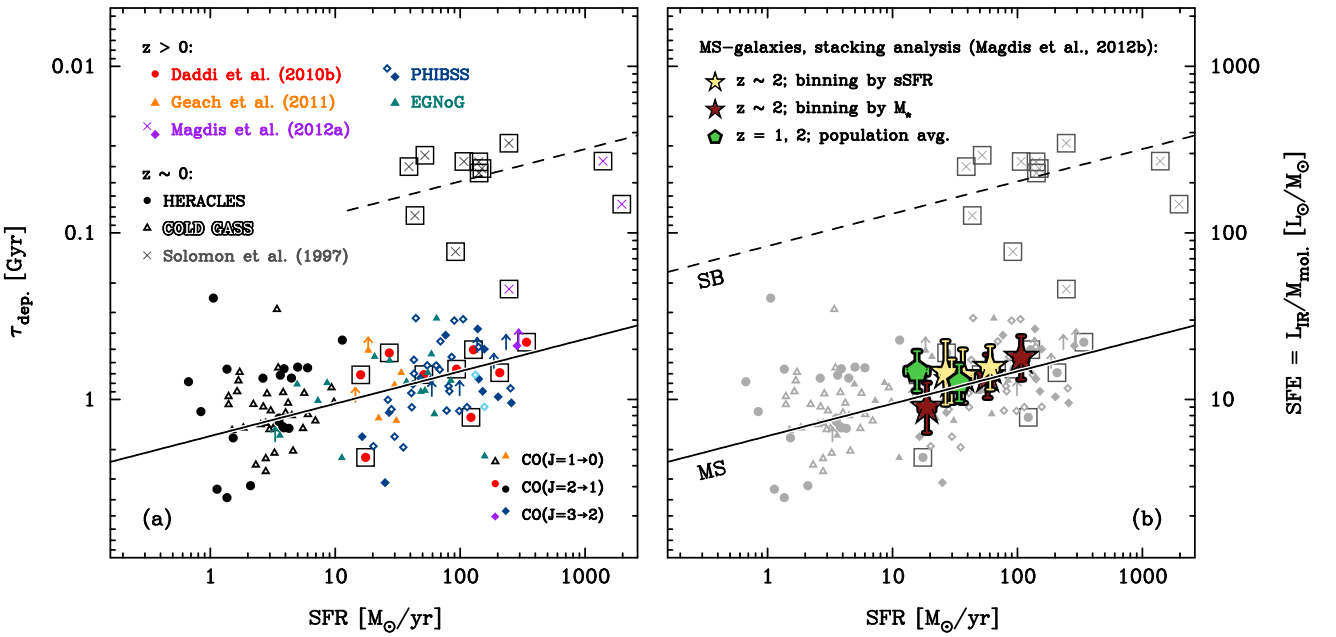

FIG. 7.—: Dependence of SFE (see scale on right) and gas depletion time $\tau_{\rm dep.}$ (scale on left) on SFR for individual galaxies in our calibration sample (panel *a*) and for stacked galaxies from Magdis et al. (2012b; panel *b*). (All data and symbols as in Figure 2.b and 4.b).

8 we then plot the normalized SFE/$\langle$SFE$\rangle_{\rm MS}$ as a function of the normalized sSFR, sSFR/$\langle$sSFR$\rangle_{\rm MS}$, which in the 2-SFM framework is a good measure of starburstiness. The stellar mass- and redshift-dependent MS average $\langle$sSFR$\rangle_{\rm MS}$ is calculated according to Equation A1. With this choice for the representation of the data, MS galaxies occupy the same region of parameter space regardless of their redshift. Our small reference sample of SB galaxies, on the other hand, is clearly offset from the MS population in the plane of normalized SFE and sFSR. Note that we assign statistically estimated CO-to-H_2 conversion factors based on a $M_\star$- and SFR-dependent metallicity $Z(\mathrm{SFR}, \mathrm{M}_\star)$ to the majority of the normal galaxies in our reference sample, but that $\alpha_{\rm CO}$ has been directly measured for our subsample of starbursting galaxies. While the scatter of the normal galaxies about the MS average $\langle$SFE$\rangle_{\rm MS}$ is thus model-dependent, the strong SFE excess found for SBs is not an artefact of, e.g., assuming *a priori* Milky-Way- and ULIRG-like conversion factors for MS galaxies and SBs, respectively. Figure 8 shows that the sSFR and SFE excess of the strongest SBs in the sample are of a similar order of magnitude. This suggests that there is some kind of link between the SFR enhancement (or "boost" in the terminology of Section 4) and the increased SFE that SBs display. The empirical calibration of this relation is the topic of the next section.

5.1.2. *Star Formation Efficiency in Normal and Starbursting Galaxies: the 2-SFM Description*

Stellar mass and SFR are fundamental parameters in the 2-SFM description of SFGs. The tight and apparently redshift-independent integrated Schmidt-Kennicutt law found in Section 3.2 links the SFR and gas mass of MS galaxies and hence provides a straightforward recipe to extend the 2-SFM framework to their molecular gas properties. At fixed stellar mass, in which case SFR/$\langle$SFR$\rangle_{\rm MS} \equiv$ sSFR/$\langle$sSFR$\rangle_{\rm MS}$ we can write

$$\log\left(\frac{\mathrm{SFE}}{\langle \mathrm{SFE}\rangle_{\rm MS}}\right) = (1-\beta_2) \times \log\left(\frac{\mathrm{sSFR}}{\langle \mathrm{sSFR}\rangle_{\rm MS}}\right) \qquad (23)$$

for the relation between normalized SFEs and sSFRs. This slow variation across the spread of the MS with $\mathrm{SFE} \propto \mathrm{sSFR}^{0.19\pm0.03}$ is superimposed on the data in Figure 8(b).
The 2-SFM framework distinguishes between MS galaxies and starbursting systems that support an elevated level of SF activity compared to what is assumed to be an initial, pre-burst state where such galaxies were indistinguishable from the large population of secularly evolving, normal SFGs. Having derived a prescription that links the SFE of MS galaxies to their offset from the MS in Equation 23 we now seek a similar relation for the starbursting fraction of the population. We adopt the following parameerization to describe the SFE of SBs:

$$\log\left(\frac{\mathrm{SFE}}{\mathrm{SFE}_{\rm MS,\,init.}}\right) = \gamma_{\rm SFE} \times b_{\rm sSFR} \qquad (24)$$

where $b_{\rm sSFR}$ is the logarithmic boost introduced in Equation 15 and $\mathrm{SFE}_{\rm MS,\,init.}$ is the SFE in the MS state, prior to the onset of the burst-activity. Since we refer the SFE to this initial state by definition no additional normalization constant is required in Equation 24. Observationally, the amount of boosting that the SB galaxies in our reference sample have experienced is obviously unknown. We shall thus assume that their SFR enhancements correspond to the median boost (i.e. the peak location of the boost distribution, $b^{\rm max}_{\rm sSFR}$; see Equation 18) which is expected for sources with an sSFR excess as determined for these SBs. In Section 4.2.3 we derived the boost spectrum at fixed sSFR excess (or deficit), sSFR/$\langle$sSFR$\rangle_{\rm MS}$, and calculated the shifting of its peak $b^{\rm max}_{\rm sSFR}$ with the normalized sSFR. We reproduce the average trends in Figure 9(a) for both the direct boost function and the

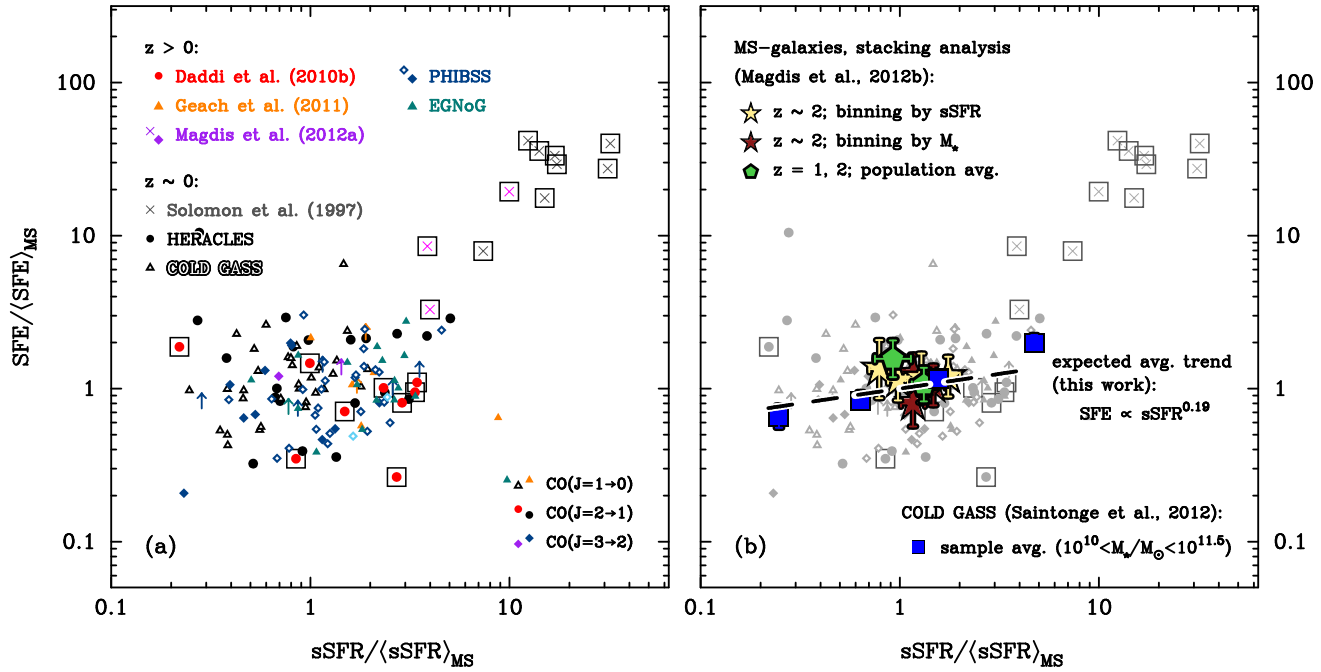

FIG. 8.—: Star formation efficiency (SFE) versus sSFR for selected main-sequence (MS) galaxies and starbursts (SBs) at $z \lesssim 3$ (*left*) and for stacked galaxies from Magdis et al. (2012b; *right)*. When normalized to the characteristic MS value, $\langle . \rangle_{\rm MS}$, a homogeneous behavior of MS galaxies at all redshifts becomes visible: SFEs vary very little within the MS while starbursting sources display enhanced SFEs that lead to their excess (s)SFR. (All data and symbols as in Figure 7. In panel (b) we also show sample SFR-averages for local COLD GASS galaxies (Saintonge et al. 2012), binned by sSFR excess.)

boost function including an explicit correction for mergers. Since the latter scenario assumes an sSFR distribution of paired, ante-merger galaxies that is narrower (see explanations in Section 4.2.2), a larger boost is required on average to reach a given sSFR excess. This fact is reflected in a steeper slope of the corresponding boost versus sSFR/$\langle$sSFR$\rangle_{\rm MS}$ relation in Figure 9(a). A conspicuous feature of this plot is the jump in average boost values at sSFR/$\langle$sSFR$\rangle_{\rm MS} \sim 3$, which is a direct consequence of the rapidly changing fraction of starbursting sources $f^{\rm SB}$ (see Figure 6, right). On the locus of the MS, most galaxies have not undergone any boosting, but at sSFR/$\langle$sSFR$\rangle_{\rm MS} > 3$ the starbursting sub-population begins to outnumber MS galaxies. This jump only occurs when the entire SFG population is taken into account. Average boost values for the starbursting subpopulation lie along the low-sSFR extension of the power-law trend at high sSFR excesses (see fine dashed lines in Figure 9(a)). In practice, burst-bearing sources with MS-like sSFRs are strongly outnumbered by normal SFGs (see Figure 6) and would in any case blend in with them because moderate SBs and "regular", secular star-formation activity are hard to tell apart. The shaded/hatched areas in Figure 9(a) indicate the uncertainty on the average relation between boost and normalized sSFR, estimated with a full accounting of the errors on (and covariance between) the parameters of the 2-SFM double log-normal decomposition of the sSFR distribution (see also Figure 1 in S12).

In Figure 9(b) we show the result of assigning representative boost values to the SBs in our sample and then fitting Equation 24. In accordance with our assumption that they experienced the median burst expected for an object with their sSFR excess, we equate SFE/$\langle$SFE$\rangle_{\rm MS}$ – the SFE normalized to the average MS value – and SFE/SFE$_{\rm MS,\,init.}$ – the SFE excess with respect to the pre-boost, MS state of each individual galaxy – for these sources. The y-axis values of the SBs in Figure 9(b) are thus identical to those in Figure 8. The x-axis values correspond to the sSFR-dependent average boost[19], which varies as shown in Figure 9(a). The associated errors span the $1\,\sigma$ range of possible average boosts resulting from the uncertainty on the sSFR measurements of the SBs. (For example, the sSFR errors of high-z GN20 and SMMJ2135-0102, which both formally lie offset from the MS by ~0.6 dex, are such that we cannot exclude that they in truth have zero SFR enhancement; this leads to their large and strongly asymmetric error bars in Figure 9(b).) We emphasize that our small reference sample of SBs does not provide sufficient statistics to justify the functional form of Equation 24. Here we simply use this data to derive the best fit given the preceding choice of a plausible parameterization; in this context, the linear relation proposed in Equation 24 is the simplest possible form that can be envisaged. The best-fitting values of the slope are $\gamma_{\rm SFE} = 1.72^{+0.17}_{-0.14}$ and 1.58 ± 0.10 for the direct and merger-corrected boost function, respectively. The quoted $1\,\sigma$ errors reflect the observational uncertainty on SFR, $M_\star$ and $M_{\rm mol.}$ (i.e. $L'_{\rm CO}$ & $\alpha_{\rm CO}$) and on the boost inferred – as plotted in Figure 9(b) for our reference SBs – but not the systematic uncertainties related to the calibration of the average sSFR and SFE of MS galaxies, nor those related to the functional form of Equation 24. It is interesting to note that Di Matteo et al. (2007) find SFE enhancements in merger simulations that exceed the

[19] As boosts between 4 and 10 have been inferred for our reference SBs, the pre-burst sSFRs of these galaxies are statistically expected to have been in the range 0.8–3 sSFR/$\langle$sSFR$\rangle_{\rm MS}$.

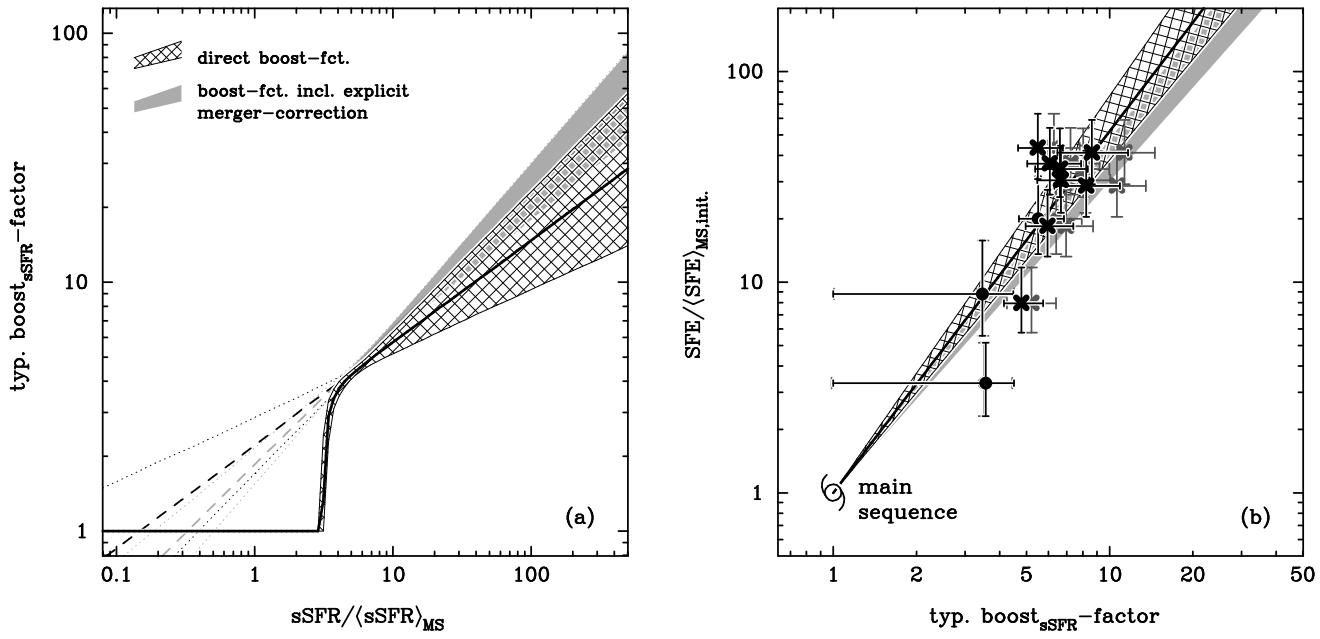

FIG. 9.—: Illustration of the two steps needed to establish a link between the star formation efficiency SFE of starbursting galaxies (normalized to the average efficiency of MS galaxies with a given H_2-mass, $\langle \mathrm{SFE} \rangle_{\rm MS}$) and their (s)SFR boost within the 2-SFM framework. (*a*) Variation of the median SFR boost of SFGs as a function of their sSFR (normalized to the $M_\star$- and redshift-dependent value of MS galaxies, $\mathrm{sSFR}/\langle \mathrm{sSFR} \rangle_{\rm MS}$). At $\mathrm{sSFR}/\langle \mathrm{sSFR} \rangle_{\rm MS} \sim 3$, where the starbursting sub-population begins to outnumber MS galaxies, the average boost rapidly rises from unity (i.e. no SFR enhancement) to values significantly larger than one. The "typical" boost of burst-bearing SFGs rises continuously after this step, in keeping with the evolution of the peak of the sSFR-dependent spectra of boosts shown in Figure 6. Two cases are considered: (1) boost function including explicit correction for merger statistics (*grey shading*, cf. Section 4.2.2), and (2) "direct" boost function (*hatched area*). The shaded/hatched areas mark the $1\,\sigma$-error on the typical boost, and were derived based on the uncertainties associated with the decomposition of the sSFR distributions of massive $z \sim 2$ SFGs into two log-normal components (for MS and starbursting galaxies, resp.; see S12 or the schematic representation in Figure 10). Bold lines at the core of the highlighted confidence regions trace the best-fit variation of the typical boost values. The formal continuation to $\mathrm{sSFR}/\langle \mathrm{sSFR} \rangle_{\rm MS} \ll 3$ of the trend line following the evolution of the typical boost of the burst-bearing sub-population only is plotted with a fine dashed line (associated uncertainties are indicated with dots). Starburst galaxies in this sSFR range are not observable in practice (see discussion in text of Section 5.1.2). (*b*) Empirical calibration of the relation between SFE enhancement and boost amplitude using a reference sample of selected SB galaxies with measured $\alpha_{\rm CO}$ (Solomon et al. 1997, Magdis et al. 2012b) and the relation between normalized sSFR and the typical boost of panel (*a*). The reference sample of SBs is located with respect to the *x*-axis using the trend lines of panel (*a*) for the 2-SFM boost function including explicit correction for merger statistics (*dark grey symbols*) and for the "direct" 2-SFM boost function (*black symbols*). (Crosses/dots are used for local/high-*z* SBs from Solomon et al. (1997) and Magdis et al. (2012b), respectively; 1 sigma-error bars plotted account for observational uncertainty on SFR, $M_\star$ and $M_{\rm mol.}$ but not systematic uncertainties, see discussion in Section 5.1.2.) The shaded/hatched areas span the 68% confidence region for a power-law relation between excess SFE and boost amplitude as parameterized in Equation 24 and passing through the MS locus highlighted schematically.

boost in SFR. The behavior of the simulations thus qualitatively matches the supra-linear relation inferred here, according to which $\mathrm{SFE}/\mathrm{SFE}_{\rm MS,\,init.} \propto (\mathrm{boost})^{\gamma_{\rm SFE}}$ with $\gamma_{\rm SFE} > 1$.

A non-linearity of this kind is virtually inevitable in order to self-consistently match the SFEs of strong SBs at the sSFR they display. If, instead, we were to describe the SFE of SBs as a linear mixing of two distinct S-K laws (one for normal galaxies and one for SBs) based on the SB contribution to the total SFR of boosted sources ($\mathcal{C}^{\rm SB}$, see Figure 6(b)), the high SFEs observed for, e.g., local ULIRGs could only be reproduced when assuming a "template" S-K law for SBs, which is offset to higher SFE than observationally seen for even the most extreme sources (cf. "strong starburst" case of Equation 4).

An immediate consequence of the inferred supra-linear relation between SFE and SFR enhancements in SB events is that the distributions of the SFG population with respect to (s)SFR and SFE are qualitatively different. (Here we consider the SFE distribution at fixed gas mass.) We illustrate this in Figure 10 for the case of the best-fitting double log-normal decomposition (eqs. 7 and 8) and SFE versus boost relation for SBs (Equation 24). While the sSFR distributions of MS galaxies and SBs blend, the two subpopulations are more strongly separated in terms of SFE. In comparison with the distribution of galaxies in the $M_{\rm mol.}$ versus SFR plane in Figure 2(b), we see that the bimodality predicted by the 2-SFM framework is less pronounced. So far, CO follow-up observations of SFGs have generally explicitly targeted either strong SBs (e.g., Solomon et al. 1997, Greve et al. 2005, Riechers et al. 2006, Ivison et al. 2011) or MS galaxies (e.g., Leroy et al. 2008, Daddi et al. 2010a, Tacconi et al. 2010, Geach et al. 2011, Magdis et al. 2012a, Tacconi et al. 2013). This selective observing strategy has thus very likely artificially deepened the expected trough between the MS and SB component in Figure 10(b) into the genuine gap that is seen in Figure 2(b). It should be clear that the detailed shape of the transition from the MS component of the SFE distribution to the offset SB component is uncertain to the same extent as we have only poor constraints on the lower part of the boost function (cf. Figure 5). However, our conclusion that the SFE distribution should be broader than the sSFR-distribution of SFGs is inevitable if the scaling between the SFE enhancement and SFR boost of SBs is

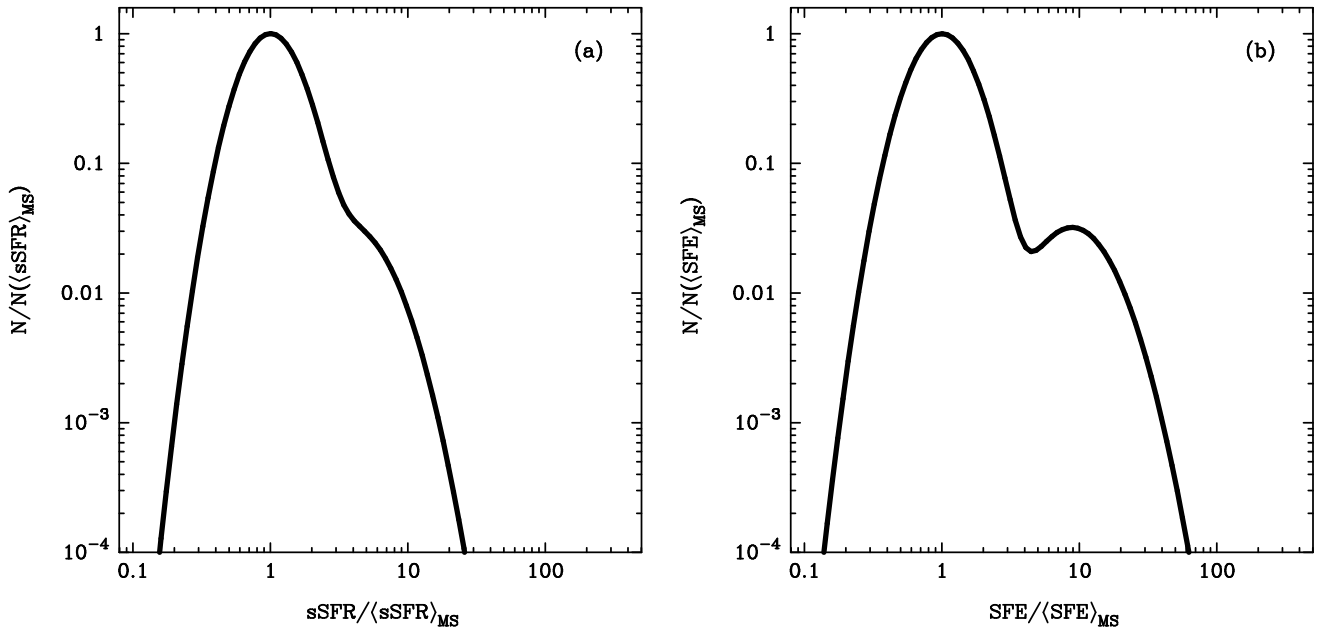

FIG. 10.—: Schematic comparison of the sSFR distribution at fixed stellar mass (*a*) with the SFE distribution at fixed molecular gas mass (*b*). The curves are representative examples, computed using the best-fit parameters of the double log-normal decomposition of the sSFR distribution (Equation 6) and of the power-law relation fitted to the dependence of SFE on boost amplitude for starbursting galaxies (Equation 24). Associated uncertainties are not shown.

supra-linear as we find here.

We now have all ingredients to provide an empirical prescription for the SFE of starbursting systems. In analogy to the expression for normal galaxies in Equation 23, we write the recipe for SBs in terms of a normalized SFE,

$$\log\left(\frac{\mathrm{SFE}}{\langle\mathrm{SFE}\rangle_{\mathrm{MS}}}\right) = \log\left(\frac{\mathrm{SFE}}{\mathrm{SFE}_{\mathrm{MS,\,init.}}}\right) + \log\left(\frac{\mathrm{SFE}_{\mathrm{MS,\,init.}}}{\langle\mathrm{SFE}\rangle_{\mathrm{MS}}}\right)$$
$$= \gamma_{\mathrm{SFE}} \times b_{\mathrm{sSFR}} + (1-\beta_2) \times \log\left(\frac{\mathrm{sSFR}_{\mathrm{MS,\,init.}}}{\langle\mathrm{sSFR}\rangle_{\mathrm{MS}}}\right) , \quad (25)$$

which is a combination of the SFE of the initial, MS state prior to boosting (second summand; see also Equation 23) and the burst-induced enhancement of this initial SFE (first summand; see also Equation 24). It is important to realize that Equation 25 stands for SFE changes in individual SBs rather than describing the sSFR dependence of the average SFE excess of the whole starbursting population. The latter trend will be discussed in the next paragraph.

By incorporating the prescriptions in Equation 23 and 25 we can predict the variation of SFE throughout the entire $M_\star$ versus SFR plane and for the entire SFG population (as opposed to individually for the subpopulation of normal galaxies and SBs). In doing so, we will again make the simplifying assumption that all recipes are independent of stellar mass, which reduces the problem to a calculation of the evolution of SFE with (s)SFR. The prediction involves several steps which we detail here in bulletized format for maximal clarity and in preparation of analogous procedures for the variation of gas fractions and α_{CO} in Sections 5.2 and 5.3, respectively:

- The hypothetical population of SFGs is distributed in $M_\star$ and SFR according to the double log-normal distribution in Equation 6.
- At each point in the $M_\star$ versus SFR plane an sSFR-dependent fraction f^{SB} of galaxies will fall into the SB category (see Figure 6, right) and hence require a different recipe for the computation of SFE than is applied to MS sources.
- For MS galaxies of a given sSFR, the SFE is computed with Equation 23.
- At each sSFR, relations 18 to 20 from Section 4.2.3 allow us to construct the spectrum of boosts b_{sSFR} and to infer the former pre-burst efficiencies, $\mathrm{SFE}_{\mathrm{MS,\,init.}}$, of the burst-bearing systems. Their SFEs then follow from Equation 25.
- A "typical" SFE – here we use the median – is calculated for the joint population of normal and starbursting galaxies. It reflects the relative importance of the two subpopulations at a given location in the $M_\star$ versus SFR plane.

Figure 11(a) shows that, beginning at the lower edge of the MS locus, the median SFE of the total SFG population initially rises slowly. Boost-bearing sources are exceedingly rare throughout most of the MS so the median, normalized SFE-value in this regime is entirely determined by the S-K relation for normal galaxies. SBs become the dominant component of the SFG population at around $3 < \mathrm{sSFR}/\langle\mathrm{sSFR}\rangle_{\mathrm{MS}} < 4$ where the global median abruptly jumps to join the trend of steadily rising SFE for the starbursting subpopulation (dotted line). The evolution of the median after this point[20] reflects the increasing boost amplitudes that are required to reach the

[20] The average SFE of starbursting systems is predicted to have a slightly sub-linear dependence on sSFR. This is the consequence of convolving the supra-linear evolution of SFE with boost amplitude (see Equation 24) with the shallow dependence of average boost amplitude on sSFR (see Figure 9).

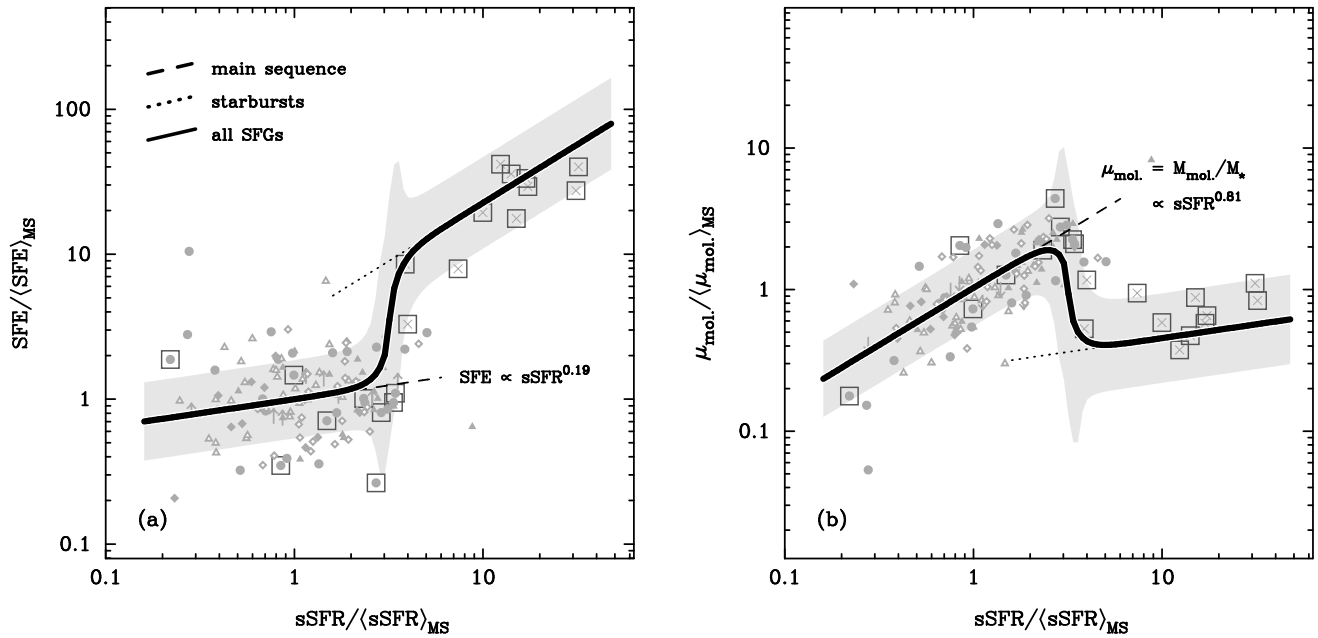

FIG. 11.—: Average variation of normalized SFE (*left*) and molecular gas mass fraction $\mu_{\rm mol.} \equiv M_{\rm mol.}/M_\star$ (*right*) with normalized sSFR, as predicted by the 2-SFM framework. Data points plotted in grey in the background are as in Figs. 8 and 12. Dashed line – expected average trend for MS galaxies (sSFR dependence as annotated adjacent to line); dotted line – expected average trend for starbursting galaxies, plotted only in the sSFR-range where SBs represent more than 10% of all SFGs ('direct' boost function assumed); solid line – average evolution for the total population of SFGs; light grey shading – expected $1\,\sigma$ scatter around average SFE variation. The scatter rises strongly over the fairly small range of sSFR where MS and starbursting galaxies occur in roughly equal numbers (see also Figure 6). The average evolution of the total population traces the variation of the median SFE ($\mu_{\rm mol.}$) of the combined SFE distribution ($\mu_{\rm mol.}$-distribution) of normal and starbursting galaxies. Its variation thus reflects the relative importance of MS and SB galaxies with offset from the MS locus $\langle {\rm sSFR}\rangle_{\rm MS}$. When normalized to the typical MS value, the predicted trends do not depend on redshift due to the simple power-law relations between SFR and molecular gas mass that are assumed in the 2-SFM framework (see Sections 5.1.2 and 5.2.1 for details).

highest sSFRs. Even though the 2-SFM framework assumes a full continuum of SFR and SFE enhancements, the changing population mix between normal and starbursting galaxies thus has lead to a "bimodal" behavior of the SFE. This general trend and the magnitude of the jump are insensitive to the details of the boost kernel mathematics because we have explicitly calibrated the relation between boost and SFE enhancement on the data (see Figure 9(b)) and because the sSFR of our reference SBs is set by observations. The exact shape of the jump hence depends on the parameters of the double log-normal decomposition and also on the SFE dispersion of MS galaxies. In plotting the average trend in Figure 11(a) we have assumed a scatter of 0.2 dex, in accordance with the measurement made on Figure 2. The scatter (indicated with light grey shading in Figure 11) abruptly increases in the transition region with its mixture of MS and SB galaxies and then at ${\rm sSFR}/\langle {\rm sSFR}\rangle_{\rm MS} \gtrsim 4$ is predicted to settle to a constant value that is somewhat larger than the 0.2 dex of the MS locus as it simultaneously reflects (a) the spectrum of initial MS states that end up at a given sSFR excess by virtue of their different SFR boosts, and (b) of the dispersion in SFEs in the pre-burst MS state. The depicted average trend also depends on the relation between SFE and boost. In Figure 11(a) we show the prediction for the case of the "direct" boost function (the SFE evolution for starbursting galaxies would steepen when using the boost function including an explicit correction for mergers) and do so only for the best-fit value of $\gamma_{\rm SFE}$. We refrain from estimating formal errors for this average trend since the systematic uncertainties (for example those pertaining to the choice of a function relating SFE excess and boost as in Equation 24) in any case strongly outweigh these.

Note that, by working with (s)SFRs that are normalized to the average MS value rather than absolute quantities, we have removed all dependence on redshift. Our prediction for the variation of SFE can thus be summarized by a single track, as shown in Figure 11(a). It is generalizable to the full range of redshifts and stellar masses by (1) multiplying (s)sSFRs by the normalization constant, $\langle {\rm sSFR}\rangle_{\rm MS}$, which is given by Equation A1, and by (2) using Equation 23 with ${\rm SFR} = M_\star \times \langle {\rm sSFR}\rangle_{\rm MS}$ to obtain the normalization, $\langle {\rm SFE}\rangle_{\rm MS}$, and thence the absolute value of SFE. While this provides a conveniently simple and flexible basis for describing SFE variations in SFGs over a large fraction of Hubble time, these trends do not represent fundamental scaling laws. Our observationally motivated purpose here is to derive the plausible variations of molecular gas-related quantities in the SFR-$M_\star$ plane, since this parameter space is an important focus of current literature, e.g., when discussing the properties of SFGs and AGN in general (e.g., Elbaz et al. 2011, Whitaker et al. 2012, Mullaney et al. 2012b, Rosario et al. 2013), and in particular also gas and dust properties (e.g., Magdis et al. 2012b, Saintonge et al. 2012, Santini et al. 2014, Magnelli et al. 2014). We do not propose that the SFE versus sSFR trends presented in this work are new laws superseding, e.g., the S-K relation. Instead, the dependence of SFE on sSFR highlighted in Figure 11 is a consequence of the different loci (see Figure 10) of "normal" and starbursting galaxies in the S-K plane

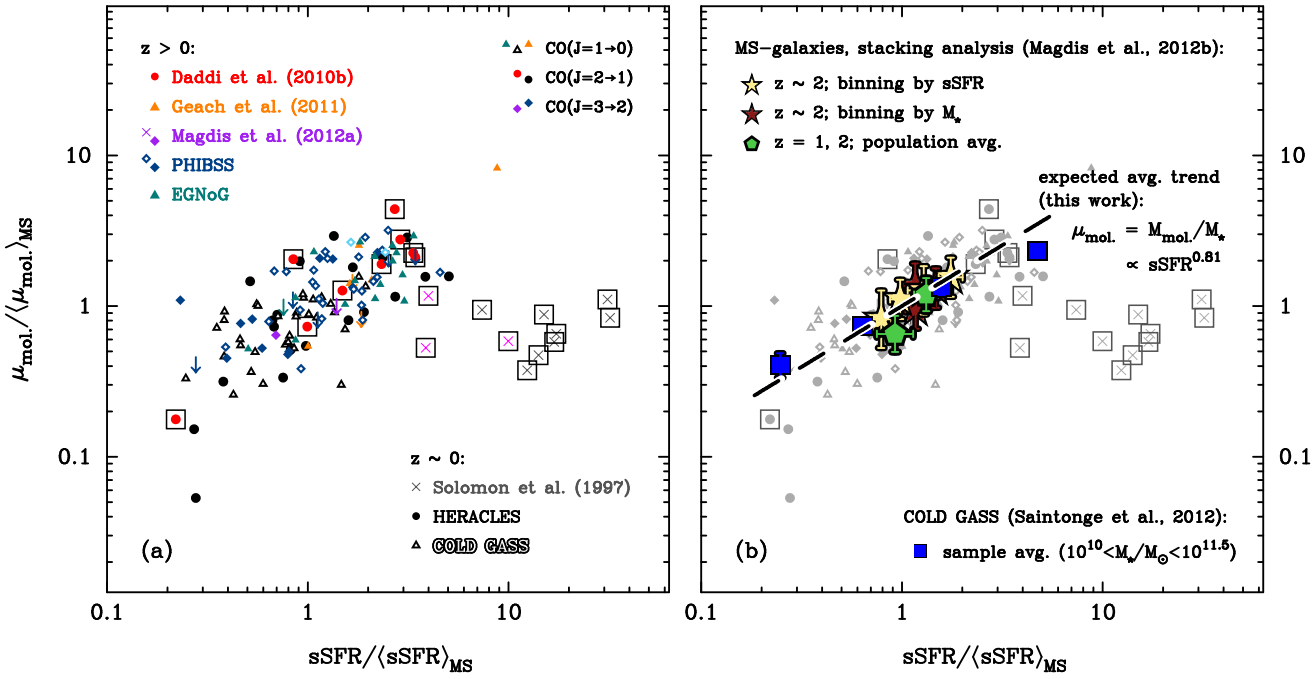

FIG. 12.—: Molecular gas mass fraction ($\mu_{\rm mol.} \equiv M_{\rm mol.}/M_\star$) versus sSFR for selected main-sequence (MS) galaxies and starbursts (SBs) at $z \lesssim 3$ (*left*), as well as for high- and low-redshift sample averages from Magdis et al. (2012b) and COLD GASS (Saintonge et al. 2012), resp. (*right*). All measurements are normalized to the $M_\star$- and redshift-dependent average of the MS and all symbols and data are identical to those used in Figure 7. At all redshifts, the gas fractions of normal galaxies rise uniformly across the MS while starbursting sources have a gas content that is somewhat lower than the MS average.

($M_{\rm mol.}$ versus SFR). The SFE trends in SFR-$M_\star$ space thus jointly reflect the balance between the relative number of starbursting ("boosted") and normal galaxies at a given $M_\star$ and SFR *and* the SFE of these two classes of galaxies.

5.2. *Molecular Gas Fractions in Star-forming Galaxies*

5.2.1. *Gas Fractions in Normal and Starbursting Galaxies*

The predictions of the previous section for the average variation of SFE in SFGs with offset from the MS locus are equivalent to a variation of the molecular gas mass $M_{\rm mol.} = \Big\{ M_\star \times {\rm sSFR}({\rm M}_\star, z) \Big\}/{\rm SFE}$. By construction, the stellar mass $M_\star$ in this expression is known in the 2-SFM approach, implying that we can directly compute the molecular gas mass to stellar mass ratio, $\mu_{\rm mol.} = M_{\rm mol.}/M_\star$, as a function of sSFR. To obtain predictions that are independent of redshift and stellar mass we again consider normalized quantities, ${\rm sSFR}/\langle {\rm sSFR} \rangle_{\rm MS}$ and $\mu_{\rm mol.}/\langle \mu_{\rm mol.} \rangle$, in Figure 11(b). The bimodal behavior of the average SFE evolution leads to two distinct regimes: (1) a nearly linear increase of the gas fraction across the MS, and (2) for strong SBs, gas fractions that vary more slowly with sSFR and are somewhat lower than the gas fraction of the average MS galaxy. (Note that as in Figure 11(a), gas fraction variations within the starbursting population are again shown for the direct boost function; using the boost function that includes the explicit correction for mergers would result in a shallower trend.) As in the case of SFE (see Figure 11(a)), the transition between these two regimes is almost step-like and characterized by a large dispersion in $\mu_{\rm mol.}$. We explore the link between gas fractions during an SB episode and prior to the onset of burst-activity in more detail in section 6.3.

We compare these expectations of the 2-SFM framework with real data in Figure 12. While our reference sample of SBs is too small to quantitatively constrain any residual variation of gas fractions at high sSFRs, the predicted rise of gas fractions across the MS is well sampled by the reference sample of normal galaxies. As discussed in Section 5.2.2, the gas fractions inferred for 90% of the MS galaxies involve an assumption about the metallicity dependence of $\alpha_{\rm CO}$. Nevertheless, they show no systematically different behavior than the eight sources (boxed symbols in Figure 12) for which measurements of $\alpha_{\rm CO}$ exist. A very similar slope (${\rm sSFR}^{0.9}$) was measured by Magdis et al. (2012b) for stacked samples of MS galaxies divided into bins of sSFR excess in which the gas mass was constrained via the far-IR dust emission. Stacking-based measurements of $\mu_{\rm mol.}$ at $z = 1$, and 2 by Magdis et al. (2012b) are shown in Figure 12(b) and found to coincide with the 2-SFM predictions and gas fractions determined on an individual basis for galaxies in our reference sample. Saintonge et al. (2012) were able to sample molecular gas mass fraction variations over a larger range in sSFR which extends to significantly below the star forming MS and also slightly into the SB regime. In their local COLD GASS data set the average $\mu_{\rm mol.}$ scales as approx. ${\rm sSFR}^{0.7}$. A significant deviation from the 2-SFM predictions for normal galaxies is only seen in their highest sSFR-bin which lies in the transition region between MS and starbursting outliers and may hence be expected to reflect the transition to the lower gas fractions in starbursting galaxies (see also the indication of an SFE increase in the COLD GASS data set at ${\rm sSFR}/\langle {\rm sSFR} \rangle_{\rm MS} = 4.5$ shown in Figure 8(b)).

5.2.2. *Gas Fraction Evolution Across Cosmic Time*

The well-defined relations between $M_\star$ and SFR, and between SFR and H_2-mass allow for a straightforward prediction of the redshift evolution of the molecular gas fraction, $f_{\rm mol.}$, in normal galaxies. Using Equation 4 we can write

$$f_{\rm mol.} \equiv \frac{M_{\rm mol.}}{M_{\rm mol.}+M_\star} = \frac{1}{1+{M_\star}/{(\rm const.\times SFR^{\beta_2})}} = \frac{1}{1+\frac{M_\star^{1-\beta_2}}{\rm const.}\times {\rm sSFR}^{-\beta_2}}\ , \quad (26)$$

where $\rm const. = 10^{\alpha_{2,\,SFR}}$. If we insert the average $\rm sSFR(\mathit{M}_\star, \mathit{z})$ of MS galaxies (parameterized as in Equation A1) into this equation we obtain an evolutionary trend, which we plot in the upper half of Figure 13 for four different stellar masses in the range $5\times10^9 < M_\star/M_\odot < 10^{11}$. The gas fractions of normal galaxies at $z \lesssim 3$ predicted in this manner are in excellent agreement with literature data based on CO line flux data, which suggests that the gas content of secularly evolving SFGs is an important driver of the cosmic sSFR evolution. Supporting evidence for this tight link between the evolution of sSFR and the gas fraction of MS galaxies was recently provided by an analysis of more than 50 SFGs at $1<z<3$ with CO-flux measurements from the PHIBSS survey in Tacconi et al. (2013; blue filled and open diamonds in our Figure 13). Combes et al. (2013), on the other hand, hold a joint redshift evolution of both SFE and gas fractions by roughly similar amounts to be responsible for the cosmic evolution of star formation activity. This apparent discrepancy can be explained by the distinctly different behaviour of normal galaxies and SBs with respect to SFE and $f_{\rm mol.}$, which we illustrate in Figure 11, and by the fact that the $0.2<z<1$ ULIRGs analyzed by Combes et al. (2011, 2013) have generally large sSFR excesses (see Figure 9 in Combes et al. 2013), while their local reference sample overlaps with the MS population. These authors hence tend to compare fairly low-efficiency $z=0$ systems with $z>0.2$ starbursting galaxies (thereby overestimating the importance of SFE for sSFR evolution) which on average have lower gas fractions than equally massive normal galaxies (leading to an underestimate of the gas fraction evolution).

The gas-to-dust ratio technique, which is more efficient than CO follow-up in terms of observing time requirements, has become increasingly popular for indirect estimation of the ISM content of high-redshift galaxies (e.g., Magdis et al. 2011, 2012b, Magnelli et al. 2012, Santini et al. 2014, Scoville et al. 2014). In the upper half of Figure 13 we have plotted the redshift evolution of gas fractions measured by Magdis et al. (2012b) and Santini et al. (2014) using this approach (see dark red stars and lines, resp.). The results from these two studies differ by a factor two, suggesting that this approach is currently still subject to systematic uncertainties. Such systematics could be caused by field-to-field variance as proposed by Santini et al. (2014) or different corrections for environmental crowding in the stacks of *Herschel* photometry that are used to determine average dust-continuum fluxes for high-z galaxy samples. The fact that metallicity estimates are central to the application of the gas-to-dust ratio technique implies that this method is also affected by the systematic offsets between different metallicity calibrations (e.g., Kewley & Ellison 2008).

The link between sSFR and gas fraction also manifests itself at fixed redshift as a variation of sSFR across the MS (see Figure 12). This is equivalent to stating that the dispersion of the MS can be at least partially ascribed to different gas fractions. In a recent morphological study of $z\sim1$ disk galaxies Salmi et al. (2012) reported that systems with clumpy substructure are found to be systematically offset to higher values of sSFR than their smoother counterparts. Since clumps are a telltale signature of violent disk instabilities in gas-rich high-redshift galaxies (e.g., Agertz et al. 2009, Ceverino et al. 2010, Förster Schreiber et al. 2011, Swinbank et al. 2011, Wuyts et al. 2012) this observation thus provides independent evidence for increasing gas fractions within the MS.

Following the publication of simulation-based recipes for the calculation of $\alpha_{\rm CO}$ by Narayanan et al. (2011), the same authors have recently questioned (Narayanan et al. 2012) the reliability of the high gas fractions reported in the literature. (Alternative predictions for $\alpha_{\rm CO}$ that make use of the observed relations between $L'_{\rm CO}$ and $L_{\rm IR}$ and SFR and H_2-mass are presented in Section 5.3.) Various additional predictions for gas fraction evolution based on numerical simulations (Davé et al. 2011, Duffy et al. 2012) or semi-analytical modeling (Fu et al. 2012, Feldmann 2013) are shown in the lower half of Figure 13. These predictions generally lie within the range of gas fractions expected in the 2-SFM framework for galaxies located on the MS, but – with the exception of the predictions in Feldmann (2013) – they show a tendency for a shallower redshift evolution of $f_{\rm mol.}$ than observed through CO-line flux measurements. Rather than being the consequence of incompatible assumptions for the calculation of $\alpha_{\rm CO}$ these differences compared to the 2-SFM predictions might reflect the well-known problem that both semi-analytical models (e.g., Fontanot et al. 2009) and cosmological hydrodynamical simulations (e.g., Weinmann et al. 2012) tend to produce too many stars too early in the history of the universe, especially in lower mass galaxies. The resulting accelerated exhaustion of gas reservoirs would then likely lead to lower gas fractions than we predict using the 2-SFM approach. Popping et al. (2012) used a similar, empirically motivated approach as the one proposed here to indirectly infer the gas content of both late- and early-type galaxies at $z<2$. Here we show the redshift evolution of $f_{\rm mol.}$ these authors derive for MS galaxies with the stellar masses plotted in Figure 13. Their expectations are in good agreement with ours at $z\lesssim1$ but begin to differ from the 2-SFM predictions at higher redshift, probably due to incompleteness in their lower-mass ($M_\star/M_\odot<10^{11}$) galaxy samples.

We end this section by plotting explicitly in Figure 14 the $M_\star$ dependence of the molecular gas fraction which was already visible in Figure 13 as a vertical offset between the evolutionary trends. Two panels with the 2-SFM predictions for $z\sim1$ and 2 are shown. In both cases the range of expected gas fractions $f_{\rm mol.} = M_{\rm mol.}/(M_\star+M_{\rm mol.})$ at fixed stellar mass can be significant, e.g., for a stellar mass of $5\times10^{10}\,M_\odot$ a $\Delta f_{\rm mol.}$ of approx. 0.5 is expected, depending on whether the source is located at a positive or negative offset of $2\,\sigma_{\rm MS}$

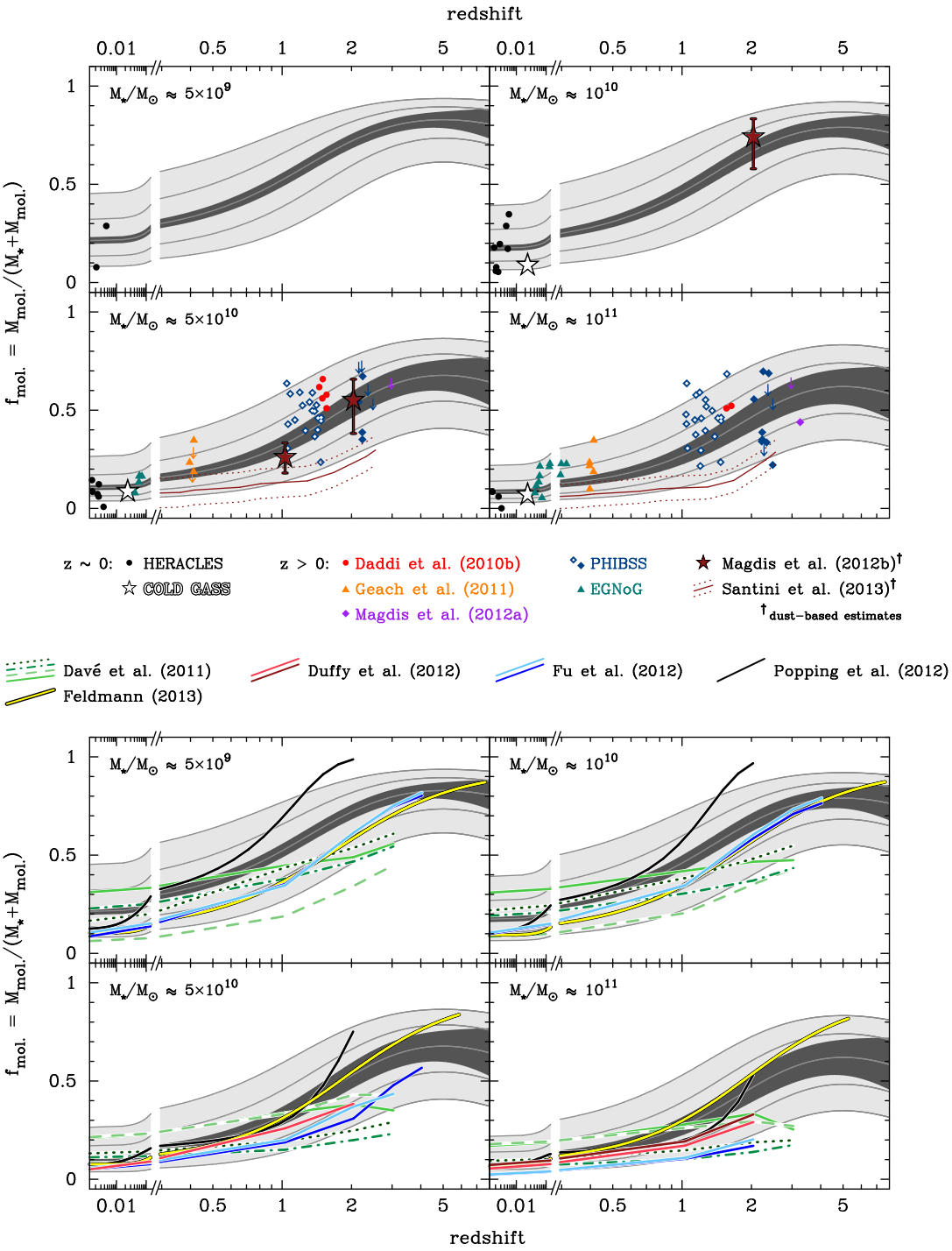

FIG. 13.—: Redshift evolution of the molecular gas fraction, $f_{\rm mol.}$, of main-sequence (MS) galaxies in four different stellar mass scales, as predicted by the 2-SFM framework based on the evolution of the sSFR and of the integrated S-K relation (see Equation 26). Upper half of figure – comparison with literature data (taken to have stellar masses within at most a factor two of the mass scale used for the analytical predictions); lower half – comparison with predictions from numerical simulations and semi-analytical modeling. The dark grey shading illustrates the uncertainty ($\pm1\,\sigma$; reflects the uncertainty of the sSFR evolution according to Equation A1 and of the integrated S-K law in Equation 4) on the evolution of $f_{\rm mol.}$ for a typical MS galaxy. Light grey areas illustrate the predicted dispersion of gas fractions. The evolution for galaxies offset by $+2/+1/0/-1/-2\,\sigma$ from the average MS locus are additionally highlighted (uppermost to lowermost medium grey line). The good agreement between predictions and data in the upper half of the figure – i.e. the observation of a synchronous evolution of sSFR and $f_{\rm mol.}$ – is consistent with the evolution of the gas reservoirs in normal galaxies being the primary driver of the cosmic sSFR evolution. Star-shaped symbols indicate gas fractions determined with stacking (Magdis et al. 2012b) or sample averaging (Saintonge et al. 2012). In the upper half of the figure two examples of indirect estimates of the gas fraction evolution based on dust mass measurements (Magdis et al. 2012b, Santini et al. 2014) are plotted in dark red. Colors and line styles used to represent different simulation predictions in the lower half of the figure are: dotted/dot-dashed/dashed/solid green lines for the vzw/cw/nw/sw (momentum-conserving/constant/no/slow wind) scenario in Davé et al. (2011); red/scarlet lines for the "L050N512"/"L100N512" realizations in Duffy et al. (2012); light/dark blue lines for "prescription 1"/"prescription 2" in Fu et al. (2012; H_2 fraction depending on local cold gas surface density and metallicity/H_2 fraction depending on ISM pressure), and for the assumption of two different SF laws for regions where atomic and molecular gas dominates, resp. (see Bigiel et al. 2008); yellow line for predictions from Feldmann (2013).

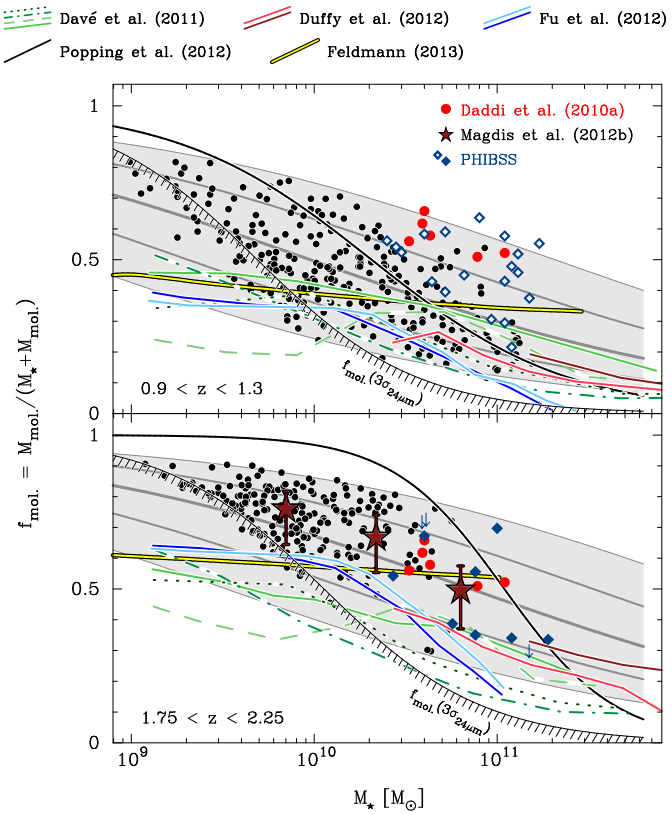

FIG. 14.—: Variation of the molecular gas fraction, $f_{\rm mol.}$, of main-sequence (MS) galaxies with stellar mass in two different redshift bins ($z\sim1$ – *top*; $z\sim2$ – *bottom*). Selected MS galaxies from Daddi et al. (2010a) and the PHIBSS survey (Tacconi et al. 2013), as well as average gas fractions determined in the stacking analysis of Magdis et al. (2012b) are plotted in color. Predictions from the 2-SFM framework and recent theoretical/numerical work in the literature are plotted with the identical symbols and color scheme as used in Figure 13. Black dots – indirect measurements of $f_{\rm mol.}$ for 24 μm-selected GOODS-S galaxies based on the inverse S-K relation calibrated in Section 3.2. The hatched line indicates the completeness limit of the statistical GOODS-S sample, as determined by the depth of the 24 μm imaging and the average redshift of the two bins displayed.

with respect to the MS. We illustrate this considerable scatter with our two statistical samples of GOODS-S galaxies (see Section 2.2), to which we apply Equation 4 to indirectly infer gas masses. In spite of the large dispersion, a clear trend of decreasing gas fractions with increasing stellar mass is seen. Semi-analytical models and simulations predict either qualitatively similar, albeit somewhat shallower trends (e.g., Davé et al. 2011, Duffy et al. 2012, Fu et al. 2012) or virtually no dependence at all of gas fractions on stellar mass (e.g., Feldmann 2013).

5.3. *The CO-to-H_2 Conversion Factor* $\alpha_{\rm CO}$

In Section 5.1.2 we showed how the sSFR-dependent SB demographics of the 2-SFM approach led to a nearly step-like variation of the SFE even if starbursting galaxies are treated as a continuous extension of normal galaxies, with depletion times that decrease in proportion to the burst strength (referred to as "boost" throughout this paper). The actual value of SFE is tightly linked to the CO-to-H_2 conversion factor, $\alpha_{\rm CO}$. In the past it has been common practice to adopt one of two discrete, "consensus" values when estimating molecular gas masses for high-redshift galaxies: $\alpha_{\rm CO}=4.4\,M_\odot\,({\rm K\,km/s\,pc^2})^{-1}$ (the conversion factor that is found to apply to GMCs in the Milky Way; e.g. Bolatto et al. 2008, Abdo et al. 2010) for normal galaxies and $0.8\,M_\odot\,({\rm K\,km/s\,pc^2})^{-1}$, a representative average for local starbursting ULIRGs (e.g., Downes & Solomon 1998). Although the collectively high luminosities of distant, CO-detected galaxies suggested that their $\alpha_{\rm CO}$ values should be ULIRG-like, the first actual estimates of $\alpha_{\rm CO}$ for $z>1$ disk galaxies (based on both dynamical arguments as in Daddi et al. 2010a or on the gas-to-dust ratio approach implemented in Magdis et al. 2011) were all broadly consistent with a Galactic $\alpha_{\rm CO}$. Going a step further, Genzel et al. (2012) subsequently were able to show that the conversion factor of high-z MS galaxies scales with gas-phase metallicity in a similar manner as the negative power laws observed for local galaxies (e.g., Wilson 1995, Israel 1997, Boselli et al. 2002, Leroy et al. 2011, Schruba et al. 2012).
The physics of the multiphase ISM that ultimately determines the exact value of $\alpha_{\rm CO}$ is complicated, regardless of whether the emission from individual star-forming regions (e.g., Glover & Mac Low 2011) or from larger scales even up to integrated emission are considered (e.g., Narayanan et al. 2011, Feldmann et al. 2012a, Papadopoulos et al. 2012). A common feature of all these theoretical or numerical calculations is a dependence of $\alpha_{\rm CO}$ on metallicity. As motivated in Section 3.2, here we adopt a shielding-based prescription for $\alpha_{\rm CO}$ from Wolfire et al. (2010), in which conversion factors vary weakly with metallicity around solar abundance but then increase quickly at $Z/Z_\odot<1/2$. The fact that SBs in the 2-SFM framework preserve a memory of their former MS state means that our predicted SB $\alpha_{\rm CO}$ values also depend on metallicity but in a more complicated way which is detailed in the following.

5.3.1. *Conversion Factors for Starbursts: Empirical Calibration of Boost Dependence*

As for the SFE (see Equation 24) we assume that $\alpha_{\rm CO}$ varies smoothly[21] with the boost of an SB,

$$\log\left(\frac{\alpha_{\rm CO}}{\alpha_{\rm MS,\,init.}}\right)=\gamma_{\alpha_{\rm CO}}\times b_{\rm sSFR}\ , \qquad (27)$$

and use our sample of reference SBs (cf. Section 2.1.3) to determine the most suitable value of $\gamma_{\alpha_{\rm CO}}$, given this choice of parameterization. Boosts $b_{\rm sSFR}$ are assigned as in Section 5.1.2 and $\alpha_{\rm CO}$ values are given in Downes & Solomon (1998) or Magdis et al. (2012b) for each SB in the reference sample. $\alpha_{\rm MS,\,init.}$ corresponds to the conversion factor of a MS galaxy with the same SFR as a reference SB, but with $L'_{\rm CO}$ and $M_{\rm H_2}$ given by the inverse integrated S-K relations in Equation 1 and 4, respectively. Since we refer the $\alpha_{\rm CO}$ to this initial state

[21] The functional form of Equation 27 is not merely motivated by its symmetry with Equation 24, it also reflects the expectation that the state of the ISM evolves continuously, e.g. depending on the strength of the tidal forces which may enhance the amplitude of the turbulent motions during galaxy-galaxy interactions (e.g., Bournaud et al. 2011b). Larger velocity gradients and higher temperatures, which are generally characteristic of the turbulent and dense starbursting ISM, both lower $\alpha_{\rm CO}$ while higher column densities increase the CO-to-H_2 conversion factor (see, e.g., Equation A4 in Papadopoulos et al. 2012).

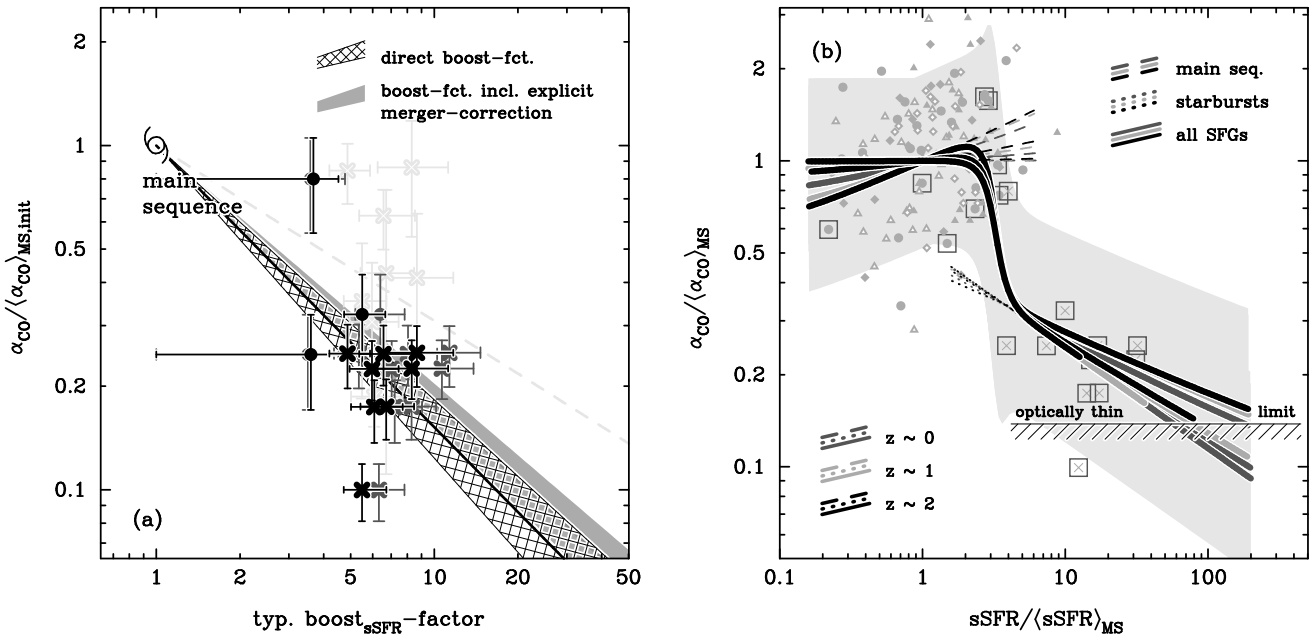

FIG. 15.—: (*a*) Empirical calibration of the decrement in $\alpha_{\rm CO}$ with the amount of (s)SFR boosting experienced by starbursts (SBs; all symbols and data as in Figure 9(b)). The decrement is referred to the CO-to-H_2 conversion factor, $\langle\alpha_{\rm CO}\rangle_{\rm MS,\,init.}$, that would be expected for each SB galaxy if it were a secularly evolving, average, normal galaxy with the same molecular gas fraction (see Section 5.3.1 for details). Starburst $\alpha_{\rm CO}$ measurements plotted in black are from dynamical modeling in Downes & Solomon (1998), light grey symbols are for $\alpha_{\rm CO}$ values derived by Papadopoulos et al. (2012) using a two-phase LVG model. (Crosses/dots are used for local/high-z SBs from Solomon et al. (1997) and Magdis et al. (2012b), respectively; 1 sigma-error bars plotted.) The shaded/hatched areas span the 68% confidence region for a power-law relation between SB $\alpha_{\rm CO}$ and boost amplitude as parametrized in Equation 27 and when fitting to $\alpha_{\rm CO}$ measurements from Downes & Solomon (1998). The light grey dashed line shows the best-fitting power-law relation inferred based on the $\alpha_{\rm CO}$ values from two-phase LVG modeling. (*b*) Predicted variation of average, normalized $\alpha_{\rm CO}$ with sSFR excess for normal MS galaxies (*dashed lines*), SBs (*dotted lines*; "direct" boost function assumed) and the total population of SFGs (*solid lines*). Data points plotted in grey in the background are as in Figure 11 (for visualization purposes in this figure an artificial dispersion has been added to galaxies with statistical estimates of $\alpha_{\rm CO}$, i.e., for all sources which are not plotted with boxed symbols; see text for details). Due to the non-linear dependence of the gas-phase metallicity on SFR and stellar mass (as parameterized by the FMR of Mannucci et al. 2010) the average $\alpha_{\rm CO}$ trends predicted by the 2-SFM framework are both stellar mass- and redshift dependent. In a given redshift bin (color-coded as shown in the upper right corner) the shallowest variation across the MS (i.e. in the range $1/6 < {\rm sSFR}/\langle{\rm sSFR}\rangle_{\rm MS} < 6$) occurs for the most massive of the three stellar mass bins considered here ($M_\star/M_\odot = 5{\times}10^9$, $5{\times}10^{10}$ and $5{\times}10^{11}$), while the steepest variation occurs for the least massive bin. At high excesses of sSFR the $\alpha_{\rm CO}$ values are predicted to decrease the most steeply in the highest and most slowly in the lowest stellar mass bin plotted. Over the range $0 < z < 2$ shown here, the variation with stellar mass is expected to be more significant than that with redshift. At the highest sSFR excesses (boosts) the $\alpha_{\rm CO}$ values in SBs plausibly asymptotically approach the lower limit set by optically thin CO line-emission.

by definition no constant term is required in Equation 27. Solving for $\gamma_{\alpha_{\rm CO}}$ we obtain $\gamma_{\alpha_{\rm CO}} = -0.82^{+0.08}_{-0.09}$ ($1\,\sigma$ errors quoted) for the case of the direct boost function and $\gamma_{\alpha_{\rm CO}} = -0.75{\pm}0.06$ for the merger-corrected boost function. The boost dependence for the two scenarios is shown in Figure 15(a), together with the SB data used for the fit. The relatively slow, sub-linear decline of $\alpha_{\rm CO}$ with boost amplitude (i.e. SFR enhancement) according to $\alpha_{\rm CO} \propto ({\rm boost})^{\gamma_{\alpha_{\rm CO}}}$ implies that to reach ULIRG-like values of the conversion factor, which are about 1/5 of the typically assumed Milky-Way-like $\alpha_{\rm CO} = 4.4\,M_\odot\,({\rm K\,km/s\,pc^2})^{-1}$, a boost by a factor of 8–10 is expected according to the 2-SFM description.

Several of the $\alpha_{\rm CO}$ measurements for our reference SBs deviate more strongly from the average trend between boost and conversion factor than was the case for the relation between SFE and boost we calibrated in Figure 9(b). As a consistency check we hence used the results of the LVG radiative transfer modeling by Papadopoulos et al. (2012) of all nine starbursting local ULIRGs in our reference sample to re-derive the logarithmic slope $\gamma_{\alpha_{\rm CO}}$ in Equation 27. We find that $\alpha_{\rm CO}$ values determined with one-phase radiative transfer models are on average consistent with the dynamical estimates of Downes & Solomon (1998), such that the resulting slope is almost identical to the previously measured one: $\gamma_{\alpha_{\rm CO}} = -0.85^{+0.08}_{-0.09}$ (direct boost function) and $\gamma_{\alpha_{\rm CO}} = -0.78^{+0.05}_{-0.06}$ (boost function corrected for merger-statistics). CO-to-H_2 conversion factors inferred with two-phase (for high- and low-excitation gas) ISM models are generally higher (see light grey crosses in Figure 15(a)), leading to a shallower slope $\gamma_{\alpha_{\rm CO}} = -0.51^{+0.10}_{-0.24}$ ($-0.46^{+0.09}_{-0.23}$) for the direct (merger-corrected) boost function. Given the good agreement between the former two estimates of $\gamma_{\alpha_{\rm CO}}$ we have adopted the dynamically constrained CO-to-H_2 conversion factors reported in Downes & Solomon (1998) throughout this paper.

We can now write an expression relating the conversion factor of an SB in general to the MS average:

$$\log\left(\frac{\alpha_{\rm CO}}{\langle\alpha_{\rm CO}\rangle_{\rm MS}}\right) = \log\left(\frac{\alpha_{\rm CO}}{\alpha_{\rm MS,\,init.}}\right) + \log\left(\frac{\alpha_{\rm MS,\,init.}}{\langle\alpha_{\rm CO}\rangle_{\rm MS}}\right)$$
$$= \gamma_{\alpha_{\rm CO}} \times b_{\rm sSFR} + [f\,({\rm SFR_{MS,\,init.}}) - f\,(\langle{\rm SFR}\rangle_{\rm MS})]\ . \quad (28)$$

Here the first term – which describes the $\alpha_{\rm CO}$ deficit of SBs with respect to the pre-boost, MS state of each indi-

vidual galaxy – corresponds to Equation 27. The second term relates the pre-boost, MS state to the MS average via the relation between $\alpha_{\rm CO}$ and metallicity (Equation 3). Eq. 28 strongly resembles Equation 25 for the normalized SFE of SBs but is nevertheless different in that the expression describing variations within the MS,

$$\begin{aligned}\log\left(\frac{\alpha_{\rm CO}}{\langle\alpha_{\rm CO}\rangle_{\rm MS}}\right) &= \log\left(\frac{\exp\left[\frac{\Delta\mathcal{A}_V(Z)}{Z/Z_\odot}\right]\,\exp^{-\Delta\mathcal{A}_V(Z)}}{\exp\left[\frac{\Delta\mathcal{A}_V(\langle Z\rangle_{\rm MS})}{\langle Z\rangle_{\rm MS}/Z_\odot}\right]\,\exp^{-\Delta\mathcal{A}_V(\langle Z\rangle_{\rm MS})}}\right)\\ &= \frac{1}{\ln(10)}\left[\Delta\mathcal{A}_V(Z)\left(\frac{Z_\odot}{Z}-1\right)\right.\\ &\qquad\left.-\Delta\mathcal{A}_V(\langle Z\rangle_{\rm MS})\left(\frac{Z_\odot}{\langle Z\rangle_{\rm MS}}-1\right)\right]\\ &= \left[f\left(\mu_{0.32}\right)-f\left(\langle\mu_{0.32}\rangle_{\rm MS}\right)\right]\\ &\equiv \left[f\left({\rm SFR}\right)-f\left(\langle{\rm SFR}\rangle_{\rm MS}\right)\right]\,, \end{aligned} \quad (29)$$

has higher order terms in log(SFR). This is caused both by the term $\Delta\mathcal{A}_V(Z) = {}^{4\,\Delta A_V(Z)}\!/\!_{\overline{A}_{V,\rm MW}}$ which is a function of the metallicity-dependent gas fraction (here we adopt the double power law dependence on metallicity of Rémy-Ruyer et al. 2014), and by the fact that our statistical estimates of metallicity involve the FMR parameter $\mu_{0.32} = \log(M_\star) - 0.32\times\log({\rm SFR})$ defined in Mannucci et al. (2010). The normalized logarithmic conversion factor for MS galaxies, $\log\left({}^{\alpha_{\rm CO}}\!/\!_{\langle\alpha_{\rm CO}\rangle_{\rm MS}}\right)$, can no longer be written as a function $f\left({}^{\rm SFR}\!/\!_{\langle{\rm SFR}\rangle_{\rm MS}}\right)$ of normalized SFR (or, equivalently, sSFR when considering a fixed bin of stellar mass). This was possible, however, in the case of SFE and $f_{\rm mol.}$ (see Sections 5.1.2 and 5.2.1) and led to a redshift- and mass-independent recipe for the evolution of the population average of these quantities with ${\rm sSFR}/\langle{\rm sSFR}\rangle_{\rm MS}$. In Figure 15(b) we plot[22] (fine dashes) the predicted variation of the median $\alpha_{\rm CO}$ of MS galaxies for three stellar mass bins ($M_\star/M_\odot = 5\times10^9$, 5×10^{10} and 5×10^{11}) and three different redshifts ($z = 0$, 1, 2). Due to the higher order (s)SFR terms in Equation 29 these trends are no longer redshift- and mass-independent; while $\alpha_{\rm CO}$ values for SFGs vary little across the MS in our highest mass bin ($M_\star/M_\odot = 5\times10^{11}$), evolution by approx. a factor two is predicted between $\pm4\,\sigma_{\rm MS}$ for stellar masses $M_\star \sim 5\times10^9\,M_\odot$. For the mass and redshifts considered here, the mass dependence of the average trends at fixed redshift is more pronounced than the redshift dependence at fixed mass. Note that although we assume the relation between boost and $\alpha_{\rm CO}$ decrement for SBs (see Equation 27) to be independent of redshift and stellar mass, the predicted average $\alpha_{\rm CO}$ trends for starbursting sources nevertheless vary with stellar mass and redshift. This is a consequence of the mass- and redshift-dependency found for the "parent" MS population. For example, the fact that at low masses conversion factors are predicted to rise across the MS implies that at fixed boost-dependent $\alpha_{\rm CO}$ decrement the $\alpha_{\rm CO}$ of high-sSFR SBs will be higher than for the highest mass bins where $\alpha_{\rm CO}$ values of normal galaxies on the MS are expected to be virtually constant. As a final comment on the description of $\alpha_{\rm CO}$ variations for starbursting sources we should point out that in practice the conversion factor cannot decrease indefinitely (as formally implied by Equation 28) but that optically thin CO line-emission sets a lower limit (see Figure 15(b)). Assuming local thermal equilibrium and a gas temperature of 40-60 K for SB sources, we estimated $\alpha_{\rm CO}$ in the optically thin approximation using standard formulae (see, e.g., Appendix A1 in Bryant & Scoville 1996) and obtained values ranging between 0.45 and $0.75\,M_\odot\,({\rm K\,km/s\,pc^2})^{-1}$. Values at the lower (higher) end of this range are generally predicted for lower (higher) redshift sources due to the evolution of the temperature of the cosmic microwave background, and with an additional contribution from the likely quite mild evolution of the dust temperature in SBs (e.g., Béthermin et al. 2012). In relative terms, at all redshifts $0 < z < 2.5$ this is about 10%–20% of the $\alpha_{\rm CO}$ values expected for massive MS galaxies if their conversion factors also increase with redshift because of the general evolution of the population toward lower metallicity.

The median $\alpha_{\rm CO}$ of the total population – computed analogously to the bulletized procedure sketched in Section 5.1.2 – is plotted with thick, solid lines in Figure 15(b). The exact shape of the transition between MS and SB regime depends both on the assumed scatter of the FMR and the dispersion of $\alpha_{\rm CO}$ at fixed metallicity (see, e.g., Mannucci et al. 2010, Genzel et al. 2012, Schruba et al. 2012). For the present case we assume these to be 0.05 dex and 0.2 dex, respectively, which leads to a step-like decrease by about a factor 2-3 at an sSFR excess ${\rm sSFR}/\langle{\rm sSFR}\rangle_{\rm MS} \sim 3$-4 with respect to the MS average. Just as for the predicted slope of the normalized $\alpha_{\rm CO}$ versus sSFR relations for normal and SB galaxies, this jump changes with redshift and stellar mass. In the next section we thus provide a more complete mapping of expected $\alpha_{\rm CO}$ variations for SFGs.

5.3.2. $\alpha_{\rm CO}$: *Predicted Variations in the SFR-$M_\star$ Plane*

To conclude this section on empirical recipes for the CO-to-H_2 conversion factor $\alpha_{\rm CO}$ we map its predicted variation within the $M_\star$ versus SFR plane for three different redshift bins in Figure 16: $z = 0$ – top row; $z = 1$ – second row; $z = 2$ – bottom row. We do this explicitly because the mapping of metallicity into the $M_\star$ versus SFR plane following Mannucci et al. (2010) is such that the variation of the metallicity-dependent $\alpha_{\rm CO}$ we adopt for 2-SFM framework is not self-similar (i.e. independent of stellar mass and redshift as was the case for SFE and $f_{\rm mol.}$; see Figure 11) and hence cannot be represented with a single, sSFR-dependent recipe.

The individual panels of Figure 16 show the variation of $\alpha_{\rm CO}$ in $M_\star$-SFR space for the total SFG population, for MS galaxies and for SBs (columns 1 to 3). We have superimposed contours of constant $\alpha_{\rm CO}$ and in particular indicated the isolines for Milky-Way-like and ULIRG-like conversion factors with a bold red and blue line, respectively. Due to the increasing normalization of the MS with redshift, metallicities at fixed stellar mass decrease with redshift (this reflects the well-established, measured evolution of the mass-metallicity relation, e.g., Kobulnicky & Kewley 2004, Erb et al. 2006, Liu et al. 2008, Zahid et al. 2013). While this evolution to lower enrichment is expected to be quite strong at the smallest stellar masses plotted in these figures ($M_\star \sim 10^9\,M_\odot$) the evolution is less strong for those galaxies of stellar mass $M_\star \sim 3\times10^{10}\,M_\odot$ that contribute most to the cosmic SFR density over the redshift range considered

[22] All predictions shown in Figs. 15(b) and 16 assume the "direct" boost function and the corresponding best-fit value of $\gamma_{\alpha_{\rm CO}}$.

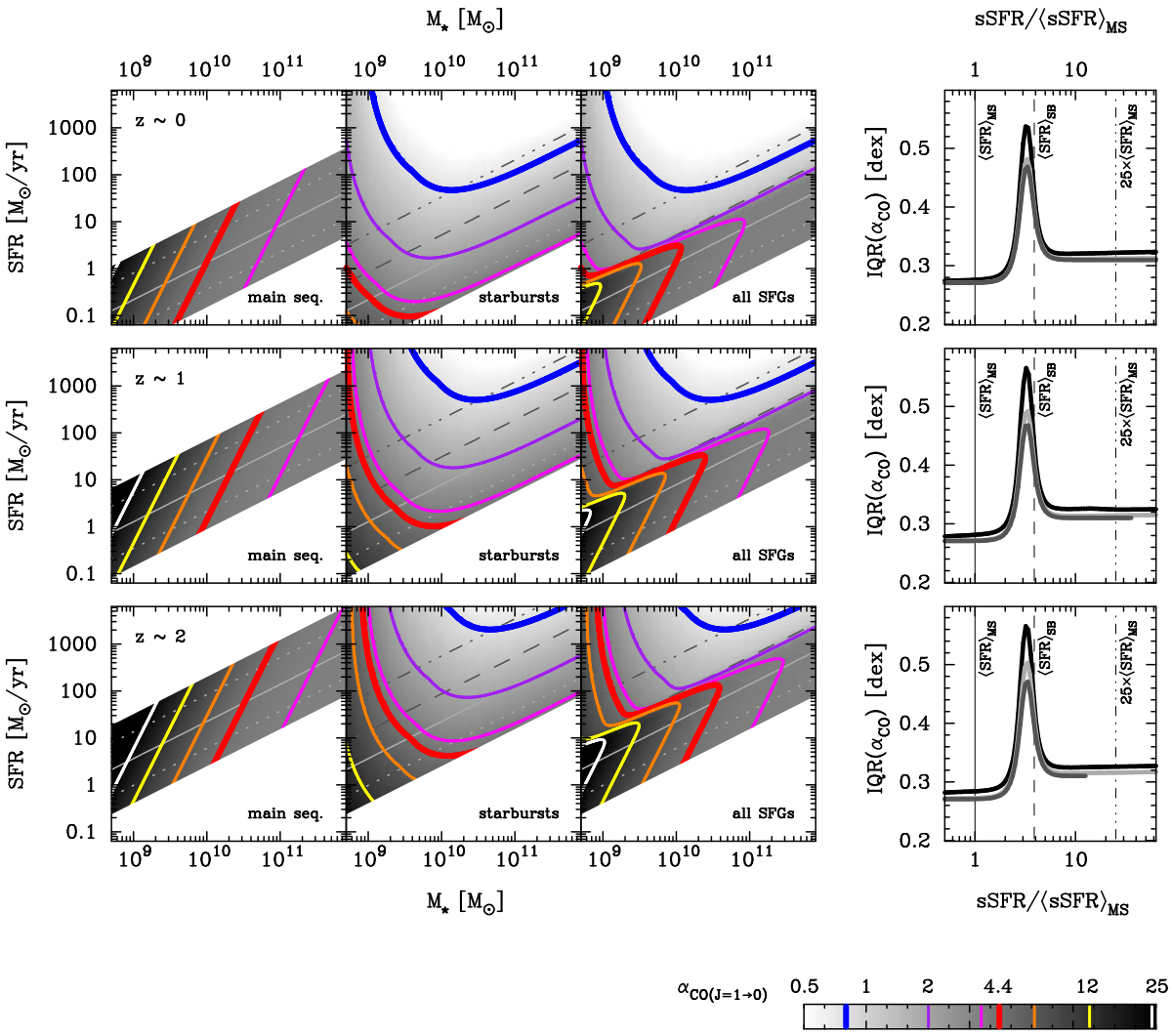

FIG. 16.—: Predicted variations of the CO-to-H_2 conversion factor, α_{CO} (for the $J=1\rightarrow0$ transition and assuming the 'direct' boost function), in the SFR-$M_\star$ plane for main-sequence (MS) galaxies, starbursting galaxies and for the combined population of normal SFGs and starbursts (SBs; *first, second & third column*, resp.) at $z\sim0$, 1 and 2 (*from top to bottom*). α_{CO} variations are mapped within ±5 times the dispersion (σ_{MS}) of the MS for the normal galaxies and between -5 σ_{MS} and arbitrarily high sSFR excesses for SB galaxies and the total SFG population (columns 2 & 3). Lines of constant $\alpha_{CO}=0.8$, 2, 3.5, 4.4, 6.5, 12 & 24 are superimposed in blue, purple, magenta, red, orange, yellow and white (standard values of a ULIRG and Milky Way conversion factor – $\alpha_{CO}=0.8$ & 4.4 – are highlighted with bold lines). Values plotted in columns 1–3 represent the median for the respective (sub-)population. Grey diagonal lines trace lines of constant sSFR at: $\pm3\,\sigma_{MS}$ – dotted; $\langle sSFR\rangle_{MS}$ – solid; $\langle sSFR\rangle_{SB}$ – long dashes; $25\times\langle sSFR\rangle_{MS}$ – dash-dot-dot. Column 4 shows the scatter of α_{CO} (visualized here by the interquartile range IQR of logarithmic α_{CO} values) around the average trends for the total SFG population (cf. col. 3) at stellar mass $M_\star/M_\odot=5\times10^9$ (*black*), 5×10^{10} (*light grey*) and 5×10^{11} (*dark grey*). Vertical lines correspond to the lines of constant sSFR plotted in columns 1–3. The dispersion rises strongly over a fairly small range of sSFR where $f^{SB}\sim50\%$ (see also Figures 6 and 15(b)).

here (e.g., Karim et al. 2011). As a consequence, we expect that the conversion factor of such galaxies remains quite similar to the classic Milky Way value of $4.4\,M_\odot\,(K\,km/s\,pc^2)^{-1}$ over the range $0<z<2$. Specifically, for a galaxy of stellar mass $M_\star\sim3\times10^{10}\,M_\odot$ that is located directly on the average MS locus, the recipes developed in Section 5.3.1 predict $\alpha_{CO}\simeq3.8$ in the local universe and $\alpha_{CO}\simeq4.5$ at $z\sim2$. Note that this prediction is not the coincidental outcome of choosing a specific slope and/or normalization of the relation between α_{CO} and metallicity in Equation 3. It would also hold for any of the other relations shown in Figure 3 as these all attain quite similar, Milky-Way-like conversion factors around solar metallicity. For our calculations we have assumed that the same relation between α_{CO} and metallicity holds at all redshifts. Under these circumstances, the weak positive evolution of α_{CO} predicted here is purely due to the lower metallicities of high-redshift galaxies. This evolutionary trend could vanish entirely or even tend toward lower values of the conversion factor if large fractions of the star-forming ISM in high-redshift galaxies have densities significantly higher than GMCs in the Milky Way (see, e.g., Bolatto et al. 2013; and references therein) or if conversion factors scale inversely with CO surface intensity, as proposed by Narayanan et al. (2011) based on simulations. Lower conversion factors in high-redshift galaxies would bring CO-based gas mass measurements into better agreement with those estimates based on the gas-to-dust ratio technique that are systematically lower (e.g., Santini et al. 2014, Scoville et al. 2014; but see also

Magdis et al. 2012b). However, it is presently unclear if these reports on lower gas masses should be interpreted as evidence that systematic overestimates of the conversion factor produce too high gas masses when these are derived from CO-data. For example, $\alpha_{\rm CO}$ measurements for *individual* galaxies (rather than stacked populations) at $1<z<2$ (e.g., Magdis et al. 2012b, Magnelli et al. 2012) made with the gas-to-dust ratio technique give values that are inconsistent with a strong decrease of conversion factors at high redshift. Likewise, dynamical constraints on the CO-to-H_2 conversion factors in BzK-galaxies (Daddi et al. 2010a) favor Milky-Way-like values. Future studies of high-redshift galaxies with ALMA should be able to clarify whether or not the $\alpha_{\rm CO}$ of normal galaxies has a similar metallicity-dependence at all redshifts.

For variations of the conversion factor of starbursting sources in the $M_\star$ versus SFR plane (second column of Figure 16) we expect two different regimes to exist. At high stellar masses, the $\alpha_{\rm CO}$ values of the parent, MS population vary little (both across the MS with a given bin of stellar mass and between stellar mass bins); the boost-dependent $\alpha_{\rm CO}$ decrement alone hence determines the value of SB conversion factors. As a consequence, lines of equal SB $\alpha_{\rm CO}$ are nearly parallel to the MS locus. At low stellar masses, lines of constant SB $\alpha_{\rm CO}$ run nearly perpendicular to the isolines on the MS locus. This is due to the rapid variation of $\alpha_{\rm CO}$ for normal galaxies, which has the effect that ever higher boost amplitudes are required in order for SBs of successively lower stellar mass to reach equal absolute values of $\alpha_{\rm CO}$ (e.g. the standard local ULIRG value $0.8\,M_\odot\,(\mathrm{K\,km/s\,pc^2})^{-1}$). Starting at an (s)SFR excess of about $+3\,\sigma_{\rm MS}$, SBs begin to dominate the MS population by number. The transition between the MS locus and the SB-dominated part of $M_\star$-SFR space is characterized by both a sudden drop of the average $\alpha_{\rm CO}$ (see Figure 15(b)) and an abrupt increase of the dispersion of $\alpha_{\rm CO}$, which is a result of the heterogeneous mixture of starbursting and high-sSFR MS galaxies in this transition region. This is illustrated in the panels in column 4 of Figure 16 where we plot the evolution of the interquartile range of $\alpha_{\rm CO}$ values measured in the total SFG population (i.e. including both SBs and normal galaxies). On the MS ($\mathrm{sSFR}/\langle\mathrm{sSFR}\rangle_{\rm MS}\lesssim 3$) the scatter in $\alpha_{\rm CO}$ is caused by the metallicity dispersion of the of FMR at fixed $M_\star$ and SFR plus the dispersion of $\alpha_{\rm CO}$ at fixed metallicity and is hence relatively small. The $\alpha_{\rm CO}$ scatter for SB galaxies is larger than that on the MS locus because it reflects both the dispersion of $\alpha_{\rm CO}$ at fixed $M_\star$ and SFR on the MS, and the fact that the shape of the boost function implies that SBs at a given $\mathrm{sSFR}/\langle\mathrm{sSFR}\rangle_{\rm MS}$ have been boosted to higher (s)SFR starting from a range of positions on the MS.

6. DISCUSSION: TOWARD A SIMPLE DESCRIPTION OF MOLECULAR GAS IN STAR-FORMING GALAXIES

6.1. *The Boost Function: Astrophysical Context and Limitations*

In Section 4.2.1 we provided simple arguments for why the existence of a statistical link (due to a so far unspecified process) between the populations of MS galaxies and SBs is a natural expectation. Here we discuss which processes might be responsible for such a link and how SF activity may reflect cosmological accretion of dark matter (DM) and baryons.

6.1.1. *Star Formation Enhancements in Simulations and Observations*

Based on a suite of simulated interacting galaxies (with comparable masses and a representative range of both orbital configurations and morphologies) Di Matteo et al. (2007) and Di Matteo et al. (2008) derived the SFR evolution of major mergers as compared to the evolution of identical, isolated galaxies. In Figure 5 we plotted the maximal SFR enhancements reported in Di Matteo et al. (2008), averaged between the Tree-SPH (smoothed particle hydrodynamics) simulations and grid-based N-body simulations carried out by these authors. Both the 2-SFM boost function and the distribution of simulated SFR enhancements have a clearly defined peak. The exact position of this peak (which corresponds to $\langle x\rangle_{\rm BK}$ in the 2-SFM formalism) in the simulations depends on the gas content of the galaxies. In local disk galaxies (simulated total gas fractions between 10 and 30%) the most frequently encountered maximal SFR excess is approx. a factor of three, while for gas-rich simulated galaxies ($f_{\rm mol.}\sim 50\%$) reminiscent of high-z disks it is twice as large, mainly because these tend to become Jeans-unstable and form dense gas clumps when perturbed. The 2-SFM boost function peaks at a roughly four-fold SFR enhancement but it should not be directly compared to the simulation results because not all SBs that contributed to the shape of the underlying (s)SFR distribution in Rodighiero et al. (2011) can have been "caught" at the peak of the SB activity. With respect to the results of Di Matteo et al. (2007, 2008), observable distributions of SFR boosts for interacting galaxies will likely be modified if minor mergers and fly-bys, as well as the relative timing of SB events, are accounted for. If SFR enhancements in merger-driven SBs depend on the mass ratio of the galaxies involved (e.g., Cox et al. 2008), then the boost distribution including minor mergers should be broader. Likewise, fly-bys and asynchronous burst-activity plausibly shift and skew the boost distribution to lower SFR enhancements.

Although the distribution of SFR enhancements caused by interactions between galaxies is poorly constrained, observationally, there have been numerous studies aimed at quantifying the integrated contribution of excess SF associated with mergers/interactions to the cosmic SFR density at redshifts $z<2$ (e.g., Robaina et al. 2009, Kampczyk et al. 2013, Kaviraj et al. 2013). One attempt is the recent determination of the distribution of SFR enhancements in SDSS galaxy pairs by Scudder et al. (2012) which we plot in blue in Figure 5. Compared to the boost distribution in the simulations of major mergers in Di Matteo et al. (2008) it is indeed displaced to systematically lower SFR enhancements. In addition to the expected shifting and skewing, the fact that the SDSS pair sample does not include mergers in which final coalescence has already taken place implies that their distribution of SFR enhancements represents a lower observational limit to the total local SFR excess distribution caused by interactions. The simulations of Di Matteo et al. (2007) and Di Matteo et al. (2008) encompass a

broad variety of orbital configurations of merging galaxy pairs and have been statistically weighted to reflect the dependence of the collision rate on the relative velocities and impact parameters. However, they do not provide information on the contribution of minor interactions, nor are they carried out in a fully cosmological framework that accounts for, e.g., the preferential alignment of galaxies in different locations within the cosmic web (e.g., Hahn et al. 2010). This additional step was taken in simulations by Hopkins et al. (2010), such that their spectrum of merger-induced surplus SFR should be similar to the measurement of Scudder et al. (2012). Hopkins et al. (2010) incorporated the results of their own high-resolution merger simulations (Hopkins et al. 2009) in a cosmological (DM) framework and were able to predict SFR distributions of secularly evolving and starbursting galaxies (see Figure 7 in Hopkins et al. 2010) that, in qualitative terms, resemble the split into MS and SB activity we proposed in S12 and which seem broadly consistent with the expected modifications to the boost distributions of Di Matteo et al. (2008) discussed at the end of the last paragraph. For galaxies with a stellar mass of $10^{11}\,M_{\odot}$, where we can compare with our own double log-normal decomposition according to Equation 6, the approach of Hopkins et al. (2010) predicts (1) an SFR boost distribution for SBs that is broader and more skewed to low boosts, and (2) typical SFR enhancements that are smaller (for simulated $z\sim0$ and 2 mergers) in comparison to both the outcome of the major merger simulations of Di Matteo et al. (2008) and also the 2-SFM boost function.

To infer that galaxy-galaxy interactions cannot be the sole trigger of SB activity, based only on the mismatch between the 2-SFM and measured or simulated boost distributions, would, however, be premature. The approach of decomposing an sSFR distribution into two components – as done in Section 4.2 – leads to inherently poor constraints on the shape of the boost function at low boosts (see cross-hatched area in Figure 5) since galaxies with small sSFR enhancements blend in entirely with the MS population. This "maximization" of the MS contribution in Equation 6 will hence cause a truncation of the lower part of the boost function. On the other hand, the distinction between secularly evolving and only weakly starbursting systems itself is not clear-cut because minor merger events occur frequently. If all galaxies that have experienced minimal boosting are regarded as SBs, then a boost distribution that goes to zero at a (s)SFR excess of zero (boost = 1) is unrealistic. The 2-SFM boost function should thus best be viewed as the signature of strong boosting where a significant fraction of the ISM fuels SB activity. Despite this limitation it is interesting that the peak position of the 2-SFM boost function at an excess (s)SFR of a factor of four corresponds exactly to the average SFR boost that was measured by Hwang et al. (2011) for FIR-selected galaxies at $z=0$ and $z=1$ undergoing an interaction with a late-type neighbor. In another study Kampczyk et al. (2013) demonstrate that SF, as traced by optical line emission, is boosted by roughly a factor four for the most closely bound (physical separation $<30\,h^{-1}$ kpc) kinematic pairs at $0.2<z<1$ from the zCOSMOS survey. Park & Choi (2009) investigated the interaction-induced SFR boosting in local late-type galaxy pairs and found an increase of the equivalent width of the Hα-line by an identical factor four when the two galaxies were separated by less than 1% of the virial radius of the companion's halo. This constancy of the average SFR excess is reminiscent of the evidence for only mild evolution of the shape of the boost function we presented in S12. Furthermore, it is worth noting that notwithstanding the uncertainties concerning the shape of the lower end of the 2-SFM boost function, Béthermin et al. (2012) successfully used it as the basis for matching observed IR source counts. Their analysis was a good test of the viability of the 2-SFM description of SBs since it employed different IR SEDs for MS galaxies and SBs.

6.1.2. *Link to Dark Matter*

Merging and SF activity – even in the "secular" mode – reflect the accretion of DM and the primordial gas bound to the DM halos. It is thus interesting to check whether there are clear similarities between the distribution of SFRs of galaxies of a given mass and the accretion of DM onto the corresponding parent halos. Dekel et al. (2009) determined the DM infall rates at the virial radius of >100 simulated DM halos with mass $10^{12}\,M_{\odot}$ at $z\sim2.5$, which typically host $\sim10^{11}\,M_{\odot}$ galaxies. For these systems (which have masses comparable to the galaxies used by Rodighiero et al. 2011 to construct distributions of sSFR) the DM accretion spectrum shows an extended tail of high accretion rates which is dominated by "major" merging activity where the mass ratio between accreted and parent DM halo is fairly high. It is obviously tempting to associate this feature of the DM accretion rate distributions in the simulations presented in Dekel et al. (2009) to the tail of excess SFRs contributed by SB galaxies while the smooth accretion would then fuel the sustained secular mode of SF that is characteristic of SFGs on the MS. This was already proposed by Dekel et al. (2009), who also point out that in this context the abbreviation "SFG" could legitimately stand for "stream-fed galaxy". In analogy to our split of the sSFR-distribution in Equation 6, T. Goerdt et al. (in prep.) have decomposed the DM accretion rate distribution for such $z=2.5$ DM halos with virial mass $10^{12}\,M_{\odot}$ into two log-normal contributions and find that the one shifted to high accretion rates contributes approx. 10% to the infalling mass budget. This value is strikingly similar to the $14.2^{+1.7}_{-1.3}$% (68% confidence limits) we inferred in S12 for the contribution of burst-like SF to the total SFRD at $z=2$.

6.2. *Universal Star Formation Laws and the Distribution of Galaxies in the Schmidt-Kennicutt Plane*

The tightness of the SF law (dispersion $\sim$0.2 dex or less than a factor two) that we found using our newly "homogenized" literature data in Section 3.2 is remarkable and points to a very direct and apparently ubiquitous link between the global molecular content of galaxies and how much of it is being converted into stars. It is akin to stating that, for normal disk galaxies out to at least $z\simeq2.5$, once the SFR has been measured the size of the associated molecular gas reservoir can be inferred with high accuracy, and vice-versa. In our calibration of the integrated S-K law in Section 3, we adopted a statistical

(metallicity-dependent) estimate of the CO-to-H_2 conversion factor, $\alpha_{\rm CO}$, for 90% of the normal galaxies in our reference sample when we were translating the observed correlation between $L_{\rm IR}$ and $L'_{\rm CO}$ to a more physical relation between SFR and $M_{\rm mol.}$. While using an average $\alpha_{\rm CO}$ and neglecting the associated scatter in principle artificially reduces the dispersion of the S-K law, it is not inconceivable that a dispersion in $\alpha_{\rm CO}$ has produced the observed width of the $L_{\rm IR}$ versus $L'_{\rm CO}$ relation. Simulations by Feldmann et al. (2012b) for example suggest that on kiloparsec-scales and above variations in the conversion factor can be as large as 0.15 dex. The underlying SF law thus might be intrinsically even tighter than the 0.2 dex we measure here. To truly test the universality of the "normal"-galaxy S-K law there are at least two complementary ways forward. On the one hand, it will be important to compile samples of galaxies for which SF and gas estimates rely on strictly identical tracers (e.g. the ground-state transition of ^{12}CO). On the other hand, it may prove worthwhile to assess in detail (e.g. by means of a full sampling of the SLEDs of molecular gas tracers) how SF proceeds in different phases of the ISM. Having the capability of doing this in a resolved fashion, we also have the potential to reveal what causes the mild SFR dependence of SFE, which manifests itself as a non-linear slope of the integrated S-K relation (SFR $\propto M_{\rm mol.}^{1.2}$). Saintonge et al. (2012) have proposed that the rise of SFE across the MS is due to morphological "stabilization" of the ISM in bulged galaxies (see Martig et al. 2009), which are more abundant on the lower part of the MS locus. Resolved studies of the SF law will also be able to reveal whether a similar mechanism is responsible for the SFE increase with redshift in massive galaxies; while it could be due to the increasing absence of bulged galaxies at high redshift (e.g., Oesch et al. 2010), it seems just as plausible that SF in an increasingly turbulent medium including massive star-forming clumps would proceed in a more efficient fashion.

The variations of SFE with SFR among normal galaxies are small compared to the strong SFE enhancements that are observed in starbursting systems. In Section 5.1.2 we introduced an empirical, supra-linear scaling between the SFE and (s)SFR increase during SB episodes. This relation can be understood very intuitively by the balance between the three quantities involved: SFR and $M_\star$, which grow in the burst-phase, and $M_{\rm mol.}$ which decreases as gas is converted into stars. SFE, as the ratio between SFR and $M_{\rm mol.}$, thus inevitably increases more strongly than sSFR. An immediate consequence of this is that we expect a more spread-out distribution of SFEs than is observed. In Figure 10 we illustrate how, in the 2-SFM framework, the overlapping sSFR distributions of normal galaxies and SBs move apart into a more clearly double-peaked SFE distribution. Discrete recipes for the assignment of CO-to-H_2 conversion factors to normal galaxies and SBs are thus not the only way to obtain a bimodal distribution of galaxies in the S-K plane; this can also be achieved with a more physical, continuous description of SF in SBs. Width and depth of the trough we predict between the "sequence of disks" and "sequence of starbursts" in the S-K plane depend on the shape of the lower end of the boost function (see discussion in Section 6.1). Our model of an unbiased profile through the S-K plane at fixed gas mass does highlight, however, that observations of large cosmological volumes are necessary to fully sample the actual distribution of galaxies with respect to SFE: the relative amplitude of the SFE distributions of SBs and MS galaxies in Figure 10 is expected to be a factor of 30 and the contrast between the peak of the SB distribution and the trough merely a factor two. A first attempt to construct a representative sampling of S-K space using the COLD-GASS survey was presented in Saintonge et al. (2012; see their Figure 6b) and demonstrated just how insignificant SBs are in determining the shape of the SF law for the bulk of the population.

6.3. *The Consumption of Gas Reservoirs During Starbursts*

As a consequence of the high efficiency with which gas is converted to stars in SB episodes, the gas reservoir in the host galaxy is used up more quickly than it can be replenished by accretion from the intergalactic medium. In Section 5.2.1 (see Figures 11 and 12) we showed that the overall gas fractions (i.e. gas fractions taking into account the molecular and stellar mass content throughout the whole starbursting galaxy) of SBs in our reference sample are indeed in general lower than the average gas fraction of galaxies which reside on the MS. We can use the 2-SFM description of SBs to explicitly calculate how we expect the gas content of starbursting galaxies to change once they have left their MS state. Given that each of the SBs in our calibration sample was observed in a different stage, this should be viewed as a comparison between the gas fraction prior to the onset of the burst and the gas fraction which would be measured approximately half-way through the SB event. If we consider the gas-to-stellar mass ratio $\mu_{\rm mol.} \equiv M_{\rm mol.}/M_\star$, the relation between pre-burst ($\mu_{\rm mol.}^{\rm pre-burst}$) and mid-burst gas content takes a simple and only boost-dependent form (see Figure 17(b)):

$$\mu_{\rm mol.}/\mu_{\rm mol.}^{\rm pre-burst} = ({\rm boost_{sSFR}})^{1-\gamma_{\rm SFE}} \quad . \qquad (30)$$

Here we have used that $\mu_{\rm mol.} = {\rm sSFR}/{\rm SFE}$ and that the sSFR and SFE of the SB are ${\rm sSFR}/{\rm sSFR^{pre-burst}} = {\rm boost_{sSFR}}$ and ${\rm SFE}/{\rm SFE^{pre-burst}} = ({\rm boost_{sSFR}})^{\gamma_{\rm SFE}}$, respectively. In Figure 17(a) we plot the variation of the typical ratio between mid-burst and pre-burst gas-to-stellar mass ratio as a function of sSFR excess. This average trend is the result of pairing up each point on the dotted curve for the evolution of $\mu_{\rm mol.}$(sSFR) for SBs in Figure 11(b) with a position on the corresponding relation for normal galaxies (dashed line in the same figure) by means of the boost-value $b_{\rm sSFR}^{\rm max}$ at the peak of the sSFR-dependent boost distribution (see Figure 6 and Section 4.2.3). Note that this calculation assumes the stellar mass in the starbursting galaxy and its pre-burst, MS state to be equal. By neglecting the fact that stellar mass has been added to the system during the first phase of the burst, our estimate of the ratio of mid-burst to pre-burst gas fraction effectively represents an upper limit. This simplification also makes the average trends in Figure 17 independent of stellar mass and redshift, because all dependence of the absolute value of the pre-burst gas fraction on these two factors (see e.g. Figure 14) is eliminated. The hatched/shaded regions straddling the median trend for $\mu_{\rm mol.}/\mu_{\rm mol.}^{\rm pre-burst}$ reflect the $1\,\sigma$

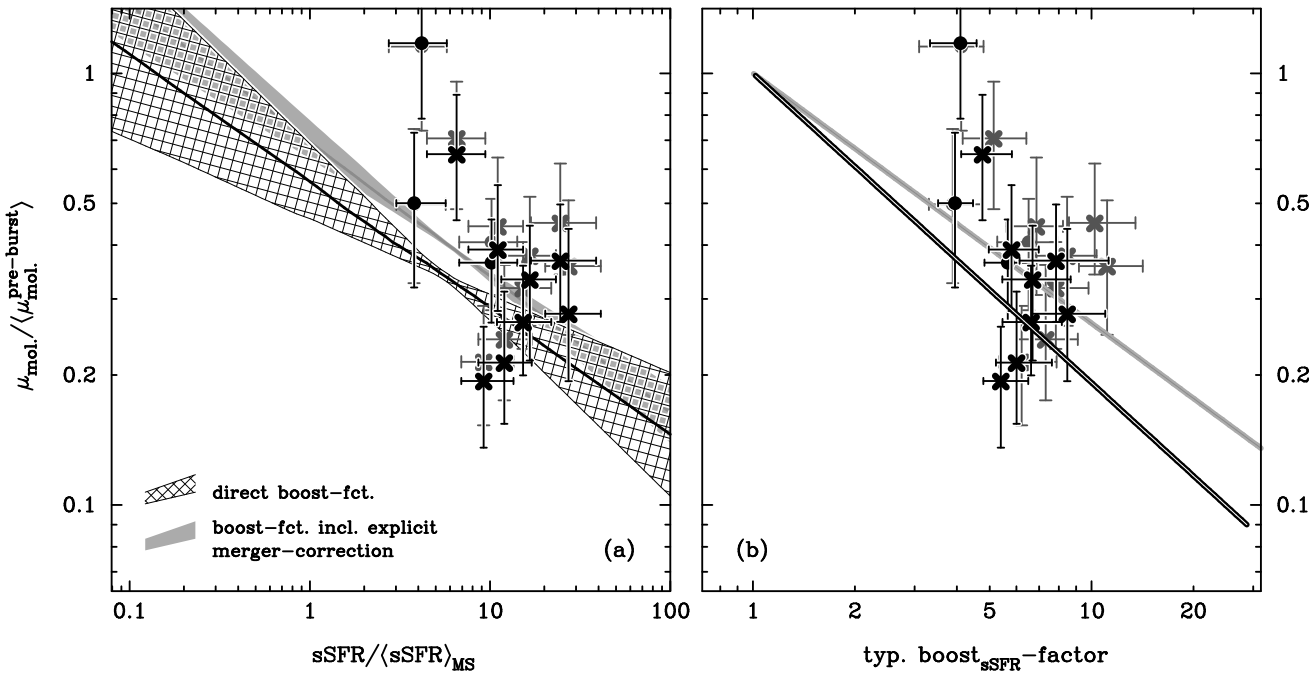

FIG. 17.—: (*a*) Predicted ratio between the molecular gas-to-stellar mass ratio of starbursts (SBs), $\mu_{\rm mol.} \equiv M_{\rm mol.}/M_\star$, and the average expected mass ratio $\langle \mu_{\rm mol.}^{\rm pre-burst} \rangle$ prior to the onset of the burst (i.e. during a phase of secular growth on the main sequence (MS)). The variation with sSFR reflects the different sSFR-dependence, for normal galaxies and SBs, of molecular gas-to-stellar mass ratios predicted by the 2-SFM description (see Figure 11(b); dashed and dotted lines, resp.). All symbols are as in Figure 9. The pre-burst gas-to-stellar mass ratios of SB galaxies from Downes & Solomon (1998) and Magdis et al. (2012b) were inferred assuming that these sources experienced the median (s)SFR boost expected for sources with the same sSFR excess (see Figure 6). (*b*) Dependence of the ratio $\mu_{\rm mol.}/\langle \mu_{\rm mol.}^{\rm pre-burst} \rangle$ on the sSFR boost of SB galaxies (see Equation 30). The black (grey) line shows the 2-SFM prediction for the average trend for the direct (merger-corrected) boost function.

uncertainty on the relation between average boost and sSFR (see also Figure 9(a)).

Based on the theoretical understanding derived from the 2-SFM approach, we are for the first time also able to infer – in a statistical sense – the pre-burst gas fractions of the SB galaxies in our reference sample, i.e. of eight local ULIRGs from Downes & Solomon (1998) and of three high-redshift SBs studied by Magdis et al. (2012b). We do so under the same assumptions as already used to derive the theoretical curve discussed above and superimpose our estimates on the 2-SFM prediction in both panels of Figure 17. Given that the typical sSFR excess of our reference SBs is about a factor of 10, their median $\mu_{\rm mol.}/\langle \mu_{\rm mol.}^{\rm pre-burst} \rangle$ of $\sim$0.35 is in quite good agreement with the 2-SFM prediction for the scenario of the "direct" boost function (black line in Figure 17(a)). For the most common SBs, which have an (s)SFR boost equal to four, the molecular mass-to-stellar mass ratio half-way through the burst is expected to lie around 35% (45%) of its initial value for the direct (merger-corrected) boost function.

It is interesting to explicitly compare our constraints on the gas fraction decrease during the SB phase with that expected in the case that the SB is triggered by a major merger. We approximate the SFR evolution during the interaction-induced burst by a top-hat function such that, at a time $t_{1/2}^{\rm merger}$ after the beginning of the burst, stellar mass and gas mass become $M_\star = M_\star^{\rm pre-burst} + {\rm SFR} \times t_{1/2}^{\rm merger}$ and $M_{\rm mol} = M_{\rm mol}^{\rm pre-burst} - {\rm SFR} \times t_{1/2}^{\rm merger}$. We write the mid-burst gas fraction as

$$
\begin{aligned}
f_{\rm mol.} &= \frac{M_{\rm mol.}}{M_{\rm mol.} + M_\star} = f_{\rm mol.}^{\rm pre-burst} - \frac{{\rm SFR} \times t_{1/2}^{\rm merger}}{M_{\rm mol.} + M_\star} \\
&= f_{\rm mol.}^{\rm pre-burst} - f_{\rm mol.} \, \frac{{\rm SFR} \times t_{1/2}^{\rm merger}}{M_{\rm mol.}} \\
&= f_{\rm mol.}^{\rm pre-burst} - f_{\rm mol.} \, \frac{\rm SFE}{{\rm SFE}^{\rm pre-burst}} \, \frac{t_{1/2}^{\rm merger}}{\tau^{\rm pre-burst}} \, ,
\end{aligned}
$$

and rearrange terms to obtain an expression for the ratio of the pre- and mid-burst gas fractions:

$$
f_{\rm mol.}/f_{\rm mol.}^{\rm pre-burst} = \left(1 + ({\rm boost})^{\gamma_{\rm SFE}} \, \frac{t_{1/2}^{\rm merger}}{\tau^{\rm pre-burst}} \right)^{-1} . \quad (31)
$$

Here we used that the total mass ($M_{\rm mol} + M_\star$) stays constant and that the SFE before and during the SB are related by the power-law in Equation 24. With a typical boost of approx. a factor of 6 and $\gamma_{\rm SFE} \sim 1.7$ (direct boost function) we find $f_{\rm mol.}/f_{\rm mol.}^{\rm pre-burst} \sim 0.5$ for $\tau^{\rm pre-burst} \approx 1\,{\rm Gyr}$ (the gas depletion time scale of MS galaxies) and $t_{1/2}^{\rm merger} \approx 50\,{\rm Myr}$ (we take this number to be about half the time for which interaction-induced SF is sustained in numerical simulations of galaxy mergers; e.g., Di Matteo et al. 2008, Bournaud et al. 2011b). Accounting for the mass and redshift dependence of the con-

version[23] between relative gas fractions and gas-to-stellar mass ratios, this corresponds to values of $\mu_{\rm mol.}/\mu_{\rm mol.}^{\rm pre-burst}$ in the range of 0.4–0.5. Obviously, the simple calculation leading up to Equation 31 will in reality be complicated by, e.g., gas loss and heating in merging systems (e.g., Cox et al. 2004), the modified balance between the atomic and molecular hydrogen phase in dense, turbulent media, and IMF variations as have been proposed for SB regions (e.g., Baugh et al. 2005, Papadopoulos et al. 2011, but see also Tacconi et al. 2008, Hayward et al. 2013). Taken at face value, the reasonable consistency of the estimates of the gas fraction decrease as per eqs. 30 and 31 may indicate that neither of these three factors plays a major role (or that these competing effects compensate each other).

Systematic comparisons between the molecular gas fractions of normal and starbursting galaxies will reveal whether the trends we proposed based on our small sample are robust. Further tests of the 2-SFM framework will now be discussed in Section 6.4.

6.4. *Observational Validation of Assumptions and Predictions Made by the 2-SFM Approach*

The 2-SFM framework as we have developed it so far has produced a remarkably simple description of SFGs over the last 10 Gyr. One may legitimately wonder whether this simplicity is the true imprint of fundamental laws that govern galaxy formation in a cold DM Universe or the outcome of an incomplete or selective view of the star-forming population due to observational limitations. The answer to this question depends to some extent also on the scope of any investigation. The occurrence of extreme behavior in rare outliers or small scale processes with little impact on global system properties – while relevant for a complete understanding of all complex aspects regulating SF – does not imply a general inadequacy of a simpler approach, as we have been advocating here, which aims to provide a panoramic treatment. Further confirmation of the validity of the 2-SFM description will instead involve both (a) revisiting some of its key ingredients and (b) testing its predictions.

Concerning point (a), the main focus should lie on verifying our hypothesis that galaxies with stellar mass significantly below $M_\star/M_\odot = 10^{10}$ follow the same relations that were calibrated on galaxies which are more massive than this threshold. The universality of the S-K law, for example, will soon be routinely tested with ALMA down to low stellar masses and out to high redshift by targeted observations of lensed galaxies. With deeper follow-up of molecular transitions, it will also be possible to identify evolution in the normalization (e.g., Tacconi et al. 2013) and curvature of the SF laws. A second assumption of the 2-SFM framework is that the double log-normal decomposition of the sSFR distribution is applicable also at $z \neq 2$. To ascertain this, tracers of dust-obscured SF are indispensable as extinction-corrected SFR measurements underestimate the true SFR of dusty SBs (e.g., Hughes et al. 1998, Trentham et al. 1999, Buat et al. 2005, Chapman et al. 2005, Daddi et al. 2007a, Casey et al. 2013) and place these on the locus of the star-forming MS. Obtaining good statistics on the rare starbursting sources (comoving number densities are of the order of $10^{-5}\,{\rm Mpc}^{-3}$) at the high-end tail of the sSFR distribution hence requires a combination of wide-area IR or radio surveys with complementary deep optical or UV data. A non-universality of the double log-normal decomposition in Equation 6 would introduce more variation in the simple SFE versus sSFR excess relations, etc. than is currently suggested by the fairly limited data. Any evolution in the sSFR decomposition into normal galaxies and SBs would imply a more complex, redshift-dependent behaviour of average scaling relations in the space of normalized molecular gas properties than is shown in Figure 11. A more fundamental question is whether the $z \sim 2$ sSFR distribution of Rodighiero et al. (2011), on which we perform the decomposition to begin with, is accurate. Little is known about the lower tail of the sSFR distribution, but it is unlikely that low-sSFR outliers to the MS should be responsible for a significant amount of SF activity (see S12, and references therein). In the absence of a single SF tracer to map out the distribution of galaxies in the SFR-$M_\star$ plane, the two-pronged approach of Rodighiero et al. (2011) for reconstructing it with two different diagnostics (IR emission for dust-obscured galaxies and UV-emission for the bulk of the MS population) relies on the consistency of the associated SF estimates. Extinction-corrected UV-fluxes and IR measurements at $z \sim 2$ are known to agree in an average sense (e.g., Daddi et al. 2007a), but the dispersion about the mean extinction correction could potentially contribute to the observed scatter of the MS of SFGs. The analysis of the MS at $0.5 < z < 1.3$ by Salmi et al. (2012) suggests that at least at these redshifts the dispersion of the sequence is mainly intrinsic. Since in Rodighiero et al. (2011) the sSFR distributions of galaxies with $M_\star \geq 10^{11}\,M_\odot$ are identical when computed with UV- or IR-emission, this seems to hold for the high-mass end of the $z \sim 2$ MS as well.

Concerning point (b), the analysis of this paper produced predictions that will be tested in future CO follow-up observations. With a good sampling of the transition region between MS and SB galaxies in the SFR–$M_\star$ plane ($^{\rm sSFR}/_{\langle {\rm sSFR} \rangle_{\rm MS}} \in [3,\ 5]$), these observations will quantify the scatter of, e.g. SFE and determine whether it is indeed larger than elsewhere, as is expected for a heterogeneous mixture of normal galaxies and SBs. While we predict such an increased dispersion to be measurable even using direct observables, e.g., $L'_{\rm CO}$ and $L_{\rm IR}$, an estimate of the CO-to-H_2 conversion factor $\alpha_{\rm CO}$ is necessary to calculate actual values of SFE and gas fractions. Our predictions for the variation of $\alpha_{\rm CO}$ in the SFR–$M_\star$ plane in Section 5.3.2 are in principle testable, but obtaining high-confidence measurements of $\alpha_{\rm CO}$ will remain a challenging task that is best tackled using different, complementary strategies in parallel. The gas-to-dust ratio technique employed by Leroy et al. (2011), Magdis et al. (2011, 2012b), Magnelli et al. (2012) is powerful, in that

[23] The relative gas fraction and gas-to-stellar mass ratio of the pre- and mid-burst state are related by

$$f_{\rm mol.}/f_{\rm mol.}^{\rm pre-burst} = \mu_{\rm mol.}/\mu_{\rm mol.}^{\rm pre-burst} \left(\frac{1+\mu_{\rm mol.}^{\rm pre-burst}}{1+\mu_{\rm mol.}} \right) .$$

For the massive SFGs discussed here, an initial gas-to-stellar mass ratio $\mu_{\rm mol.}^{\rm pre-burst}$ of ∼5-10% and 50-100% is expected at low and high-redshift, respectively. The term in brackets should thus vary between roughly 1.1 and <2.

it can provide constraints on the conversion factor for large data sets. However, the large scatter in measured gas-to-dust ratios in local, low-metallicity and low-mass galaxies (e.g., Draine & Li 2007, Galliano et al. 2008, Galametz et al. 2011, Rémy-Ruyer et al. 2014) indicates that this method becomes highly inaccurate for $z > 3$ galaxies and galaxies with stellar mass $M_\star \ll 10^{10}\,M_\odot$. An alternative approach is to interpret dynamical constraints from CO line profiles in the context of numerical simulations to infer $\alpha_{\rm CO}$ as proposed by Daddi et al. (2010a). However, even barring the systematic uncertainties on model DM distributions, the application of this method to large data sets may be impracticable as it requires high signal-to-noise data and a fine spectral sampling of the emission feature.

Finally, we note that the (s)SFR boost of SBs, although much less easily determined than their (s)SFR excess with respect to the average of the MS population, is in principle measurable using high-fidelity and ideally also spatially resolved spectroscopy. When compared to the output of stellar evolution models, this kind of data would allow a detailed reconstruction of the SFH of boosted sources prior to the onset of burst activity. It would hence also reveal whether galaxies that show a strong sSFR excess are truly experiencing short-term boosting of their activity at all redshifts or whether they are merely a high-intensity tail of the "normal" population. The episodic and merger-related nature of ULIRGs at low redshift is well-accepted (e.g., Sanders & Mirabel 1996; and references therein) but is harder to prove for SBs in the distant universe (e.g., Tacconi et al. 2006, Daddi et al. 2009, Ivison et al. 2013). The supporting evidence which has been accumulating in recent years, however (e.g., IR diagnostics, ISM temperatures, host galaxy structure and kinematics; see also our overview in the introduction and the discussion in Section 6.1), is at the basis of our proposed split into SB and normal galaxy populations and the assumption that it provides a valid description of the star-forming population of much of the history of the universe.

7. SUMMARY

The 2-Star Formation Mode ("2-SFM") framework provides a conceptually simple and self-consistent scheme for the prediction of basic properties of the star-forming galaxy (SFG) population. It relies on basic observables – e.g. the evolution of specific star formation rate (sSFR) in main-sequence (MS) galaxies or their stellar mass ($M_\star$) distribution – and their mathematical description – e.g. the Schechter function parametrization of the stellar mass function or slope and normalization of the Schmidt-Kennicutt (S-K) law – to produce an analytico-empirical description of the statistical properties of SFGs which can be both predictive and help (re)interpret existing measurements. A central ingredient of the 2-SFM framework is the distinction between "normal" SFGs that reside on the star-forming MS and starbursts (SBs) that are much rarer and regarded here as a "perturbation" of the MS state (see Section 4.1) that is probably dynamically induced or induced by interactions. We recently applied this approach successfully for the prediction of IR luminosity functions at $z \lesssim 2.5$ in S12 and of galaxy number counts between 24 and 1100 μm and at 1.4 GHz in Béthermin et al. (2012). In this article we have investigated the observational evidence that the molecular gas properties of massive ($M_\star \gtrsim 10^{10}\,M_\odot$) SFGs are amenable to a similarly simplified description as their IR-emission.

We use a sample of approx. 130 normal SFGs (see Sections 2.1.1 and 2.1.2) to calibrate scaling relations that allow us to predict – in anticipation of future complete and unbiased surveys of the ISM content of galaxies – how molecular gas properties of secularly evolving SFGs at $z < 3$ vary depending on their SFR and stellar mass. When all involved quantities are normalized to the value a given observable takes for an average MS galaxy, these trends become strikingly simple (and in general also independent of redshift). In particular, we find that:

1. All literature measurements of SFR and $M_{\rm mol.}$ in massive ($M_\star > 10^{10}\,M_\odot$) MS galaxies at $z < 3$ are compatible with the existence of a universal (i.e., redshift-invariant) star formation (SF) law for such systems. This integrated S-K relation is slightly supra-linear ($\mathrm{SFR} \propto M_{\rm mol.}^{1.2}$) and tight (dispersion $\sim$0.2 dex; see Figure 2).

2. Star formation efficiency (SFE) varies very little across the MS (see Figure 8) while the molecular gas mass fractions, $M_{\rm mol.}/M_\star$, increase almost linearly with (s)SFR for MS galaxies of a fixed stellar mass.

3. Changes in the sSFR of MS galaxies are strongly correlated with changes of the molecular gas fraction, implying that both the dispersion of the MS and the cosmic evolution of sSFR in general reflect variations of the gas content of normal galaxies (see Figure 13).

Based on this characterization of gas in the MS population, we are then able to predict the molecular gas properties of SB galaxies which – in the 2-SFM approach – start out as normal galaxies that subsequently experience boosting to higher (s)SFRs. In this paper we go beyond assuming that there are two discrete modes of SF. Instead, we adopt a continuous description of SFE-variations for SBs, in which small SFR enhancements translate to small SFE increases as well. By considering the excess SFR and excess SFE of observed SB galaxies with measured CO-to-H_2 conversion factors $\alpha_{\rm CO}$, we infer that SFE grows more strongly in the burst-phase than SFR (see Section 5.1.2). Taking into account the changing, sSFR-dependent mixture of SB and normal galaxies that constitutes the total star-forming population, this leads to the following expectations:

4. Normal SFGs and SBs are separated more strongly in the S-K plane than in the space of $M_\star$ and SFR (see Figure 10). However, a separation that is as discrete as currently suggested by observations is not expected and is likely the outcome of the incomplete sampling of the S-K plane in surveys explicitly targeting strong SBs and average MS galaxies.

5. Even if SBs are treated as a continuous extension of normal galaxies, with depletion times that decrease in proportion to their burst-related (s)SFR

enhancement, a nearly step-like, roughly tenfold increase of the SFE is predicted at the sSFR where starbursting sources begin to outnumber the MS population (see Figure 11(a)).

6. A similar, albeit less pronounced step-like behavior is predicted for molecular gas fractions (see Figure 11(b)): while these continuously rise across the MS (see point 2 above), the higher SFE of SBs causes their gas fractions to decrease to a value that is smaller than the average observed for a typical MS galaxy. In Section 6.3 we provide recipes for how much gas fractions are expected to drop, depending on the intensity of the SB, if – as is expected for, e.g., merger-induced SBs – the timescale for the exhaustion of the molecular fuel reservoir is much shorter than the timescale for accretion of pristine gas from the cosmic web.

Based on the systematic difference between the $L'_{\rm CO}/L_{\rm IR}$ and $M_{\rm H_2}/L_{\rm IR}$ ratios of SBs, we derive an empirical recipe for the CO-to-H_2 conversion factor, $\alpha_{\rm CO}$, of SB galaxies (see Section 5.3.1). In combination with an assumed metallicity dependence of $\alpha_{\rm CO}$ for MS galaxies, we are able to predict $\alpha_{\rm CO}$ variations for SFGs throughout the $M_\star$ versus SFR plane (see Section 5.3.2). Due to the flatness of the mass-metallicity relation at high stellar masses, the conversion factor of Milky-Way-mass galaxies is expected to resemble the canonical Milky Way value even at the cosmic epoch when the SF history of the universe peaked.

Our understanding of molecular gas at high redshift will progress rapidly in the near future as the ALMA observatory acquires increasing volumes of data that will quickly outgrow the currently available information. The 2-SFM description of SFGs provides a flexible methodological framework that can adapt to future findings, e.g. by re-calibrating the relation between SFR boosts and SFE enhancements once larger samples of SB galaxies become available, or by recalibrating the Schmidt-Kennicutt relation should new measurements reveal that the relation between SFR and molecular gas mass is more complex than it appears at present. The simple, analytico-empirical description of molecular gas in star-forming galaxies developed in the present work will be used to infer the evolution of molecular gas mass functions and CO luminosity functions, as well as CO source counts in two forthcoming papers.

We thank F. Bournaud, A. Cibinel, P. Di Matteo, S. Ellison, R. Feldmann, A. Karim, K. Kraljic, S. Lilly, G. Popping, F. Renaud, D. Riechers and F. Walter for helpful discussions/suggestions, as well as J. Scudder for providing the data shown in Figure 5 and A. Leroy for kindly sharing new HERACLES measurements with us ahead of publication. We are grateful to both our referees for a careful reading of the paper and valuable suggestions for improvements.

M.T.S., M.B. and E.D. acknowledge financial support from the EC through ERC-StG/ UPGAL 240039 and grant ANR-08-JCJC-0008. S.J. was supported by ERC-grant ERC-StG-257720.

This article is partly based on observations with AKARI, a JAXA project with the participation of ESA. It has also made use of NED which is operated by the Jet Propulsion Laboratory, California Institute of Technology, under contract with the National Aeronautics and Space Administration. Much of the analysis presented here was carried out in the Perl Data Language (PDL; Glazebrook & Economou, 1997), which can be obtained from `http://pdl.perl.org`.

APPENDIX

LITERATURE MEASUREMENTS OF SPECIFIC STAR FORMATION RATE IN MS GALAXIES

The locus of the MS is known to depend on sample selection (e.g., Karim et al. 2011) and, in particular, on how actively star-forming the sample under consideration is. With the aim of deriving a representative, average evolution we gathered measurements from several recent studies of the distribution of SFGs in the ($M_\star$, SFR) plane that employed different selection criteria (e.g., different color cuts or selection by morphology, by near-IR flux/mass or by SFR), chose different SF tracers (e.g., UV, IR or radio emission) and/or adopted a variety of measurement techniques (e.g. individual detections versus source stacking). By considering two separate mass scales at 5×10^9 and $5\times10^{10}\,M_\odot$ we obtain a constraint on the typical exponent ν of the $M_\star$ dependence of sSFR, $\mathrm{sSFR}\propto {M_\star}^\nu$. We find that an exponent $\nu\simeq$-0.2 reproduces the systematic shift between the sSFR evolution of galaxies in the two $M_\star$-bins (see Figure 18). This slope agrees closely with the value $\nu=$-0.21$\pm$0.04 we adopted (based on the $z\sim2$ MS presented in Rodighiero et al. 2011) in our previous publications investigating the viability of the 2-SFM framework (see S12, Béthermin et al. 2012). Our literature compilation covers the redshift range $z<7$, with a majority of the measurements tracing the steep rise of sSFR in MS galaxies out to $z\sim3$. At $z>4$, drop-out samples constrain the sSFR evolution at $M_\star\sim5\times10^9\,M_\odot$, but they do not contain enough high-mass galaxies to probe the evolution in our second, more massive bin.

We parameterize the evolution of sSFR with a smoothly varying function of redshift with five free parameters which we fit to the data in Figure 18:

$$\mathrm{sSFR}(M_\star,\,z) = N(M_\star)\exp\left(\frac{A{\cdot}z}{1+B{\cdot}z^C}\right)\ ,\ \text{where} \tag{A1}$$

$$N(M_\star) = N(5{\times}10^{10}\,M_\odot)\,10^{\nu\,\log\left(M_\star/[5\times10^{10}\,M_\odot]\right)}$$
$$A = 2.05^{+0.33}_{-0.20}$$
$$B = 0.16^{+0.15}_{-0.07}$$
$$C = 1.54\pm0.32$$

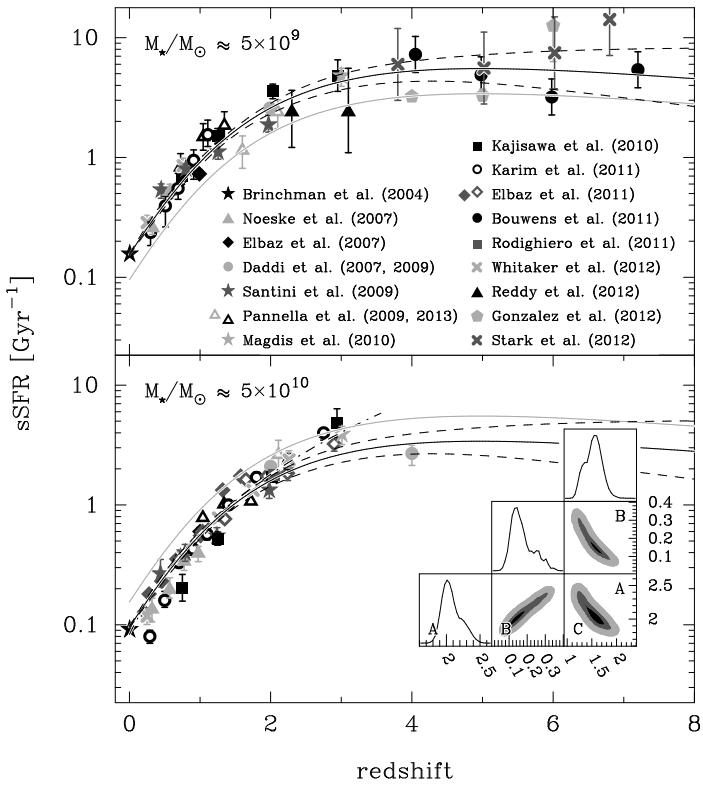

FIG. 18.—: Redshift dependence of the sSFR of SFGs with stellar mass $M_\star/M_\odot \approx 5\times10^9$ (*top*) and 5×10^{10} (*bottom*), as published in the recent literature (see legend; where necessary, literature values from adjacent mass bins were used to interpolate to the mass scales displayed here). Measurements derived based on image-stacking are indicated with open symbols and error bars denote the uncertainty on the sSFR average rather than the sSFR scatter in the population. Solid/dashed black lines – the best-fit evolution of the sSFR – parameterized as in Equation A1 (see inset panels on lower right for the covariance between the free parameters of the fit) – and associated $2\,\sigma$-errors.; light grey lines – sSFR evolution in the other of the two stellar mass bins depicted in the figure, for comparison; dot-dashed line – evolution according to $(1+z)^{2.8}$ as used in S12 for the range $z \lesssim 2$.

Here ν is the slope of the log(sSFR) versus log($M_\star$) relation as above and the normalization at a stellar mass of $5\times10^{10}\,M_\odot$ is $N(5\times10^{10}\,M_\odot) = 0.095^{+0.002}_{-0.003}\,\mathrm{Gyr}^{-1}$. The quoted uncertainties are 68% confidence limits as determined by a Monte Carlo Markov Chain (10^6 realizations).

In Figure 18 the $1\,\sigma$-errors on the average sSFR evolution according to Equation A1 are marked by dashed lines. Due to the abundant data (e.g., Noeske et al. 2007, Elbaz et al. 2007, Daddi et al. 2007b, 2009, Pannella et al. 2009, Karim et al. 2011, Rodighiero et al. 2011, Whitaker et al. 2012) and their generally high fidelity (error bars on the individual literature measurements span the statistical uncertainty on the mean rather than the population dispersion), formal uncertainties at $z < 2$ are small but increase steadily thereafter, reflecting the much sparser data at the highest redshifts. The growing formal errors do not include the systematic evolutionary uncertainties at $z > 3$, where the sSFRs of drop-out galaxies have been subject to frequent revision on an almost yearly basis. Initial measurements at $4 < z < 8$ by Stark et al. (2009) and González et al. (2010) – subsequently modified by Bouwens et al. (2012) to account for dust-extinction – suggested a much more gradual sSFR evolution than expected by most theoretical models (see, e.g., Weinmann et al. 2011, and references therein). The most recent efforts have focused on quantifying the impact of nebular emission lines (e.g., Schaerer & de Barros 2010, Stark et al. 2013, de Barros et al. 2014, González et al. 2014) on stellar mass measurements. It is presently unclear, however, whether corrections for nebular emission cause significant deviations from the nearly flat evolution that was found prior to their implementation: line-corrected sSFR values scatter about the Bouwens et al. (2012) measurements[24] at $z < 6$ and only then become consistently larger than non-corrected ones. Our analytical parameterization of the sSFR evolution does not trace the apparent increase at $z \geq 6$ but these high redshifts are not the main focus of this article.

[24] Independent, albeit tentative evidence for a flattening of the sSFR evolution in the range $2 < z < 4$ is provided by the similar gas fractions in $z \sim 2$ BM/BX-selected galaxies and two $z \sim 3$ LBGs by Tacconi et al. (2010) and Magdis et al. (2012a), respectively. See Magdis et al. 2012a and our Section 5.2.2 for further discussion of the co-evolution of gas fractions and sSFR with cosmic time.

REFERENCES

Abdo, A. A., Ackermann, M., Ajello, M., et al. 2010, ApJ, 710, 133
Agertz, O., Teyssier, R., & Moore, B. 2009, MNRAS, 397, L64
Aravena, M., Carilli, C., Daddi, E., et al. 2010, ApJ, 718, 177
Arnouts, S., Walcher, C. J., Le Fèvre, O., et al. 2007, A&A, 476, 137
Baldry, I. K., & Glazebrook, K. 2003, ApJ, 593, 258
Barton, E. J., Geller, M. J., & Kenyon, S. J. 2000, ApJ, 530, 660

Baugh, C. M., Lacey, C. G., Frenk, C. S., et al. 2005, MNRAS, 356, 1191
Bauermeister, A., Blitz, L., Bolatto, A., et al. 2013a, ApJ, 768, 132
Bauermeister, A., Blitz, L., Bolatto, A., et al. 2013b, ApJ, 763, 64
Behroozi, P. S., Wechsler, R. H., & Conroy, C. 2013, ApJ, 770, 57
Belli, S., Jones, T., Ellis, R. S., & Richard, J. 2013, ApJ, 772, 141
Bigiel, F., Leroy, A., Walter, F., et al. 2008, AJ, 136, 2846
Bigiel, F., Leroy, A. K., Walter, F., et al. 2011, ApJ, 730, L13
Béthermin, M., Daddi, E., Magdis, G., et al. 2012, ApJ, 757, L23
Bolatto, A. D., Leroy, A. K., Rosolowsky, E., Walter, F., & Blitz, L. 2008, ApJ, 686, 948
Bolatto, A. D., Wolfire, M., & Leroy, A. K. 2013, ARA&A, 51, 207
Boselli, A., Lequeux, J., & Gavazzi, G. 2002, A&A, 384, 33
Bouché, N., Dekel, A., Genzel, R., et al. 2010, ApJ, 718, 1001
Bouwens, R. J., Illingworth, G. D., Oesch, P. A., et al. 2012, ApJ, 754, 83
Bournaud, F., Powell, L. C., Chapon, D., & Teyssier, R. 2011, IAU Symposium, 271, 160
Bournaud, F., Chapon, D., Teyssier, R., et al. 2011, ApJ, 730, 4
Brinchmann, J., Charlot, S., White, S. D. M., et al. 2004, MNRAS, 351, 1151
Bryant, P. M., & Scoville, N. Z. 1996, ApJ, 457, 678
Buat, V., Iglesias-Páramo, J., Seibert, M., et al. 2005, ApJ, 619, L51
Buckley, J., &. James, I. 1979, Biometrika, 66, 429
Carilli, C. L., Daddi, E., Riechers, D., et al. 2010, ApJ, 714, 1407
Casey, C. M., Chen, C.-C., Cowie, L. L., et al. 2013, MNRAS, 436, 1919
Ceverino, D., Dekel, A., & Bournaud, F. 2010, MNRAS, 404, 2151
Chabrier, G. 2003, PASP, 115, 763
Chapman, S. C., Helou, G., Lewis, G. F., & Dale, D. A. 2003, ApJ, 588, 186
Chapman, S. C., Blain, A. W., Smail, I., & Ivison, R. J. 2005, ApJ, 622, 772
Chary, R., & Elbaz, D. 2001, ApJ, 556, 562
Chenu, J. Y., Carter, M., Maier, D., Bortolotti, Y., Butin, G., Serres, P., Boucher, C., Mattiocco, F., & Lazareff, B. 2007, 'New SIS receivers for the IRAM Plateau de Bure interferometer', Joint 32nd International Conference on Infrared and Millimeter Waves, 2007 and the 2007 15th International Conference on Terahertz Electronics. IRMMW-THz., IEEE Conference Proceedings, 176-177
Combes, F., García-Burillo, S., Braine, J., et al. 2011, A&A, 528, A124
Combes, F., García-Burillo, S., Braine, J., et al. 2013, A&A, 550, A41
Cowie, L. L., & Barger, A. J. 2008, ApJ, 686, 72
Cox, T. J., Primack, J., Jonsson, P., & Somerville, R. S. 2004, ApJ, 607, L87
Cox, T. J., Jonsson, P., Somerville, R. S., Primack, J. R., & Dekel, A. 2008, MNRAS, 384, 386
da Cunha, E., Charmandaris, V., Díaz-Santos, T., et al. 2010, A&A, 523, A78
Cresci, G., Mannucci, F., Sommariva, V., et al. 2012, MNRAS, 421, 262
Cucciati, O., Tresse, L., Ilbert, O., et al. 2012, A&A, 539, A31
Daddi, E., Dickinson, M., Morrison, G., et al. 2007a, ApJ, 670, 156
Daddi, E., Alexander, D. M., Dickinson, M., et al. 2007b, ApJ, 670, 173
Daddi, E., Dannerbauer, H., Elbaz, D., et al. 2008, ApJ, 673, L21
Daddi, E., Dannerbauer, H., Stern, D., et al. 2009, ApJ, 694, 1517
Daddi, E., Bournaud, F., Walter, F., et al. 2010a, ApJ, 713, 686
Daddi, E., Elbaz, D., Walter, F., et al. 2010b, ApJ, 714, L118
Dale, D. A., Gil de Paz, A., Gordon, K. D., et al. 2007, ApJ, 655, 863
Damen, M., Labbé, I., Franx, M., et al. 2009, ApJ, 690, 937
Dannerbauer, H., Daddi, E., Riechers, D. A., et al. 2009, ApJ, 698, L178
Davé, R., Finlator, K., & Oppenheimer, B. D. 2011, MNRAS, 115
de Barros, S., Schaerer, D., & Stark, D. P. 2014, A&A, 563, A81
Dekel, A., Birnboim, Y., Engel, G., et al. 2009, Nature, 457, 451
Denicoló, G., Terlevich, R., & Terlevich, E. 2002, MNRAS, 330, 69
Dessauges-Zavadsky, M., Christensen, L., D'Odorico, S., Schaerer, D., & Richard, J. 2011, A&A, 533, A15
Di Matteo, P., Combes, F., Melchior, A.-L., & Semelin, B. 2007, A&A, 468, 61
Di Matteo, P., Bournaud, F., Martig, M., et al. 2008, A&A, 492, 31
Downes, D., & Solomon, P. M. 1998, ApJ, 507, 615
Draine, B. T., & Li, A. 2007, ApJ, 657, 810
Duffy, A. R., Kay, S. T., Battye, R. A., et al. 2012, MNRAS, 420, 2799
Dunne, L., Ivison, R. J., Maddox, S., et al. 2009, MNRAS, 394, 3
Elbaz, D., Daddi, E., Le Borgne, D., et al. 2007, A&A, 468, 33
Elbaz, D., Hwang, H. S., Magnelli, B., et al. 2010, A&A, 518, L29
Elbaz, D., Dickinson, M., Hwang, H. S., et al. 2011, A&A, 533, A119
Erb, D. K., Shapley, A. E., Pettini, M., et al. 2006, ApJ, 644, 813
Feldmann, R., Gnedin, N. Y., & Kravtsov, A. V. 2012a, ApJ, 747, 124
Feldmann, R., Gnedin, N. Y., & Kravtsov, A. V. 2012b, ApJ, 758, 127
Feldmann, R. 2013, MNRAS, 433, 1910
Förster Schreiber, N. M., Genzel, R., Bouché, N., et al. 2009, ApJ, 706, 1364
Förster Schreiber, N. M., Shapley, A. E., Genzel, R., et al. 2011, ApJ, 739, 45
Frayer, D. T., Ivison, R. J., Scoville, N. Z., et al. 1998, ApJ, 506, L7
Fontanot, F., De Lucia, G., Monaco, P., Somerville, R. S., & Santini, P. 2009, MNRAS, 397, 1776
Fu, J., Kauffmann, G., Li, C., & Guo, Q. 2012, MNRAS, 424, 2701
Galametz, M., Madden, S. C., Galliano, F., et al. 2011, A&A, 532, A56
Galliano, F., Dwek, E., & Chanial, P. 2008, ApJ, 672, 214
Geach, J. E., Smail, I., Coppin, K., Moran, S. M., Edge, A. C., & Ellis, R. S. 2009, MNRAS, 395, L62
Geach, J. E., Smail, I., Moran, S. M., MacArthur, L. A., Lagos, C. d. P., & Edge, A. C. 2011, ApJ, 730, L19
Geach, J. E., Chapin, E. L., Coppin, K. E. K., et al. 2013, MNRAS, 432, 53
Genzel, R., Tacconi, L. J., Gracia-Carpio, J., et al. 2010, MNRAS, 407, 2091
Genzel, R., Tacconi, L. J., Combes, F., et al. 2012, ApJ, 746, 69
Gilbank, D. G., Bower, R. G., Glazebrook, K., et al. 2011, MNRAS, 414, 304
Glover, S. C. O., & Mac Low, M.-M. 2011, MNRAS, 412, 337
González, V., Labbé, I., Bouwens, R. J., et al. 2010, ApJ, 713, 115
González, V., Bouwens, R., Illingworth, G., et al. 2014, ApJ, 781, 34
Graciá-Carpio, J., Sturm, E., Hailey-Dunsheath, S., et al. 2011, ApJ, 728, L7
Greve, T. R., Bertoldi, F., Smail, I., et al. 2005, MNRAS, 359, 1165
Gruppioni, C., Pozzi, F., Rodighiero, G., et al. 2013, MNRAS, 432, 23
Guo, K., Zheng, X. Z., & Fu, H. 2013, ApJ, 778, 23
Hahn, O., Teyssier, R., & Carollo, C. M. 2010, MNRAS, 405, 274
Hayward, C. C., Narayanan, D., Kereš, D., et al. 2013, MNRAS, 428, 2529
Heinis, S., Buat, V., Béthermin, M., et al. 2014, MNRAS, 437, 1268
Heisler, C. A., & Vader, J. P. 1994, AJ, 107, 35
Hodge, J. A., Carilli, C. L., Walter, F., et al. 2012, ApJ, 760, 11
Hopkins, P. F., Hernquist, L., Cox, T. J., et al. 2006, ApJS, 163, 1
Hopkins, P. F., Cox, T. J., Younger, J. D., & Hernquist, L. 2009, ApJ, 691, 1168
Hopkins, P. F., Younger, J. D., Hayward, C. C., Narayanan, D., & Hernquist, L. 2010, MNRAS, 402, 1693
Howell, J. H., Armus, L., Mazzarella, J. M., et al. 2010, ApJ, 715, 572
Hughes, D. H., Serjeant, S., Dunlop, J., et al. 1998, Nature, 394, 241
Hwang, H. S., Elbaz, D., Magdis, G., et al. 2010, MNRAS, 409, 75
Hwang, H. S., Elbaz, D., Dickinson, M., et al. 2011, A&A, 535, A60
Isobe, T., Feigelson, E. D., & Nelson, P. I. 1986, ApJ, 306, 490
Israel, F. P. 1997, A&A, 328, 471
Ivison, R. J., Chapman, S. C., Faber, S. M., et al. 2007, ApJ, 660, L77
Ivison, R. J., Papadopoulos, P. P., Smail, I., et al. 2011, MNRAS, 412, 1913
Ivison, R. J., Swinbank, A. M., Smail, I., et al. 2013, ApJ, 772, 137
Juneau, S., Narayanan, D. T., Moustakas, J., et al. 2009, ApJ, 707, 1217
Juneau, S., Dickinson, M., Alexander, D. M., & Salim, S. 2011, ApJ, 736, 104
Kajisawa, M., Ichikawa, T., Yamada, T., et al. 2010, ApJ, 723, 129
Kampczyk, P., Lilly, S. J., de Ravel, L., et al. 2013, ApJ, 762, 43
Kaplan, E. L. & Meier, P. 1958, J. Am. Statist. Assoc., 53, 457
Karim, A., Schinnerer, E., Martínez-Sansigre, A., et al. 2011, ApJ, 730, 61
Kartaltepe, J. S., Dickinson, M., Alexander, D. M., et al. 2012, ApJ, 757, 23
Kaviraj, S., Cohen, S., Windhorst, R. A., et al. 2013, MNRAS, 429, L40
Kawada, M., Baba, H., Barthel, P. D., et al. 2007, PASJ, 59, 389

Kennicutt, R. C., Jr. 1998a, ApJ, 498, 541
Kennicutt, R. C., Jr. 1998b, ARA&A, 36, 189
Kewley, L. J., & Dopita, M. A. 2002, ApJS, 142, 35
Kewley, L. J., & Ellison, S. L. 2008, ApJ, 681, 1183
Kobulnicky, H. A., & Kewley, L. J. 2004, ApJ, 617, 240
Kroupa, P. 2001, MNRAS, 322, 231
Krumholz, M. R., Dekel, A., & McKee, C. F. 2012, ApJ, 745, 69
Lara-López, M. A., Cepa, J., Bongiovanni, A., et al. 2010, A&A, 521, L53
Lara-López, M. A., López-Sánchez, Á. R., & Hopkins, A. M. 2013, ApJ, 764, 178
Larson, D., Dunkley, J., Hinshaw, G., et al. 2011, ApJS, 192, 16
Laskar, T., Berger, E., & Chary, R.-R. 2011, ApJ, 739, 1
Lee, J. C., Gil de Paz, A., Kennicutt, R. C., Jr., et al. 2011, ApJS, 192, 6
Leitner, S. N. 2012, ApJ, 745, 149
Leroy, A. K., Walter, F., Brinks, E., Bigiel, F., de Blok, W. J. G., Madore, B., & Thornley, M. D. 2008, AJ, 136, 2782
Leroy, A. K., et al. 2009, AJ, 137, 4670
Leroy, A. K., et al. 2011, ApJ, 737, 12
Leroy, A. K., Walter, F., Sandstrom, K., et al. 2013, AJ, 146, 19
Liu, X., Shapley, A. E., Coil, A. L., Brinchmann, J., & Ma, C.-P. 2008, ApJ, 678, 758
Magdis, G. E., Rigopoulou, D., Huang, J.-S., & Fazio, G. G. 2010, MNRAS, 401, 1521
Magdis, G. E., Daddi, E., Elbaz, D., et al. 2011, ApJ, 740, L15
Magdis, G. E., Daddi, E., Sargent, M., et al. 2012a, ApJ, 758, L9
Magdis, G. E., Daddi, E., Béthermin, M., et al. 2012b, ApJ, 760, 6
Magnelli, B., Elbaz, D., Chary, R. R., Dickinson, M., Le Borgne, D., Frayer, D. T., & Willmer, C. N. A. 2009, A&A, 496, 57
Magnelli, B., Elbaz, D., Chary, R. R., Dickinson, M., Le Borgne, D., Frayer, D. T., & Willmer, C. N. A. 2011, A&A, 528, A35
Magnelli, B., Saintonge, A., Lutz, D., et al. 2012, A&A, 548, A22
Magnelli, B., Lutz, D., Saintonge, A., et al. 2014, A&A, 561, A86
Magrini, L., Sommariva, V., Cresci, G., et al. 2012, MNRAS, 426, 1195
Maiolino, R., Neri, R., Beelen, A., et al. 2007, A&A, 472, L33
Mannucci, F., Cresci, G., Maiolino, R., Marconi, A., & Gnerucci, A. 2010, MNRAS, 408, 2115
Martig, M., Bournaud, F., Teyssier, R., & Dekel, A. 2009, ApJ, 707, 250
Mihos, J. C., & Hernquist, L. 1996, ApJ, 464, 641
Monaco, P., Murante, G., Borgani, S., & Dolag, K. 2012, MNRAS, 421, 2485
Moshir, M., Kopman, G., & Conrow, T. A. O. 1992, *IRAS* Faint Source Survey, Explanatory supplement version 2, JPL, Pasadena
Moustakas, J., Kennicutt, R. C., Jr., Tremonti, C. A., et al. 2010, ApJS, 190, 233
Mullaney, J. R., Daddi, E., Béthermin, M., et al. 2012a, ApJ, 753, L30
Mullaney, J. R., Pannella, M., Daddi, E., et al. 2012b, MNRAS, 419, 95
Narayanan, D., Cox, T. J., Shirley, Y., et al. 2008, ApJ, 684, 996
Narayanan, D., Krumholz, M., Ostriker, E. C., & Hernquist, L. 2011, MNRAS, 418, 664
Narayanan, D., Bothwell, M., & Davé, R. 2012, MNRAS, 426, 1178
Noeske, K. G., Weiner, B. J., Faber, S. M., et al. 2007, ApJ, 660, L43
Oesch, P. A., Carollo, C. M., Feldmann, R., et al. 2010, ApJ, 714, L47
Oliver, S., Frost, M., Farrah, D., et al. 2010, MNRAS, 405, 2279
Omont, A., Petitjean, P., Guilloteau, S., et al. 1996, Nature, 382, 428
Pannella, M., Carilli, C. L., Daddi, E., et al. 2009, ApJ, 698, L116
Pannella, M., Elbaz, D., Daddi, E., et al. 2014, arXiv:1407.5072
Papadopoulos, P. P., Thi, W.-F., Miniati, F., & Viti, S. 2011, MNRAS, 414, 1705
Papadopoulos, P. P., van der Werf, P., Xilouris, E., Isaak, K. G., & Gao, Y. 2012, ApJ, 751, 10
Park, C., & Choi, Y.-Y. 2009, ApJ, 691, 1828
Peng, Y.-J., Lilly, S. J., Kovač, K., et al. 2010, ApJ, 721, 193
Perley, R. A., Chandler, C. J., Butler, B. J., & Wrobel, J. M. 2011, ApJ, 739, L1
Pettini, M., & Pagel, B. E. J. 2004, MNRAS, 348, L59
Pilyugin, L. S. 2001, A&A, 374, 412
Popping, G., Caputi, K. I., Somerville, R. S., & Trager, S. C. 2012, MNRAS, 425, 2386
Reddy, N. A., & Steidel, C. C. 2009, ApJ, 692, 778
Reddy, N. A., Pettini, M., Steidel, C. C., et al. 2012, ApJ, 754, 25
Rémy-Ruyer, A., Madden, S. C., Galliano, F., et al. 2014, A&A, 563, A31
Renaud, F., Kraljic, K., & Bournaud, F. 2012, ApJ, 760, L16
Richard, J., Jones, T., Ellis, R., et al. 2011, MNRAS, 413, 643
Riechers, D. A., Walter, F., Carilli, C. L., et al. 2006, ApJ, 650, 604
Riechers, D. A., Cooray, A., Omont, A., et al. 2011, ApJ, 733, L12
Robaina, A. R., Bell, E. F., Skelton, R. E., et al. 2009, ApJ, 704, 324
Robertson, B. E., & Kravtsov, A. V. 2008, ApJ, 680, 1083
Rodighiero, G., et al. 2010, A&A, 515, A8
Rodighiero, G., Daddi, E., Baronchelli, I., et al. 2011, ApJ, 739, L40
Rosario, D. J., Santini, P., Lutz, D., et al. 2013, ApJ, 771, 63
Rujopakarn, W., Rieke, G. H., Eisenstein, D. J., & Juneau, S. 2011, ApJ, 726, 93
Saintonge, A., et al. 2011a, MNRAS, 415, 32
Saintonge, A., Tacconi, L. J., Fabello, S., et al. 2012, ApJ, 758, 73
Salim, S., Rich, R. M., Charlot, S., et al. 2007, ApJS, 173, 267
Salmi, F., Daddi, E., Elbaz, D., et al. 2012, ApJ, 754, L14
Salpeter, E. E. 1955, ApJ, 121, 161
Sanders, D. B., Soifer, B. T., Elias, J. H., et al. 1988, ApJ, 325, 74
Sanders, D. B., & Mirabel, I. F. 1996, ARA&A, 34, 749
Sandstrom, K. M., Leroy, A. K., Walter, F., et al. 2013, ApJ, 777, 5
Santini, P., Fontana, A., Grazian, A., et al. 2009, A&A, 504, 751
Santini, P., Maiolino, R., Magnelli, B., et al. 2014, A&A, 562, A30
Sargent, M. T., Béthermin, M., Daddi, E., & Elbaz, D. 2012, ApJ, 747, L31 (S12)
Schaerer, D., & de Barros, S. 2010, A&A, 515, A73
Schmidt, M. 1959, ApJ, 129, 243
Schruba, A., Leroy, A. K., Walter, F., et al. 2012, AJ, 143, 138
Scoville, N., Aussel, H., Sheth, K., et al. 2014, ApJ, 783, 84
Scudder, J. M., Ellison, S. L., Torrey, P., Patton, D. R., & Mendel, J. T. 2012, MNRAS, 426, 549
Skibba, R. A., Engelbracht, C. W., Dale, D., et al. 2011, ApJ, 738, 89
Skrutskie, M. F., Cutri, R. M., Stiening, R., et al. 2006, AJ, 131, 1163
Solomon, P. M., Downes, D., Radford, S. J. E., & Barrett, J. W. 1997, ApJ, 478, 144
Solomon, P. M., & Vanden Bout, P. A. 2005, ARA&A, 43, 677
Sommariva, V., Mannucci, F., Cresci, G., et al. 2012, A&A, 539, A136
Stark, D. P., Ellis, R. S., Bunker, A., et al. 2009, ApJ, 697, 1493
Stark, D. P., Schenker, M. A., Ellis, R., et al. 2013, ApJ, 763, 129
Swinbank, A. M., Smail, I., Longmore, S., et al. 2010, Nature, 464, 733
Swinbank, A. M., Papadopoulos, P. P., Cox, P., et al. 2011, ApJ, 742, 11
Tacconi, L. J., Neri, R., Chapman, S. C., et al. 2006, ApJ, 640, 228
Tacconi, L. J., Genzel, R., Smail, I., et al. 2008, ApJ, 680, 246
Tacconi, L. J., et al. 2010, Nature, 463, 781
Tacconi, L. J., Neri, R., Genzel, R., et al. 2013, ApJ, 768, 74
Teyssier, R., Chapon, D., & Bournaud, F. 2010, ApJ, 720, L149
Trentham, N., Kormendy, J., & Sanders, D. B. 1999, AJ, 117, 2152
U, V., Sanders, D. B., Mazzarella, J. M., et al. 2012, ApJS, 203, 9
Walter, F., Bertoldi, F., Carilli, C., et al. 2003, Nature, 424, 406
Walter, F., Brinks, E., de Blok, W. J. G., et al. 2008, AJ, 136, 2563
Weinmann, S. M., Neistein, E., & Dekel, A. 2011, MNRAS, 417, 2737
Weinmann, S. M., Pasquali, A., Oppenheimer, B. D., et al. 2012, MNRAS, 426, 2797
Weiß, A., De Breuck, C., Marrone, D. P., et al. 2013, ApJ, 767, 88
Whitaker, K. E., van Dokkum, P. G., Brammer, G., & Franx, M. 2012, ApJ, 754, L29
Wilson, C. D. 1995, ApJ, 448, L97
Wolfire, M. G., Hollenbach, D., & McKee, C. F. 2010, ApJ, 716, 1191
Wuyts, S., Förster Schreiber, N. M., van der Wel, A., et al. 2011, ApJ, 742, 96
Wuyts, S., Förster Schreiber, N. M., Genzel, R., et al. 2012, ApJ, 753, 114
Wyder, T. K., Martin, D. C., Schiminovich, D., et al. 2007, ApJS, 173, 293
Yamamura, I., Makiuti, S., Ikeda, N., et al. 2010, VizieR Online Data Catalog, 2298, 0
Zahid, H. J., Geller, M. J., Kewley, L. J., et al. 2013, ApJ, 771, L19